論文 / 著書情報
Article / Book Information

題目(和文)	
Title(English)	Study on glass formation from ZrF_4_- and AlF_3_-based fluoride melts
著者(和文)	矢野哲司
Author(English)	Tetsuji Yano
出典(和文)	学位:工学博士, 学位授与機関:東京工業大学, 報告番号:乙第2721号, 授与年月日:1995年2月28日, 学位の種別:論文博士, 審査員:
Citation(English)	Degree:Doctor of Engineering, Conferring organization: Tokyo Institute of Technology, Report number:乙第2721号, Conferred date:1995/2/28, Degree Type:Thesis doctor, Examiner:
学位種別(和文)	博士論文
Type(English)	Doctoral Thesis

STUDY ON GLASS FORMATION FROM ZrF_4- AND AlF_3-BASED FLUORIDE MELTS

(ZrF_4系およびAlF_3系フッ化物融液からのガラス形成に関する研究)

by

Tetsuji Yano

CONTENTS

CHAPTER 1

INTRODUCTION

Fluoride glasses was found accidentally in the growth process of single phase crystal of $2ZrF_4$-BaF_2-NaF in 1975. The first report about the vitrification of this new fluoride glass system was done by M. Poulain, M. Poulain, J. Lucas and P. Brun [1]. The most impressive information, which caused the numerous research efforts all over the world since then, was the estimation of extremely low transmission loss in the mid-IR region of the order of 10^{-3}dB/km [2], which is due to the wide optical window from UV(~220nm) to IR(~7μm) . This estimated value is two orders of magnitude lower than that of SiO_2 fibre practically used at the present and means that the optical fibre telecommunication without any relay for the amplification of light signals would be possible over the long distance like from Tokyo to SanFrancisco.

Firstly, the researches on the glass forming system were concentrated into the incorporation of other fluoride compounds into ZrF_4-BaF_2 binary system in order to enlarge the glass forming region [3]. The extremely poor glass forming ability of melt has been, even now, one of the big obstacles to be overcome, because the precipitation of crystalline would occur in the preparation process to cause the serious light scattering. For this, the multiplication technique of glass composition has mainly been taken in order to improve the glass forming ability. The main target which has been mainly researched by a lot of researchers was focused to ZrF_4-BaF_2-based glass, because this system shows higher glass forming ability among fluoride glass systems. Table 1-1 shows the typical ZrF_4-BaF_2-based systems developed by

the multiplication of the glass composition with the critical cooling rate R_C [4]. The critical cooling rate R_C means the slowest cooling rate to vitrify the melt and although empirical, is considered to be one of the best and most realistic scale for the quantitative evaluation of the glass forming ability in the melting-quenching process. R_C value has been lowered about 4 orders of magnitude in ZBLAN system compared to in ZBG ternary system, and the multiplication of the composition successfully improved the glass forming ability. Recently, InF_3-based glass systems also become to get much attention because its low phonon energy is found to be fascinating to raise up the quantum efficiency of Up-conversion optical function of doped rare earth ions [5]. Table 1-2 lists the main glass forming systems reported by several researchers. In a general view, the systems of the fluoride glass can be classified into about four groups ;

1) ZrF_4-, HfF_4- and ThF_4-based systems (IVB group)

2) AlF_3-, GaF_3-, and InF_3-based systems (IIIA group)

3) MnF_2- and FeF_3-based systems (Transition metal group)

4) ZnF_2-, CdF_2-based systems (IIB group)

Only BeF_2 has been well known as the glass forming fluoride compound since about 50 years ago [6], and the existing glass forming criteria, which has successfully depicted the glass formation in the oxide systems, has also well explained its glass forming ability, because the same analogy of SiO_2 structure can be applied to it. Since the discovery of new fluoride glass* system represented by ZrF_4-based systems, the structural studies have been extensively carried out for these systems, because the existing glass forming rules could not predict and

* After that, the word of ' fluoride glass(es) ' does not include BeF_2 -based system.

explain their glass forming ability. Several techniques of elastic scattering method by X-ray and neutron [7], inelastic scattering method like Raman spectroscopy [8], and computer simulation method of Molecular Dynamics simulation [9] have been employed and the following features of glass structure have been reported in ZrF_4-BaF_2 system.

A) The main flames of glass networks are consisting of ZrF_n polyhedra

B) High coordination number of fluorine about zirconium ions of 7-8.

C) There exist the edge sharing linkages among ZrF_n polyhedra.

D) The necessity of the coexistence of modifiers like barium ions.

From a view point of the empirical rules over oxide systems, the above features are anomalous to explain the formation of glass. Zachariasen rules [10] have been well acknowledged as the guideline of the glass forming conditions, which offer the structural chemical recognition way to consider the glass forming ability of compounds. There are four conditions proposed,

1) oxygen does not bond more than 3 cations.

2) the coordination number of cation about oxygen is less than 4.

3) the coordination units link each other in the corner sharing manner, neither edge nor face sharing.

4) more than 3 oxygen in the coordinate unit are located in bridging site.

Compared the features A-D of ZrF_4-BaF_2 glass with the above rules, B and C do not satisfy the Zachariazen rules, 2 and 3, respectively. This means that ZrF_4 compound has to be classified far from the glass forming progenitor. In order to explain these inconsistency and understand the glass formation mechanism in fluoride glasses, the several criteria have been proposed by several authors at the present.

Baldwin and Mackenzie [11] classified fluoride compounds into the glass former, intermediate and modifier along with single bond strength as shown in Table 1-3 similar to those carried out in oxide glass systems by Sun [12]. This can also explain almost of the glass forming compounds observed and give some guideline to estimate the role of the respective fluoride compounds in the glass. In fluoride compounds, almost the same border line to distinguish the glass formers, intermediates and modifiers, respectively, could be obtained and their values are almost the same as in the oxide systems. The compounds classified into glass formers of ZrF_4, HfF_4, AlF_3 etc, are actually contained as the main component in the glass forming system and this means that the higher single bond strength should be favored as the constituents of glass-forming network. However, fluoride glass former can not form the glass in single compound and needs some appropriate modifier. In this aspect, this table can not offer enough information about modifiers and intermediate to be co-introduced with glass formers. In addition, this classification does not offer any explanation about high coordination number of the former compounds, which is the negative factor from the view point of the ordinary acknowledgment about glass formation.

Poulain [13] proposed another scale to estimate the ability of the glass progenitor. He classified the halide compounds with the relative electric field strength of cation (F_C) against anion (F_A), and ruled out the condition of glass formation to be F_C/F_A=2.5-10 (Table 1-4). His criteria also proposed the guideline to understand the glass forming behavior. His idea was based on the nonperiodic packing concept; i.e. fluorine ions create the potential cationic sites exceeding the available number of cations. The higher field strength enforces the interaction of cation-anion and enhance the random packing of fluoride ions. The additional modifiers

like Ba^{2+} stabilize to preclude the close-packing of anion. His proposed criterion provides some aspect of the role of modifier ions, which is indispensable for glass progenitor to form the glass. However, the quantitative estimation of glass forming ability from F_C/F_A values can not be attained and the repulsion effects among fluorine ions are completely neglected in his scale.

The above two criteria, in some meaning, can play a role in the determination or design of the glass composition, but they do not offer any structural scheme of the devitrification process of the melt. Returning to the definition of ' GLASS ', non-periodicity of liquid phase is quenched into the solid of meta-stable condition without crystallization and the secondary transition of ' glass transition temperature ' will appear. In other word, the relaxation time of the melt structure increases with the temperature decrease and delays the attainment of the equilibrium condition. The liquid-like structures remain even under liquidus temperature and are finally frozen in the solid state. For this, the relaxation time changes widely from 10^{-12} to 10^{2} second. This time-functional behavior is the most representative feature of ' GLASS '. In several properties of ' GLASS ', viscosity, η, directly reflects the relaxation time, because it has the following relation with the relaxation time τ.

$$\eta = G_{\infty} \tau$$

Viscosity-temperature relationship of glass forming liquids have been known to expressed well by the special manner (Fig. 1-1), in which temperature is normalized by glass transition temperature. As shown in this figure, the viscosity-temperature relation changes uniformly from Arrhenius to non-Arrhenius behavior depending on the subjects. Angell [14] classified this phenomena in terms of ' fragility ' of melts. The glass melts showing viscosity change in

Arrhenius form are identified as 'strong' liquid, while ones in non-Arrhenius form are ' fragile' liquids. Most of oxide glass system like SiO_2, B_2O_3, etc. can be classified into ' strong liquid ', because they show near Arrhenius viscosity-temperature relationship. On the other hand, fluoride glass systems in this study are able to be classified as the ' extremely fragile' liquid, because the liquidus viscosity is quite low and the steep viscosity change is observed above glass transition temperature. These characteristic viscosity change means that the viscous flow phenomena is quite different in low temperature region from in high temperature region, meaning that certain structural changes which are characteristic in fluoride glass melt should occur, especially near liquidus temperature. As shown previously, the fluoride glass with higher glass forming ability are actually developed like ZBLAN glass, but its R_c value of 0.7K/min is quite high compared with oxide glasses, e.g. $2x10^{-4}$ K/s in SiO_2, 10^{-16}K/s in B_2O_3 and 10^{-23}K/s in P_2O_5[15]. These differences are consistent with those found in viscosity-temperature relationship. In order to understand the glass formation of fluoride melts, the investigation of the structural changes above Tg must be the most important factor.

In addition to the above mentioned features, we have to take into account the fact that the glass forming ability and the thermal stability* against the crystallization of fluoride

*Therma stability also reveals the scale to evaluate the glass formig ability. It has been often used in the investigation of the glass forming system to know how easy to prepare the glass from the melt. Several equation have been proposed. Poulain et al. [16] also proposed and summarized as follows;

Thermal stability	$\Delta T=Tx-Tg$
Hurby's criterion	$H_r=(Tc-Tg)/(Tm-Tc)$
Weighted thermal stability	$H'=(Tx-Tg)/Tg$
Poulain's criterion	$S=(Tc-Tx)(Tx-Tg)/Tg$

Because the temperature parameters used in the above equations like Tx,Tc, etc. are usually measured by Differential Thermal Analysis by heating at a rate of 10K/min from the glass. Therfore, the melt passes firstly the nucleation temperature range before the crystalline growth region. In this thesis, The term 'Thermal Stability' is used as the scale to evaluate the stability of the melt on heating, and 'Glass Forming Ability' is on cooling from the melt above liquidus temperature.

glass melts were reported to be quite sensitive to the glass preparation process, i.e. the different heat and/or atmospheric treatment often produces the glass with different properties like the thermal stability, even when the same glass compositions are molten. The various kinds of the preparation processes have been proposed. The reactive atmosphere process (RAP) are commonly used in the preparation of Halide glasses. In the case of fluoride glass system, the reactive gas species have been introduced into the melting atmosphere like NF_3, SF_6, CCl_4, etc [17]. The RAP melting method have been employed mainly to reduce the amount of impurity, especially oxygen relating species. As shown in the reports by Mitachi and Tick [18], oxygen impurities changed dynamically the critical cooling rate R_C only in ppm order and showing how sensitively the fluoride melts are influenced to the small amount of anion impurities. On the other hand, no report is found in which small amount of cation influenced the glass forming ability. These results have induced the complexity and the confusion in the consideration of the melting process and this troublesome features of fluoride melts have made it difficult to improve the preparation process. There have not been reported of the systematic investigations of the relation of the preparation process (or impurity) and the stability of the melt. However, the various reports of the crystallization behaviors suggested that there are some keys to understand the glass formation of fluoride glass melt.

From the backgrounds mentioned above, this thesis intends to clarify the following matters about ZrF_4- and AlF_3-based fluoride glass systems.

(I) the structural changes of the melt occurring during cooling, which reflect on the characteristic viscosity-temperature relationship

(II) the general rules working beyond the glass formation of fluoride melts; the

difference in the glass forming scheme among inorganic glasses.

(III) the effects observed in the glass forming ability of the melt in which the non-fluorine anions are incorporated.

In CHAPTER 2, a new simulation method of 'Non-equilibrium Molecular Dynamics method (NEMD)' is proposed and developed, which can be utilized to calculate shear viscosity of inorganic melts with ionic coulomb interactions. In addition to the precise prediction of the viscosity values, this is also intended to understand the viscous flow phenomena of the liquid, especially the glass forming liquid, from the view points of the microscopic dynamic motion of ions . Its accuracy and the analysis way of the results are tested by utilizing it to the simple alkaline halide melt of NaCl and proves its availability.

In CHAPTER 3, the developed simulation method of NEMD for shear viscosity is applied to the glass forming fluoride melt of Zr-Ba-Na-F and compared with the experimental data. The some important factors that have to be taken care in case of glass forming liquid are proposed and the availability of NEMD for the glass forming liquid are discussed. By taking the appropriate particle number, the viscosity-temperature relation have been well simulated and the potentials of NEMD method for the glass forming ionic liquid have been proved. The microscopic analysis utilizing MD trajectories offered the informative results about coordination number in ZrF_n polyhedra and their population and linkage form and key of the structural changes on the glass formation was illustrated and correlated with the characteristic viscosity change of Zr-Ba-Na-F glass melt.

In CHAPTER 4, the viscosity-temperature relations are measured for ZrF_4BaF_2-LaF_3-

AlF_3-NaF glass melts with the different glass forming ability and thermal stability. The effects of the viscosity near liquidus temperature and the compositional difference on the glass forming ability are discussed and the structural schemes on the glass formation proposed in CHAPTER 3 are examined from the view point of modifier ions of Ba^{2+} and Na^{+}.

In CHAPTER 5, the glass forming ability of ZBLAN glass melts is investigated from a view point of the crystallization behavior. The crystalline developing curves are drawn for respective phases precipitated for the glass containing non-fluorine ions of OH^- and Cl^-. In spite of a small amount of their content, the crystallization behaviors were heavily influenced and chlorine showed remarkable effects on the glass forming ability. Their effects in the glass melts have been discussed from the crystalline structures informations of precipitating phases and the glass forming ability of ZrF_4-BaF_2-based fluoride melts have been considered based on the idea of the stability of ZrF_n polyhedra and their linkage.

CHAPTER 6 deals with another fluoride glass system of AlF_3-based YF_3-AlF_3-BaF_2-CaF_2. Chlorine ions are incorporated into this glass system and their glass forming ability and thermal stability are investigated based on the glass forming schemes of ZrF_n-BaF_2-based fluoride melt proposed in CHAPTER 2-5. The appropriate chlorine incorporation maximized both of the glass forming ability and the thermal stability, which are comparable and/or superior to ZBLAN and ZBGA glasses. The precipitation of the crystalline in bulk was heavily suppresses and the fragility of melt decreased. These behaviors have been discussed from the view point of AlF_n polyhedra linkages by comparing with ZrF_4-based system.

CHAPTER 7 summarizes all the results and discussions, and mentions briefly about the overview on the glass formation of fluoride glass formation.

REFERENCES

[1] M. Poulain, M. Poulain, J. Lucas and P. Brun, Mater. Res. Bull., 10 (1975) 243

[2] S. Shibata, M. Horiguchi, K. Jinguji, S. Mitachi, T. Kanamori and T. Manabe, Electr. Lett., **17** (1981) 775-777

[3] e.g., J. Lucas, M. Chanthanasihn, M. Poulain, M. Poulain, P. Brun and M. J. Weber, J. Non-Cryst. Solids, **27** (1978) 273, M. Poulain, M. Chanthanasihn and J. Lucas, Mater. Res. Bull., **12** (1977) 151, A. Lecoq and M. Poulain, J. Non-Cryst. Solids, **34** (1979) 101, S. Mitachi and T. Manabe, Jpn. J. Appl. Phys., **19** (1980) L313

[4] T. Kanamori, Mater. Sci. Forum, **19&20** (1987) 363

[5] e.g., C. Guery, J. L. Adam and J. Lucas, J. Lumine. **42** (1988) 181

[6] V. M. Goldschmidt, Skrifter Norske Videnskaps Akad (Oslo). I. Math-naturwiss. Kl. No. 8, 7

[7] e.g., R. Coupé, D. Louër, J. Lucas and J. Lé0onard, J. Am. Ceram. Soc., **66** (1983) 523, J. Lucas, C. A. Angell and S. Tamaddon, Mater. Res. Bull., **19** (1984) 945

[8] e.g., R. M. Almeida and J. D. Mackenzie, J. Chem. Phys., **74** (1981) 5954, R. M. Almeida and J. D. Mackenzie, J. Chem. Phys., **78** (1983) 6502

[9] e.g., C. A. Angell, P. A. Cheeseman and S. Tamaddon, J. de Phys., **43** (1982) C9-381

[10] W. H. Zachariasen, J. Am. Chem. Soc., **54** (1932) 3841

[11] C. M. Baldwin and J. D. Mackenzie, J. Am. Ceram. Soc., **62** (1979) 537

[12] K. M. Sun, J. Am. Ceram. Soc., **30** (1947) 277

[13] M. Poulain, Nature, **293** (1982) 279

[14] C. A. Angell; in *Relaxation in Complex Systems*, ed. K. Ngai and G. B. Wright, National

Technical Information Service, U. S. Department of Commerce, Sprigerfield, VA 22161, 1 (1985); J. Non-Cryst. Solids, **73** (1985) 1

[15] Z. Strnad; in *Glass-Ceramic Materials*, Elsevior, 1 (1986): C. A. Vreeswijk, R. G. Gossink and J. M. Stevels, J. Non-Cryst. Solids, **16** (1974) 15

[16] M. Saad and M. Poulain, Mater. Sci. Forum, **19&20** (1987) 11

[17] e.g., M. G. Drexhage, C. T. Moynihan, B. Bendow, E. Gboji, K. H. Chung and M. Saleh-Boulos, Mater. Res. Bull., **16** (1981) 943 ; E. Gboji, K. Chung, C. T. Moynihan and M. G. Drexhage, J. Am. Ceram. Soc., **64** (1981) C51

[18] S. Mitachi and P. A. Tick, Mater. Sci. Forum, **32&33** (1988) 197

Table 1-1. The typical ZrF_4-BaF_2-based fluoride glass systems and their critical cooling rates. [4]

Glass	Composition (mol%)								R_c (K/min)
	ZrF_4	BaF_2	GdF_3	LaF_3	YF_3	AlF_3	LiF	NaF	
ZBG	63	33	4	–	–	–	–	–	370
ZBGA	60	32	4	–	–	4	–	–	70
ZBLAL	52	20	–	5	–	3	20	–	26
ZBLYAL	49	22	–	3	3	3	20	–	26
ZBLAN	51	20	–	4.5	–	4.5	–	20	~0.7
ZBLYAN	47.5	23.5	–	2.5	2	4.5	–	20	~1.1

Table 1-2. The examples of the typical fluoride glass forming systems.

ZrF_4-BaF_2
ZrF_4-BaF_2-NaF
ZrF_4-BaF_2-LaF_3
ZrF_4-BaF_2-NdF_3
ZrF_4-BaF_2-GdF_3
ZrF_4-BaF_2-ThF_4
ZrF_4-BaF_2-UF_4
ZrF_4-ThF_4-MF_3 (M=La,Nd,Y,Lu,Sc,Al)
ZrF_4-BaF_2-AlF_3-MF_n
(MF_n=LiF,NaF,CaF_2,LaF_3,NdF_3,LaF_3)
ZrF_4-BaF_2-AlF_3-YF_3
ZrF_4-BaF_2-LaF_3-AlF_3-NaF

HfF_4-BaF_2-LaF_3
HfF_4-BaF_2-ThF_4
HfF_4-BaF_2-ThF_4
HfF_4-BaF_2-LaF_3-AlF_3

AlF_3-PbF_2
AlF_3-BaF_2-CaF_2
AlF_3-YF_3-BaF_2-CaF_2

ScF_3-BaF_2-MF_n (MF_n=NaF,YF3,ThF4)
InF_3-ScF_3-BaF_2
InF_3-GaF_3-BaF_2
InF_3-CdF_2-BaF_2
GaF_3-CdF_2-BaF_2
GaF_3-BaF_2-NaF

MnF_2-BaF_2-LnF_3
MnF_2-BaF_2-CrF_3
MnF_2-BaF_2-ThF_4

ZnF_2-CdF_2-BaF_2
ZnF_2-BaF_2-LnF_3
ZnF_2-AlF_3-ThF_4-MF_2 (M=Mg,Ca,Sr,Ba)
ZnF_2-BaF_2-MF_3-ThF_4 (M=Yb,Lu)

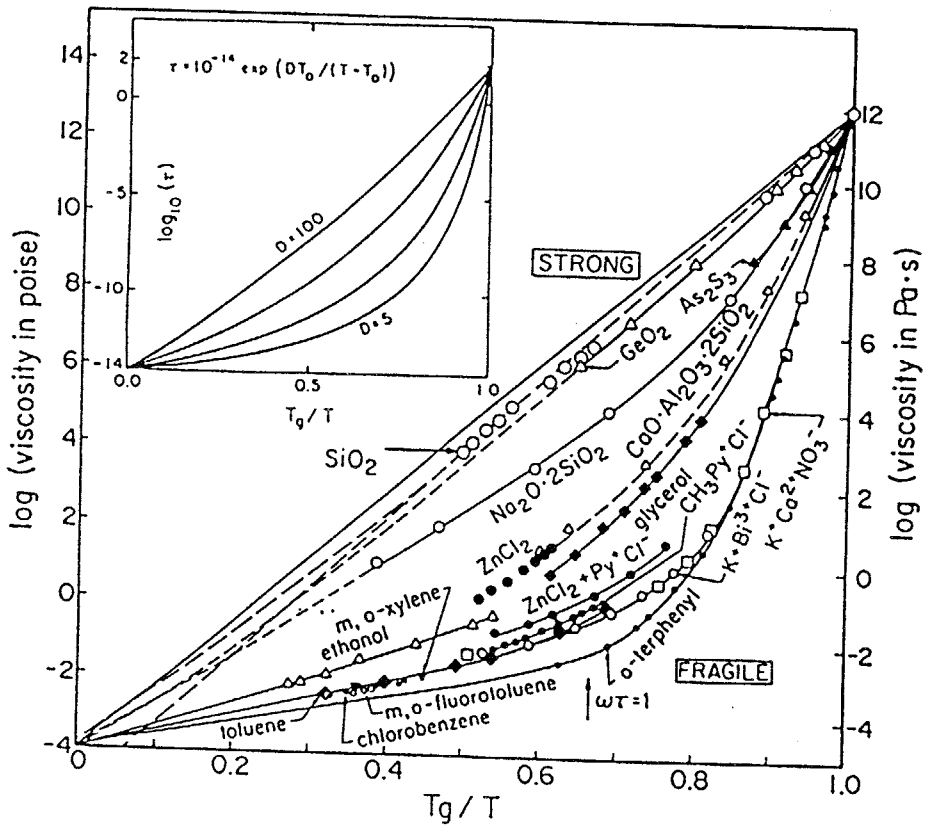

Fig. 1-1 The viscosity-temperature relations of glass forming liquids. Temperature is normalized by the respective glass transition temperature. The figure interpolated is the relaxation time-temperature relations. The relaxation time is simply connected with viscosity by the factor of the shear modulus G_∞.

Table 1-3. The relationships of glass formation of fluorides according to the single bond strength proposed by Baldwin and Mackenzie [11].

M in MF_n	Valence	Dissociation energy per MF_n (kcal/mole)	Coordination number	Single bond strength (kcal/mole)
Glass formers				
Ti	4	585	6	98
Sc	3	539	6	90
Be	2	537	4	89
Hf	4	688	8	86
Zr	4	681	8	85
Al	3	496	6	83
Intermediates				
Cr	3	431	6	72
Y	3	570	8	71
B	3	275	4	69
Fe	3	408	6	68
Nd	3	537	8	67
Pb	4	350	6	58
Sb	3	340	6	57
Mg	2	339	6	57
Modifiers				
Si	4	319	6	53
Co	2	304	6	51
Ga	3	403	8	50
Ni	2	297	6	50
Mn	2	296	6	49
Ca	2	371	8	46
Sr	2	369	8	46
Ba	2	368	8	46
Zn	2	253	6	42
Cu	2	250	6	42
Bi	3	324	8	41
Cr	2	320	8	40
Li	1	203	6	34
Pb	2	245	8	31
Na	1	182	6	30
K	1	176	6	29
Cd	2	233	8	29
Ag	1	167	6	28
Cs	1	166	6	28
Tl	1	141	6	24
Hg	2	178	8	22

[a] After Baldwin and Mackenzie (1979).

Table 1-4. The criterion of the glass formation of fluorides based on the electric field strength proposed by M. Poulain [13].

Cation	Anion	F_A*	F_C*	F_A/F_C	Glass progenitor	Ref.
Al^{3+}	F	0.78	5.6	7.2	Yes	19
Be^{2+}	F	0.78	7.4	9.5	Yes	19
Zr^{4+}	F	0.78	5	6.4	Yes	12
Hf^{4+}	F	0.78	5.2	6.7	Yes	20
Ga^{3+}	F	0.78	4.8	6.1	Yes	14
Fe^{3+}	F	0.78	4.7	6.0	Yes	14
Cr^{3+}	F	0.78	4.9	6.3	Yes	14
Th^{4+}	F	0.78	3.8	4.9	Yes	15, 16
Y^{3+}	F	0.78	3.1	4.0	Yes	21, 22
Zn^{2+}	F	0.78	2.8	3.6	Yes	22
Si^{4+}	F	0.78	15.4	19.7	No	
Mo^{6+}	F	0.78	14.6	18.7	No	
Ca^{2+}	F	0.78	1.78	2.3	No	
NaF	F	0.78	0.85	1.1	No	
Zn^{2+}	Cl	0.55	3.33	6.0	Yes	19
Bi^{3+}	Cl	0.55	2.91	5.3	Yes	23

CHAPTER 2

DEVELOPMENT OF NON-EQUILIBRIUM MOLECULAR DYNAMICS SIMULATION METHOD OF VISCOSITY FOR IONIC MELTS

2-1. INTRODUCTION

As mentioned in CHAPTER 1, the viscosity-temperature relationship is the most representative property of glass forming liquid and the various features of liquids like the structure, interatomic forces, intermolecular interaction, thermal decomposition or reaction etc. reflect on it in very complex manner. However, it gives much informations to understand the glass forming behavior.

Viscosity and viscous flow phenomena of glass forming liquids have been investigated by a lot of researchers for a long time in order to clarify the origins to change its value widely from 10^{-2} to 10^{15} poise. They have been employed the methods of the constructing of some physical [1] and thermodynamical models [2] into some mathematical expressions. Their proposed equations show the excellent expression of the measured data and the abstract schemes of viscous flow phenomena have been well depicted to various glass forming liquids. However, in some cases, they include some parameters which can not be given any physical and/or chemical meaning, causing the lack of the structural chemical illustrations imaged from the equations. Fluoride glass is one of such representatives, which does not obey Arrhenius [3] nor Vogel-Tanmann-Fulcher expression [4], but Cohen-Grest equation [5]. The latter includes the four parameters which do not have any physical meaning.

The investigation and the build-up of the full illustration of the glass and glass melt structures are considered to be the ultimate goal for the glass sciences. There are often used a lot of experimental techniques to investigate the glass structures like spectroscopic measurement like IR, Raman scattering, NMR etc. but they often offer only the informations on the short range structures. The viscous flow phenomena are relating to the longer range structures and their cooperative motions, especially the dynamics of the motion of the structural flames of glass network. The above mentioned investigation techniques can be said to be not enough to understand and illustrate the viscous flow mechanisms.

Molecular Dynamics simulation (MD) method have been used more widely in the field of the material science, because it has been rapidly progressed accompanying with the rapid advance of the capacity and performance of computer. MD simulation technique has also been employed in the glass science and proposed a lot of advances of the understanding for the structural analysis results by using with the elastic scattering measurements [6]. The most impressive advantages of MD method can be listed as follows;

(i) available to know the strict information about the coordinates of ions consisting the materials.

(ii) available to know the dynamic motion of particles from the time-trajectories, which can be used to calculate the vibrational spectrum like Raman scattering, the transport properties like viscosity, diffusion constant, etc.

(iii) available to simulate the system under some special condition like the high temperature, the high pressure, the instantaneous phenomena etc., under which no experimental technique is available.

Concerning the viscosity, the information of the dynamical motion of particles are necessary and indispensable to clarify the viscous flow phenomena. It is clear from the above mentioned advantages, MD simulation method is considered to be applicable to investigate the viscosity of liquids, and there are much potential to introduce the microscopic point of view in this field.

In this CHAPTER, a new simulation method of shear viscosity called as ' Non-equilibrium Molecular Dynamics ' has been developed in order to utilize it for the inorganic liquids. With respect to the interactions between particles, it is firstly preferred for the ionic interaction to be available, because this kind of the interaction envelops the objective materials over the inorganic materials. The availability and the accuracy are tested by its application to the molten simple alkali halide of NaCl.

2-2. VISCOSITY IN MD SIMULATIONS

The investigation of viscosity by MD simulation method have been carried out by several researchers [7]. Their employing techniques were

1) using Stokes-Einstein relationships

$$\eta = k_B T / 6\pi\delta D$$

where δ is the radius of the particle and D is the self-diffusion constant at temperature T.

2) using Green-Kubo relation [8]

$$\eta = \frac{V}{k_B T}\int_0^\infty \langle P^{\alpha\beta}(t)\cdot P^{\alpha\beta}(0)\rangle dt$$

where V is the cell volume, $P^{\alpha\beta}(t)$ is the tensor value at time *t*.

Recently, a new calculation method of MD simulation has been proposed and carried out to simulate shear viscosity of liquids [9]. This is called as ' Non-equilibrium Molecular Dynamics (NEMD)' and the above two approaches have been classified as Equilibrium Molecular Dynamics (EMD) against this. There are also several ways in NEMD approach [10], but the main difference with EMD exists in the replica construction way. In this thesis, the algorithm by Lees and Edwards [11] is employed. Overview of NEMD methods are reviewed in detail by Evans et al. [12] and the features of NEMD cas be summarized as follows;

(i) the external forces can induce efficiently the output like shear stress.

(ii) the similar condition as the experiment can be created.

(Iii) there is less influence of the pre-history of the structure on the results than in EMD.

(iv) there needs less time-trajectories than in EMD.

On the other hand, there are also pointed out some matters to be payed attention when utilizing NEMD method. The point can be expressed as follow;

The external forces are relatively much larger than the actually applied in experiment. This is mainly due to the cell size problem and common in all MD simulation method, but whether such a condition induces some meaningful

behavior for considering the realistic phenomena or not ?

On considering the relaxation process against the external force, there has to be cared the relation between its frequency and the relaxation time as seen in various relaxation experiments [13]. The large force would change the susceptibility of the system and show the non-linearity. In this CHAPTER, the way of the analysis about these phenomena has been also examined to obtain the appropriate viscosity value along with the observed non-linear behaviors of liquids.

2-3. NEMD VISCOSITY CALCULATION

A. NEMD ALGORITHM

The fundamental algorithm of NEMD simulation for shear viscosity is based on the idea of homogeneous shear formation proposed by Lees and Edwards [11]. Fig. 2-1(a) shows the arrangement of the unit cell and its replicas which are settled to define boundary condition for the calculation of Coulombic interactions among particles. This formula has been widely employed in equilibrium MD method, where the replicas are always fixed in the same position. In contrast, NEMD method for shear viscosity uses the time-dependent arrangement of replicas: the replica arrays are displaced in the special manner in order to create Couette flow in the unit cell as shown in Fig. 2-1(b). The shear stresses are spontaneously caused by the velocity gradient of particles in the cell and their values have much correlation with the flow mechanism of the composing particles and the formed liquid structures.

In this study, the subject liquids of the simulation are the ionic melts with Coulombic interaction forcing over a long distance, which is largely different from the L-J liquid previously

studied. Coulombic interactions among charged particles are calculated by using Ewald method[14]. In Ewald calculation (Eq. 2-1), the sum over the vectors in real space and reciprocal space must be modified because of the displacement of replicas in NEMD.

$$\Phi_i = \Phi_{Ii} + \Phi_{IIi} + \Phi_{IIIi}$$

$$\Phi_{Ii} = Z_i e^2 \sum_j Z_j \sum_{\mathbf{n}} \frac{\operatorname{erfc}(\alpha|\mathbf{r}_{ijn}|)}{|\mathbf{r}_{ijn}|}$$

$$\Phi_{IIi} = \frac{Z_i e^2}{\pi V} \sum_j Z_j \sum_{\mathbf{k}} \left[\exp\left(\frac{-\pi^2|\mathbf{k}|}{\alpha^2}\right) \frac{1}{|\mathbf{k}|^2} \cos(2\pi\mathbf{k}\cdot\mathbf{r}_{ij}) \right] \qquad (2\text{-}1)$$

$$\Phi_{IIIi} = \frac{Z_i^2 e^2 \alpha}{\sqrt{\pi}}$$

The displacement of the replica cells to form Couette flow means that the vectors in real and reciprocal space in Eq. (2-1) change every step. Therefore the real space vector **n** and the reciprocal space vector **k** are expressed in Eqs. (2-2) and (2-3), respectively.

$$\mathbf{n} = \begin{pmatrix} 1 & \gamma t & 0 \\ 0 & 1 & 0 \\ 0 & 0 & 1 \end{pmatrix} \begin{pmatrix} l \\ m \\ n \end{pmatrix} \qquad (2\text{-}2)$$

$$\mathbf{k} = \frac{2\pi}{L} \begin{pmatrix} 1 & -\frac{\gamma t}{L} & 0 \\ 0 & 1 & 0 \\ 0 & 0 & 1 \end{pmatrix} \begin{pmatrix} l \\ m \\ n \end{pmatrix} \qquad (2\text{-}3)$$

In the calculation of the repulsive term, Born-Haggins-Mayer type potential is employed:

$$\Phi_{ij} = \frac{Z_i Z_j e^2}{r_{ij}} + A_{ij} \exp\left(-\frac{r_{ij}}{\rho}\right) \tag{2-4}$$

The motion of particles are calculated in the manner of Newtonian equation with Verlet argolithm[15] and the temperature of system is controlled by the velocity scaling factors. Under shear flow created, the treatment of the particles forced out of the unit cell must be taken care. The relation of coordinates between particle i in the unit cell and its image i' in the replica (l, m, n), where l, m, and n are the integral values defining the replicating coordination against the unit cell, under shear rate γ at time t is expressed as follow:

$$\begin{pmatrix} x_i' \\ y_i' \\ z_i' \end{pmatrix} = \begin{pmatrix} x_i \\ y_i \\ z_i \end{pmatrix} + L \begin{pmatrix} 1 & \gamma t & 0 \\ 0 & 1 & 0 \\ 0 & 0 & 1 \end{pmatrix} \begin{pmatrix} l \\ m \\ n \end{pmatrix} \tag{2-5}$$

where (x_i, y_i, z_i) and (x'_i, y'_i, z'_i) reveal the coordinates of particles i and i' in the unit cell and the replica cell, respectively. When the particle is forced out of the unit cell, its image must be replaced at the appropriate position in the unit cell. Its position is defined by Eq. (2-5) and its velocity must also be corrected. The relation of velocity between i and i' can be obtained by differentiating Eq. (2-5) about time t as Eq. (2-6):

$$\begin{pmatrix} v_x' \\ v_y' \\ v_z' \end{pmatrix} = \begin{pmatrix} v_x \\ v_y \\ v_z \end{pmatrix} + L \begin{pmatrix} 0 & \gamma & 0 \\ 0 & 0 & 0 \\ 0 & 0 & 0 \end{pmatrix} \begin{pmatrix} l \\ m \\ n \end{pmatrix} \tag{2-6}$$

As seen in Eq. (2-6), x-component of velocity is dependent on both shear rate and y coordinate. This means that the treatment of particle going in or out over xz plane needs some correction about x component of velocity.

The formation of Couette flow spontaneously causes the shear terms of pressure tensor. The value of $P^{\alpha\beta}$ can be obtained by using Eq. (2-7).

$$P^{\alpha\beta} = \frac{1}{V}\left\{\sum_i m_i v_{\alpha i} v_{\beta i} - \sum_{i<j}\sum \frac{r_{\alpha ij}\, r_{\beta ij}}{r_{ij}} \cdot \frac{d\Phi_{ij}}{dr_{ij}}\right\} \qquad (2\text{-}7)$$

where α and β mean the direction of axis. From Eq.(2-7) and shear rate γ, shear viscosity η is obtained from Eq. (2-8)

$$\eta = -\frac{\langle P^{\alpha\beta} \rangle}{\gamma} \qquad (2\text{-}8)$$

where the brancket < > means the average over the shearing time period. The calculation flow chart was shown in Fig. 2-2.

B. CALCULATION PROCEDURES

The objective materials of shear viscosity calculation in this CHAPTER were a simple alkaline halide melt of NaCl. This is well known as the subject with coulombic interaction between particles and is non-glass forming liquid even under the fastest cooling rate of real condition. In order to verify the program and its accuracy of calculation of shear viscosity, NaCl melt is considered to be the appropriate subject because there are a lot of reliable data

of viscosity, density, etc. For the calculation of interactions between ions, Tosi-Fumi's parameters[16] were used. In this calculation, the dipole interaction and quadrupole interaction were calculated in addition to Eq. (2-4). All of the calculation conditions are listed in Table 2-1. Temperature was settled at 1100K near the melting point of 1131K. The number of particles was 216. The length of the unit cell were determined from the density of melts at this temperatures. The density values in the literatures[17] are expressed by Eq.(2-9).

$$\rho=1.560-0.53\times10^{-3}\,(T_K-1073) \qquad (2\text{-}9)$$

For every series of calculations, the initial positions of particles were determined as following calculation flow ; (I) starting from the random positions and the velocity with Gaussian distribution and calculated for 10000 steps at 5000K. (II) rapidly quenched down to the respective temperature followed by annealing for 20000 steps. The basic value of time step was settled to be 2.0 fsec for this initial calculations. The total momentum of the system was corrected at every 1000 steps. The last snap-shot of particles was used as the starting initial position and velocity for NEMD viscosity calculations.

The shear rate applied to the unit cell was changed from $1.0\times10^{10}s^{-1}$ to $1.0\times10^{13}s^{-1}$. The lowest shear rate was defined according to the value of the induced stress; the excessively low shear rate applied, the induced shear stress would be too small compared with the thermal fluctuation of stress to obtain shear viscosity. Time step value was also taken care. The basic value was 2.0 fsec, but the shorter time step was employed depending on the controllability of temperature of system.

2-4. RESULTS AND DISCUSSION

The shear rate dependence of NaCl melt at 1100K was shown in Fig. 2-3. The allow in the figure indicates the measured value by Brückner et al.[18] While the shear rate applied, the temperature of system was slightly increased because of dissipation energy, but was controlled within ±2% of the settled temperature; e.g., at the highest shear rate of $1.0\times10^{13}s^{-1}$, temperature drift was only ±8K. The simulated shear viscosity increased with the decrease of the shear rate and approached to a constant value. This so-called Non-Newtonian behavior was also reported as shear thinning effects in other NEMD shear viscosity simulations for L-J system[19], Soft-Sphere system[20]. This non-Newtonian behavior was considered to be caused by the extremely high shear rate compared with one used in the real viscosity measurement. In the Newtonian region, the applied shear rate γ is very small compared with the structural relaxation time τ ; $\gamma\tau<<1$. On the other hand, the shear rate applied in the simulation was too large to guarantee the above relation ; $\gamma\tau\sim1$. In MD simulation, only a few thousands of particles can be treated because of the problem of computer, and a small cell with the length in the order of <10nm have to be used. This means that the extremely high shear have to be applied to it to obtain the shear stress high enough to attain better S/N ratio. This might give some impression that the viscous flow occurring in the cell would be artificial. However, taking into account the structural relaxation time τ of liquid with viscosity in the order of 10^{-2} poise, these applied shear rate values at which Non-Newtonian behavior appeared would be quite unreasonable ($\tau\sim10^{-10}$s). This suggested that the simulated relaxation process in the cell have the almost the similar time-dependency to the real phenomena. Concerning the reliability of the viscous flow phenomena, the accuracy of Newtonian viscosity would

also support to confirm the reliability of the simulated phenomena.

In order to obtain Newtonian viscosity (zero-shear viscosity), η_0, the mode-mode coupling theory of KYG[21] was employed to fit the shear rate dependence in most of reports of NEMD shear viscosity simulation[19, 20]. According to this theory, viscosity might have the dependence on the square root of shear rate.

$$\eta = \eta_0 - A\,\gamma^{-0.5} \qquad (2\text{-}11)$$

On the other hand, non-Newtonian viscous behaviors were actually observed in the real subjects like silicate glass melts[22]. According to the analysis by Simmons et al.[23] against soda-lime silicate glass of NBS710, the relation between viscosity and shear rate was shown to be expressed well by the empirical equation[24];

$$\eta / \eta_0 = \frac{1}{1 + \gamma \frac{\eta_0}{\sigma_\infty}} \qquad (2\text{-}12)$$

Fig. 2-3 included the least square curve fitting results to both equations mentioned above. Apparently, KYG equation failed to express the calculated results while the latter succeeded well. In addition, Eq. (2-11) is meaningless at much higher shear rate, because it produces negative viscosity value. This reveals that the estimation of shear viscosity in Newtonian region (zero-shear viscosity) is possible and appropriate from non-Newtonian equation (2-12) applying to these simulated viscosity data obtained by NEMD simulation. Therefore, the zero-shear viscosity of NaCl melt at 1100K was evaluated to be 0.03P, which coincided well with the measured value of 0.01P. This calculation results revealed that the NEMD program developed in this study could be applied to realistic subjects with Coulombic interactions, and

present sufficiently accurate viscosity value. Although the so-called non-Newtonian behavior appeared because of the high shear rate, its phenomenon resembled well with those observed in the real liquids and could be expressed well with the empirical equation. As Simmons et al.[23] also suggested, the critical shear rate, at which the non-Newtonian behavior was observed, was considered to reveal some information of the relaxation time, but at the present we would not discuss about it because there have not been found any method of theoretical treatment about this phenomena.

2-5. CONCLUSIONS

Non-Equilibrium Molecular Dynamics simulation method for shear viscosity of ionic liquids was developed based on the algorithm proposed by Lees and Edwards. It was actually applied to the simple alkaline halide melt of NaCl and the viscosity at melting point 1100K was calculated. Viscosity values showed typical Non-Newtonian behavior above the shear rate near 10^{11} s^{-1}. The observed viscosity data could be well fitted by the empirical Non-Newtonian equation of viscosity, which has been known to express the actually observed results in measurement. Considering the relaxation in liquid, the critical shear rate at which Non-Newtonian behavior appeared would likely to correlate with the relaxation time and the reciprocal value of that shear rate was similar to one observed in the relaxation measurement. Although the applied shear rate is extremely high, the observed shear rate dependence would have some physical meaning and not be a fabrication. The resulted Newtonian viscosity consisted well with the measured data and the accuracy and the probability of this developed NEMD simulation method have been verified.

REFERENCES

[1] M. H. Cohen and D. Turnbull, J. Chem. Phys., **31** (1959) 1164

[2] G. Adam and J. H. Gibbs, J. Chem. Phys., **43** (1965) 139

[3] S. Glasstone, K. J. Laidler and H. Eyring ; Theory of Rate Process, McGraw-Hill (1941)

[4] G. S. Fulcher, J. Am. Chem. Soc., **8** (19525) 339

[5] M. H. Cohen and G. S. Grest, Phys. Rev. **B 20** (1979) 1077

[6] e.g., T. F. Soules, J. Chem. Phys., **73** (1980) 4032

[7] e.g., G. Ciccotti, G. Jacucci, I. R. McDonard, Phys. Rev., **A13** (1976) 426

[8] R. Kubo, J. Phys. Soc. Jpn., **12** (1957) 570

[9] e.g., D. M. Heyes, J. Chem. Soc., Faraday Trans. 2, **82** (1986) 1365 ; W. T. Ashrust and W. G. Hoover, Phys. Rev. Lett., **31** (1973) 206

[10] e. g., G. Ciccotii and G. Jacucci, Phys. Rev. Lett., **35** (19875) 789 ; G. V. Paoliui, G. Ciccotti and C. M. Massobrio, Phys. Rev. **A34** (1986) 1355

[11] A. W. Lees and S. F. Edwards, J. Phys. **C16** (1983) 860

[12] D. J. Evans and G. P. Morriss, Comput. Phys. Rep., **1** (1984) 297

[13] e.g., S. Sridhar and P. Tabrek, J. Chem. Phys., **88** (1988) 1170 ; E. A. Pavlatou, A. K. Rizos, G. N. Papatheodorou and G. Fytas, J. Chem. Phys., **94** (1991) 224 ; L. M. Torell, L. Borjesson and M. Elmroth, J. Phys. Condens. Matter, **2** (1990) SA207

[14] P. P. Ewald, Ann. Phys., **64** (1921) 253

[15] L. Verlet, Phys. Rev. **159** (1967) 88

[16] F. G. Fumi and M. P. Tosi, J. Phys. Chem. Solids **25** (1964) 31 ; M. P. Tosi and F. G. Fumi, J. Phys. Chem. Solids **25** (1964) 45

[17] K. Grjotheim, R. Nikolic, and H. A. Øye, Trans. Faraday Soc. **67** (1971) 640

[18] W. Brückner, K. Grjotheim, T. Ohta and H. A. Øye, Berichte Bunsen-Gesellschaft Bd.**79,** Nr.4 (1975) 344

[19] C. Massobrio, V. Pontikis and G. Ciccotti, Phys. Rev. **B39**, 2640 (1988) ; T. Naitoh and S. Ono, J. Chem. Phys. **70** (1979) 4515

[20] P. T. Cummings and T. L. Varmer, Jr., J. Chem. Phys. **89**, 6391 (1988), ; J. R. Rustad, D. A. Yuen and F. J. Spera, J. Chem. Phys. **91** (1989) 3662

[21] K. Kawasaki and D. Gunton, Phys. Rev. **A8** (1973) 2048

[22] e.g., J. H. Li and D. R. Uhlmann, J. Non-Cryst. Solids, **3** (1970) 127

[23] J. H. Simmons, R. Ochoa, K. D. Simmons, and J. J. Milles, J. Non-Cryst. Solids **105** (1988) 313

[24] C. J. Montrose, ONR Technical Report Contract No.N00014-75-C-1856, Government Printing Office, Washington, DC, Jan. 1981

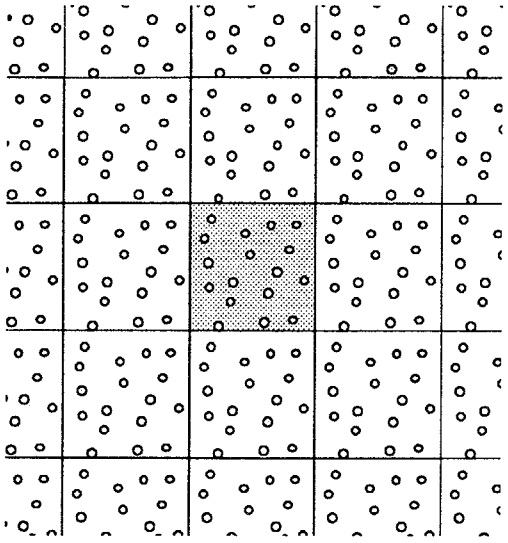

(a)

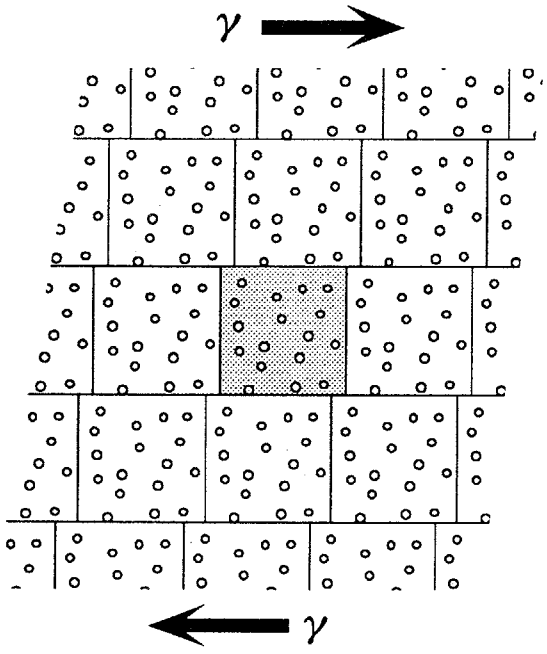

(b)

Fig. 2-1 The arrangements of the unit cell and its replicas. (a) is usually used in Equilibrium MD method and (b) is for the shear viscosity calculation by NEMD. The respective replica arrays are displaced every step along the holizontal axis.

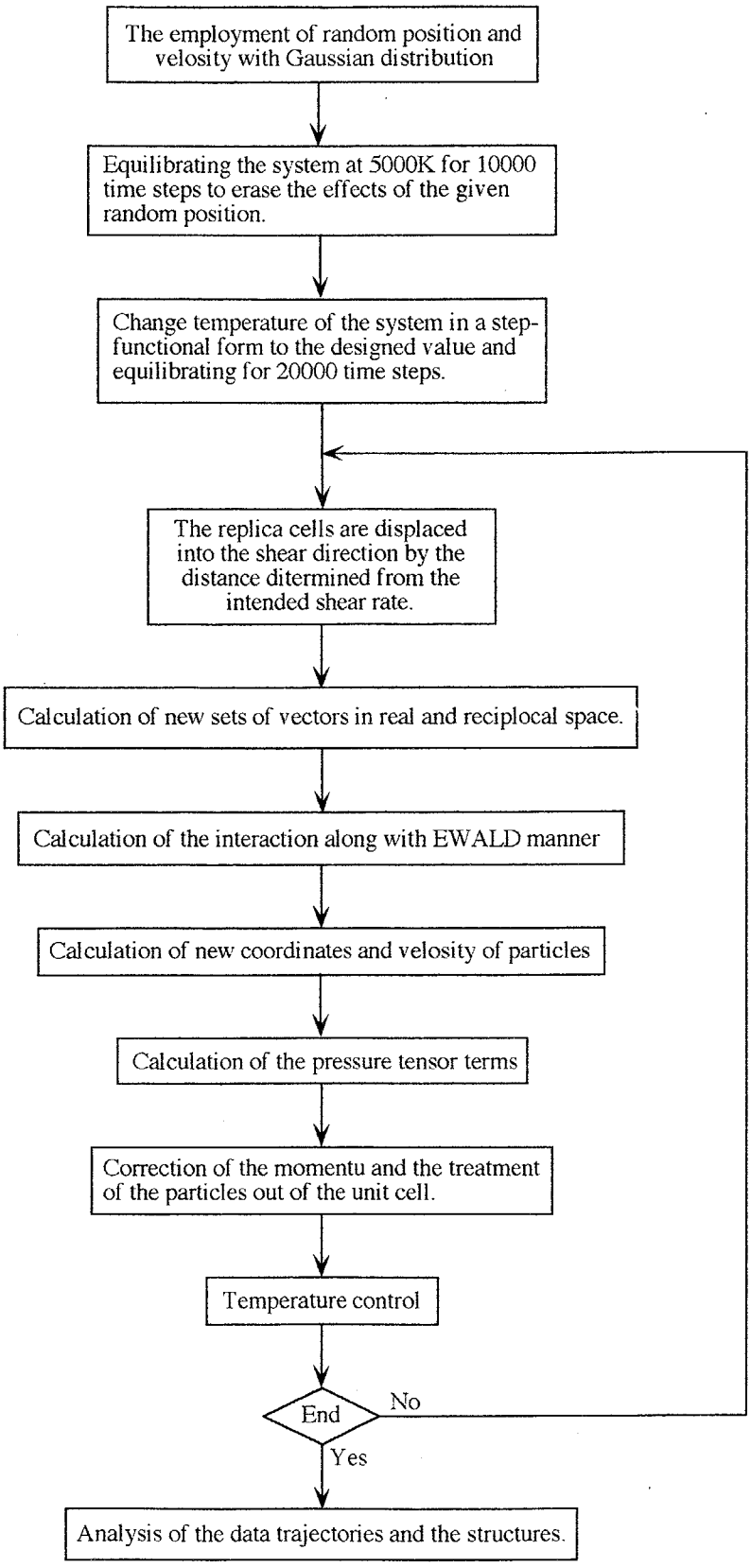

Fig. 2-2 Calculation flowchart of NEMD method for viscosity.

Table 2-1. Lists pf the calculation conditions for shear ciscosity, the apparent viscosity values, and Newtonian (zero-shear) viscosity obtained from the least square fitting to Eq. 2-12.

SYSTEM	Temperature (K)	Cell size L (nm)	Time step (fs)	No. of step	Shear rate γ (s^{-1})	Viscosity η (P)	Newtonian viscosity η_0 (P)
108Na-108Cl	1100	1.95980	5.0	80 000	1.0×10^{10}	0.0388	0.03
	1100	1.95980	2.0	20 000	4.0×10^{10}	0.0164	
	1100	1.95980	2.0	20 000	1.0×10^{11}	0.0121	
	1100	1.95980	1.0	10 000	4.0×10^{11}	0.0103	
	1100	1.95980	1.0	10 000	1.0×10^{12}	0.00686	
	1100	1.95980	0.5	10 000	4.0×10^{12}	0.00141	
	1100	1.95980	0.2	10 000	1.0×10^{13}	0.000547	

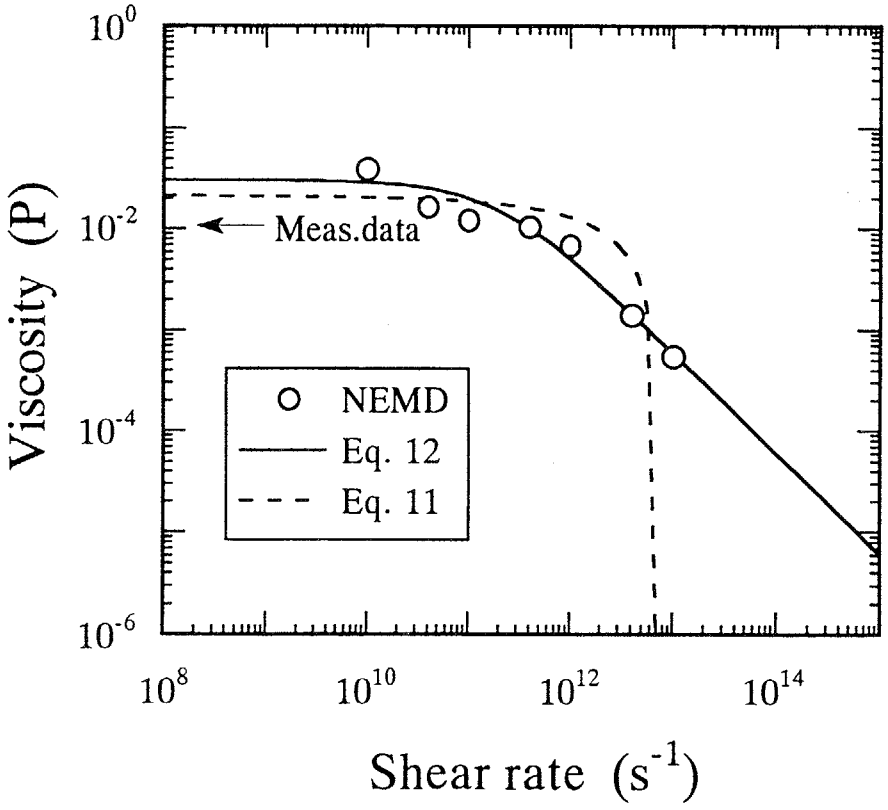

Fig. 2-3 The shear rate dependence of viscosity of NaCl melt at 1100K calculated by NEMD method. The allow inside the graph is showing the experimental value at the melting point and the curves are obtained by the least square fitting of the calculated data to Eqs. (2-11) and (2-12), respectively.

CHAPTER 3

VISCOSITY AND STRUCTURAL INVESTIGATION OF ZrF_4-BaF_2-NaF GLASS MELT BY MOLECULAR DYNAMICS SIMULATION

3-1. INTRODUCTION

As mentioned in CHAPTER 1, fluoride glass systems represented by ZrF_4-BaF_2 systems show some characteristic properties that have not been observed in oxide glass systems, and they should be much correlated with the structural features found in this system. Any existing criteria [1] applied to the oxide systems could not fully explain the glass formation of fluoride system. The viscosity-temperature relation can be said to be one of those properties and considered to hold the key to understand the glass formation of the melt, because the viscosity means directly the relaxation phenomena and their change over the wide range is just the nature of the glass forming liquid. The viscosity-temperature relation of fluoride glass melt of ZrF_4-BaF_2-based system have been measured by several researchers and acknowledged to show non-Arrhenius and non-Fulcher type behaviors [2]. Along with the classification by Angell [3], it can be expressed as 'extremely fragile'. This means that the activation energy of viscous flow widely change depending on temperature and the different viscous flow mechanisms should play a role to define the viscosity and the activation energy. In case of ZrF_4-BaF_2-based glass system, viscosity changes steeply under liquidus temperature with the temperature decrease, suggesting that some dynamical changes in the melt structure should happen. In this CHAPTER, the viscosity-temperature relation of ZrF_4-BaF_2-NaF fluoride glass melt has been investigated by using NEMD and EMD simulation methods. As shown in

CHAPTER 2, NEMD viscosity simulation method developed in this study predicted the viscosity value at the melting point of NaCl melt with sufficient accuracy. The purposes in this CHAPTER are as follows;

1) The application of NEMD simulation to the glass forming ionic liquid of ZrF_4-BaF_2-NaF fluoride melt.
2) To clarify the origin of the observed steep change in viscosity near liquidus temperature of ZrF_4-BaF_2-NaF melt.
3) To investigate the structural features of ZrF_4-BaF_2-NaF system in order to illustrate the glass forming process of fluoride glass melt.

This prospects the investigation method of the relaxation phenomena from the microscopic standpoint, which would provide useful and valuable means to clarify their complex mechanisms.

3-2. NEMD VISCOSITY CALCULATION

The objective materials of shear viscosity calculation were ZrF_4-BaF_2 system melt, ZBLAN ($53ZrF_4$-$20BaF_2$-$4LaF_3$-$3AlF_3$-20NaF in mol%). This is well known to show the highest glass forming ability among various fluoride glass systems. The parameters used in Eq. (2-4) are listed in Table 3-1. The space parameters of Zr^{4+}, Ba^{2+} and Na^+ were determined to equalize only the distances between cation and fluorine ion in the first neighbor with fluoride compound crystals by trial and error method. The minor compounds of LaF_3 and AlF_3 were intensionally excluded, because the calculation restriction about the number of treated particles made it difficult to obtain enough trajectories of La^{3+} and Al^{3+} ions. The potential curves used in this study were shown in Fig. 3-1 with ones used by Phifer et al. [4],

Boulard et al. [5], Lucas et al. [6] and Hamill et al. [7]. The calculation conditions are listed in Table 3-2. The particle number ratio of respective ions were determined along with the composition of ZBLAN and the total number of particles was changed to be 360, 720 and 1440. Temperature was changed around liquidus temperature of ZBLAN (915K) to be 700, 800, 900, 1100 and 1300K. The length of the unit cell were determined from the density of melts at the respective temperatures. The density of ZBLAN melt was measured, because there is no available data of this composition. (Details were mentioned below.)

For every series of calculations, the initial positions of particles were determined as following calculation flow ; (I) starting from the random positions and the velocity with Gaussian distribution and calculated for 10000 steps at 5000K. (II) rapidly quenched down to the respective temperature followed by annealing for 20000 steps. The basic value of time step was settled to be 2.0 fsec for this initial calculations. The total momentum of the system was corrected at every 1000 steps. The last snap-shot of particles was used as the starting initial position and velocity for NEMD viscosity calculations.

The shear rate applied to the unit cell was changed from $4.0\times10^{8}s^{-1}$ to $1.0\times10^{13}s^{-1}$. The lowest shear rate was defined according to the value of the induced stress; the excessively low shear rate applied, the induced shear stress would be too small compared with the thermal fluctuation of stress to obtain shear viscosity. Time step value was also taken care. The basic value was 2.0 fsec, but the shorter time step was employed depending on the controllability of temperature of system.

3-3. EXPERIMENTAL

A. Sample preparation

The cell sizes used in MD simulation should be determined from the measured values of the melt density because the mobility of particles in the melt is very sensitive to the fraction of free volume caused by the thermal expansion. The fluoride glass of 53mol%ZrF_4-20BaF_2-4LaF_3-3AlF_3-20NaF was prepared by the melt quenching method. 50g batch mixture from ZrF_4 of the sublimated grade, LaF_3 of 99.9% purity, BaF_2, AlF_3 and NaF of the reagent grade (Morita Chemicals) was melted in Pt crucible at 850°C for 1hr under dry N_2 gas flow. The melt was poured into the pre-heated Aluminum mold and annealed at glass transition temperature for 1hr and then cooled slowly down to the room temperature.

B. Density measurement

The density was measured by different method depending on the temperature region. The value at room temperature was measured by Archimedian method for the glass powder. For the region from *RT* to glass transition temperature T_g, the thermal expansion coefficient was used. The values at high temperature near liquidus temperature T_l were measured by Archimedian method using Pt ball. The glass cullet was remelted in Pt crucible in dry N_2 atmosphere and the weight changes of Pt ball in the melt was monitored against the temperature change. As shown in Fig. 3-2, the measurement in the temperature region from T_g to near T_l could not be performed because of the devitrification of the melt, but in this region, the linear relation against temperature was held and the values could be estimated by the least square fitting result.

$$\rho = 4.374 - 1.19 \times 10^{-3} (T_K - 537) \qquad [T > 537K] \qquad (3\text{-}1)$$

3-4. RESULTS AND DISCUSSION

A. Shear rate dependence of viscosity of Zr-Ba-Na-F melt

Figs. 3-3(a)-(c) showed the shear rate dependence of Zr-Ba-Na-F melts of 360, 720 and 1440 particle systems, respectively. The typical non-Newtonian behavior was observed in all systems at every temperature and similar to that of NaCl melt. The calculated viscosity showed higher values compared with NaCl melt at the same temperature and the shear rate region in which non-Newtonian behavior appeared was different depending on temperature and the number of particle. Temperature dependence was efficiently observed in the larger system and the shear rate at which the viscosity reached to some plateau shifted to lower value with the temperature decrease. The solids lines were drawn by the least square fitting to data by Eq. (2-12). In fluoride melt systems, the satisfying fittings could also be obtained for all calculations and Newtonian viscosity values could be estimated for respective temperature of each system. These values were listed in Table 3-2.

B. Temperature dependence of viscosity

Fig. 3-4 showed Arrhenius plots of the calculated Newtonian viscosity of Zr-Ba-Na-F melts along with the measured values. The Cohen-Grest equation curve for ZBLAN melt [8] was also drawn in the figure. Most of the simulated shear viscosity points coincided well with the measured ones and the viscosity temperature dependence was well simulated over 2

orders of magnitude from 10^{-1} to 10^{1} P. The arrow near 900K showed liquidus temperature of ZBLAN glass taken from the thermal analysis. The main feature of NEMD shear viscosity simulation compared with ones of EMD method using Green-Kubo relation [9] or Stokes-Einstein relation is to observe directly the response of the system (melt structures) against the applied strain, while the latter two methods observe the time-correlation of pressure of system or displacement of particles, which is thought to be sensitive to the prehistory of system and, in case of Green-Kubo relation, it needs huge calculation time. In this study, we have not compared NEMD simulation with the other two method, but the simulated phenomena is considered to resemble more with the realistic shear relaxation of liquid. In viscous flow phenomena, shear viscosity η is well known to have a simple relation with the stress relaxation as Eq. (3-2)

$$\eta = G_{\infty} \langle \tau \rangle \qquad (3\text{–}2)$$

where G_{∞} is the shear modulus and $\langle \tau \rangle$ is the average relaxation time. In the glass forming liquids, the increase of viscosity means not only the increase of relaxation time $\langle \tau \rangle$, but also the broadening of the relaxation distribution function. In order to succeed in simulating the accurate viscosity of glass forming liquids at different temperature, it is important how closely the dynamics of motion in MD cell reflect the real phenomena. As seen in Fig. 3-4, the viscosity-temperature relation of ZrF_4-BaF_2 glass melt shows steep increase below liquidus temperature, which is one of the most characteristic features of this glass melt and suggesting the changes in the viscous flow mechanism. Above 900K, the viscosity is quite low and the calculated shear viscosity of both 360 and 720 system revealed the same values, coinciding

well with measured ones. On the other hand, below 900K, the smaller system showed lower viscosity value, and 360 and 720 particles systems failed to show this steep viscosity change. On the other hand, 1440 system could produce successfully similar viscosity changes with temperature as the measured ones. These particle dependence below liquidus temperature was considered to have certain correlation with the difference in the viscous flow mechanism simulated. In order to clarify these differences, the structural analysis of melts was needed and discussed at the next section in detail.

C. Structural change in Zr-Ba-Na-F melt with temperature

Short range structure

The static melt structures were investigated from the trajectories of equilibrating calculation before shear applied. Fig. 3-5 showed the pair distribution functions (PDF) of main ion pairs. The strong temperature dependence was found in Zr-Zr, Zr-Ba and Zr-Na pairs. As shown in the previous study about glass structure [10], the manner of linkage between ZrF_n polyhedra is one of the most important features in fluorozirconate glasses. The main peak near 4.2Å and the shoulder near 3.9Å could be assigned to the corner bridging Zr-F-Zr and the edge sharing Zr-F_2-Zr, respectively. These bridging forms are found in various crystalline of $M_xZr_yF_z$ type compounds. The PDF results of Zr-Zr revealed that Zr ions connected each other mainly in the corner sharing form at high temperature and the bridging in edge sharing manner increased with the decrease of temperature, especially below 900K (liquidus temperature of ZBLAN glass was 915K). Fig. 3-6 plotted the frequency of Zr ions with n coordinating fluorine ions and F ions connecting with n Zr ions. As seen in the

changes in the distribution and the mean coordination number of ZrF_n, Zr ions shifted to form the higher coordinated ZrF_n polyhedra with the temperature decrease. The data of frequency about F ion also revealed that F ions in bridging form increased with the decrease of temperature. Fig. 3-7 showed the more detailed analysis results about fluorine ions. The temperature decrease caused more bridging between Zr ions and the ratio of edge sharing form increased. These structural changes found in the simulated results could be explained by the features of the polymerization models between ZrF_n polyhedra schematically illustrated in Fig. 3-8. As Phifer et al. [11] pointed out, the formation of bridging between ZrF_n polyhedra forces the change in F coordination number of Zr ions. For instance, as seen in Fig. 3-8(b), the change from the corner sharing into the edge sharing increase F coordination number of one side of Zr-Zr pair. These changes in the bridging form were actually observed by Raman measurement of ZrF_4-BaF_2-PbF_2 glass melts by Walrafen et al. [12] Raman peaks assigned to the edge sharing were lost in the spectrum at high temperature. The simulated melt structural changes with temperature coincided well with this reported result. The formation of edge sharing at low temperature, especially under liquidus temperature, was considered to be much correlated with the steep viscosity increase. The similar edge sharing were also formed between Zr and Ba ions and supported the viscosity increase, but as shown in PDF between Zr-Ba, their correlation was gradually enforced with the decrease of temperature and played 'assistant' roles in viscosity compared with Zr-F_2-Zr bridging, because of lower single bond strength [13] of Ba-F (46kcal/mol) compared with Zr-F (85kcal/mol).

Intermediate-range structures

The structural informations obtained from the equilibrium condition showed that the linkage between ZrF_n polyhedra shifted to form more edge sharing with the temperature decrease under 900K. However, any remarkable difference was not observed in PDF results of local structures around Zr ions among the systems with different particle number, even between 360 and 1440 systems, meaning that this could not explain the differences found in viscosity simulation results. In order to clarify this inconsistency, the linkage structures in the cell were investigated. Figs. 3-9 and 3-10 showed the snap shots of simulated equilibrium structures of 720 and 1440 systems before shear applied, respectively. For simplicity, only particles which joined the structural linkages of ZrF_n were drawn; modifying ions of Ba^{2+} and Na^+, non-bridging F^-, and isolating ZrF_n polyhedron were neglected. The lines mean the bridging between Zr-F in Figs. 3-9(a)-(e) and Figs. 3-10(a)-(c). In case of Figs. 3-9(f)-(j) and Figs. 3-10(d)-(f), only edge sharing were connected by line. These structures depicted well the progress of linkages between ZrF_n polyhedra with temperature decrease. It was found that the number of linkage was low and edge sharing was rare at high temperature, but at lower temperature, some larger structural units composed from a few edge shared ZrF_n appeared. This means that the edge sharing unit would not be so important in the viscous flow at high temperature, but played as a key structure at low temperature to control longer relaxation time process. These structural features were also observed in 1440 system, but the more units were formed at lower temperature in proportion to the cell volume. This revealed that the formation of edge sharing enforced the cooperative motion between ZrF_n polyhedra and the relaxation processes among these larger units played as a origin of higher viscosity in larger system.

This scheme about viscosity increase also explain the reason of glass formation of ZrF_4-based fluoride melts and coincided well with the model proposed by Phifer et al.[11].

As pointed out in Sec. C, the key in the viscosity simulation of glass forming melts was the broadness of the relaxation process simulated. From such a point of view, the simulation of higher viscosity region needs larger cell size and longer calculation time comparable to the relaxation time. In such a meaning, more than 1000 particles would be needed at least to simulate viscosity of the order of 10^1 Poise of Zr-Ba-Na-F system. This fact might reveal some limitation of computer simulation for much higher viscosity region, but this new viscosity simulation will provide certain new dynamical aspects on the relaxation phenomena of liquid, and in the technological field, it will be possible to provide a predictive tool of viscosity in the critical devitrifying temperature range.

3-5. CONCLUSIONS

In this chapter, the melt structure of ZrF_4-BaF_2-based fluoride glass of Zr-Ba-Na-F was investigated by utilizing Non-equilibrium and Equilibrium Molecular Dynamics simulation methods. The NEMD calculations well simulated the viscosity-temperature relation near liquidus temperature and the rapid viscosity change up to in the order of 10^1 poise was reproduced by employing the appropriate large cell size. It was clearly proved that the NEMD simulation method of viscosity developed in this study has high potential to be used for the inorganic glass forming systems and expected to propose a new method for the prediction of viscosity values. This method also offers the new investigation way to understand the viscous phenomena from the view point of microscopic structures.

The detailed structural analysis about Zr-Ba-Na-F melt, the keys to control the viscosity changes under liquidus temperature was found to be the linkage forms among ZrF_n polyhedra. Above liquidus temperature, quite low viscosity was caused from the lower degree of the bridging between polyhedra. Most of bridging was found to be in the corner sharing form and the coordination number of F about Zr was low. Beyond the liquidus temperature, the coordination number of ZrF_n increases and the edge sharing began to be formed. This formation of the edge sharing between polyhedra coincided well with the steep viscosity change and suggesting that they enforce the cooperativity among the structural units, which is so called as 'viscous flow unit'. Such a larger structural flames can not be depicted by the general structural function like pair distribution function (PDF), because there were not found any remarkable differences in PDFs between the systems with different cell size, while the calculated shear viscosity was different. Compared with NaCl melt in CHAPTER 2, the cell size effect have to be taken much care in the case of the glass forming liquids and by employing the appropriate cell size, this NEMD is considered to be able to depict the viscous flow phenomena similar to the real one.

The features of the glass formation of fluoride glass melt of ZrF_4-BaF_2-based system can be summarized as follows;

1) Above liquidus temperature, ZrF_n polyhedra link each other only in the corner sharing manner and the viscosity becomes quite low because such linkages weaken the cooperative motion between structural units.

2) Zr ions change their own coordination number of F with the temperature decrease and begin to form the edge sharing linkage between them at the appropriate temperature.

3) These edge sharing forms are thermally sensitive and cause the steep viscosity change between glass transition temperature and liquidus temperature.

4) Higher glass forming ability of ZrF_4 -based systems should be originated from the high flexibility of the ZrF_n polyhedra in terms of the coordination number and the bridging form.

REFERENCES

[1] W. H. Zachariazen, J. Am. Chem. Soc., **54** (1932) 3841

[2] C. T. Moynihan, R. Mossadegh, P. K. Gupta and M. G. Drexhage, Mater. Sci. Forum, **6** (1985) 655

[3] C. A. Angell, in *Relaxation in Complex Systems*, ed. K. Ngai and G. B. Wright, National Technical Information Service, U. S. Department of Commerce, Springerfield, VA, (1985), p.1

[4] C. C. Phifer, C. A. Angell, J. P. Laval and J. Lucas, J. Non-Cryst. Solids, **94** (1987) 315

[5] B. Boulard, J. Kieffer, C. C. Phifer and C. A. Angell, J. Non-Cryst. Solids, **140** (1992) 350

[6] J. Lucas, C. A. Angell and S. Tamaddon, Mat. Res. Bull., **19** (1984) 945

[7] L. T. Hamill and J. M. Parker, Mater. Sci. Forum, **6** (1985) 437

[8] W. C. Hasz, S. N. Crichton and C. T. Moynihan, Mater. Sci. Forum **32-33** (1988) 589

[9] B. J. Alder and T. E. Wainwright, J. Chem. Phys. **27** (1957) 1208

[10] J. Lucas, D. Louer and C. A. Angell, Mater. Sci. Forum **6** (1985) 449

[11] C. C. Phifer and J. Lucas, Mater. Sci. Forum, **19&20** (1987) 111

[12] G. E. Walrafen, M. S. Hokmabadi, S. Guha, P. N. Krishnan and D. C. Tran, J. Chem. Phys. **83** (1985) 4427

[13] C. M. Baldwin and J. D. Mackenzie, J. Am. Ceram. Soc. **62** (1979) 537

Table 3-1. Potential parameter list. Ion cahrge, Z_i, Pre-exponential parameter, A_{ij} (10^{-16}J), of each ion pair. $4\pi/\varepsilon_0$=2.307×10^{-28}(Jm), ρ=0.3(Å)

	Zr	Ba	Na	F
Z_i	+4	+2	+1	-1

A_{ij}	Zr	Ba	Na	F
Zr	20.07	41.23	9.61	3.48
Ba	---	84.12	19.62	6.96
Na	---	---	4.58	1.63
F	---	---	---	0.546

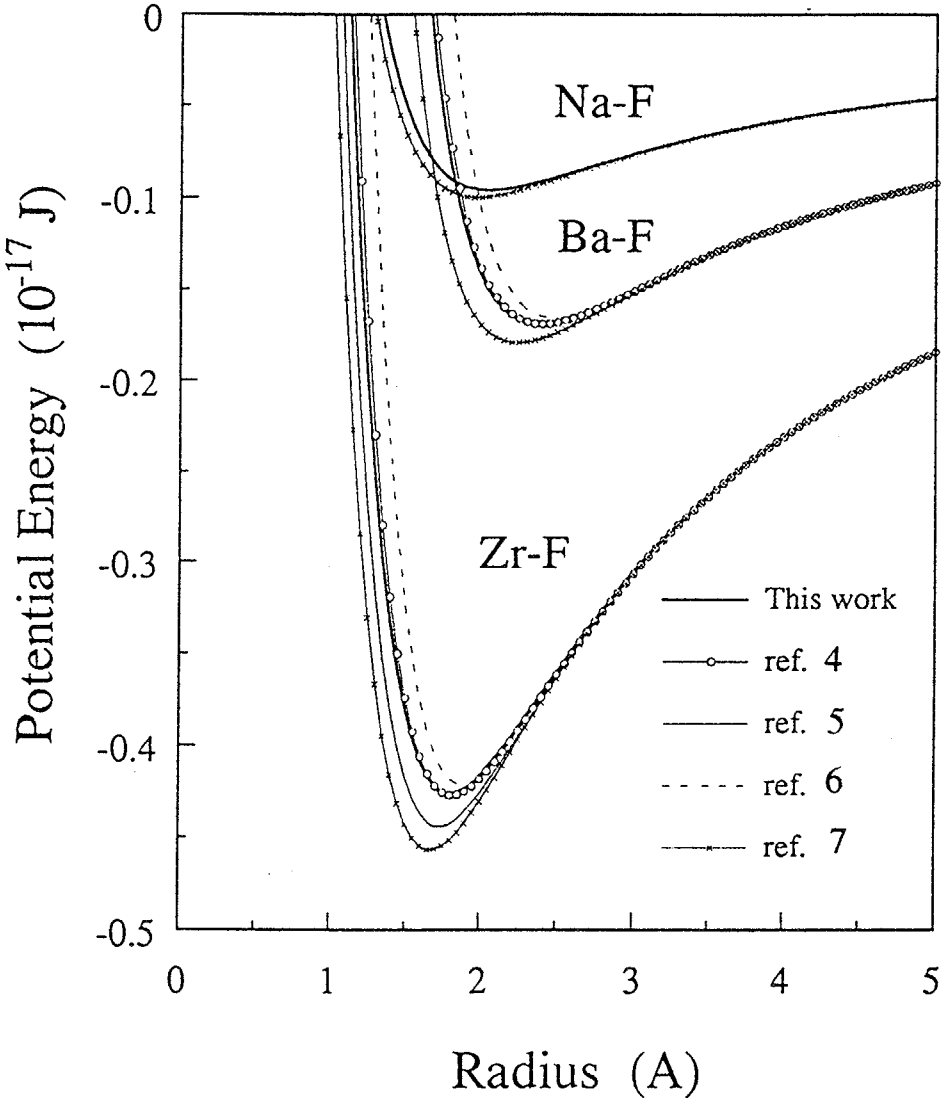

Fig. 3-1 The potential curves of the respective pair of ions used in this study. The ones used in ref. [4,5,6,7] are shown as the references.

Table 3-2. Lists pf the calculation conditions under shear applied, the apparent viscosity values, and Newtonian (zero-shear) viscosity obtained from least square fitting to Eq. 2-12.

SYSTEM	Temperature (K)	Cell size L (nm)	Time step (fs)	No. of step	Shear rate γ (s^{-1})	Viscosity η (P)	Newtonian viscosity η_0 (P)
52Zr-20Ba-20Na-268F	700	1.73032	2.0	20 000	1.0×10^{11}	0.145	0.234
	700	1.73032	2.0	10 000	4.0×10^{11}	0.0578	
	700	1.73032	2.0	10 000	1.0×10^{12}	0.0289	
	700	1.73032	2.0	10 000	4.0×10^{12}	0.00725	
	700	1.73032	2.0	10 000	1.0×10^{13}	0.00038	
52Zr-20Ba-20Na-268F	900	1.76434	2.0	50 000	4.0×10^{10}	0.207	0.320
	900	1.76434	2.0	20 000	1.0×10^{11}	0.125	
	900	1.76434	2.0	10 000	4.0×10^{11}	0.050	
	900	1.76434	2.0	10 000	1.0×10^{12}	0.0256	
	900	1.76434	2.0	10 000	4.0×10^{12}	0.00573	
	900	1.76434	2.0	10 000	1.0×10^{13}	0.00136	
52Zr-20Ba-20Na-268F	1100	1.80121	2.0	50 000	4.0×10^{10}	0.119	0.162
	1100	1.80121	2.0	20 000	1.0×10^{10}	0.0818	
	1100	1.80121	2.0	10 000	4.0×10^{11}	0.0365	
	1100	1.80121	2.0	10 000	1.0×10^{12}	0.0208	
	1100	1.80121	2.0	10 000	4.0×10^{12}	0.0044	
	1100	1.80121	2.0	10 000	1.0×10^{13}	0.00097	
52Zr-20Ba-20Na-268F	1300	1.84136	2.0	50 000	1.0×10^{10}	0.156	0.120
	1300	1.84136	2.0	20 000	1.0×10^{11}	0.0627	
	1300	1.84136	2.0	10 000	4.0×10^{11}	0.029	
	1300	1.84136	1.0	10 000	1.0×10^{12}	0.017	
104Zr-40Ba-20Na-536F	700	2.18000	2.0	50 000	4.0×10^{9}	1.04	1.12
	700	2.18000	2.0	50 000	1.0×10^{10}	0.721	
	700	2.18000	2.0	50 000	4.0×10^{10}	0.343	
	700	2.18000	2.0	50 000	1.0×10^{11}	0.175	
	700	2.18000	2.0	20 000	4.0×10^{11}	0.0665	
104Zr-40Ba-40Na-536F	800	2.20107	2.0	50 000	4.0×10^{9}	0.783	0.834
	800	2.20107	2.0	50 000	4.0×10^{10}	0.275	
	800	2.20107	2.0	50 000	4.0×10^{11}	0.0603	
104Zr-40Ba-40Na-536F	900	2.22293	2.0	50 000	1.0×10^{10}	0.600	0.489
	900	2.22293	2.0	50 000	4.0×10^{10}	0.307	
	900	2.22293	2.0	50 000	1.0×10^{11}	0.162	
	900	2.22293	2.0	20 000	4.0×10^{11}	0.0614	
104Zr-40Ba-	1100	2.26937	2.0	50 000	1.0×10^{10}	0.309	0.289
	1100	2.26937	2.0	50 000	4.0×10^{10}	0.178	
	1100	2.26937	2.0	20 000	1.0×10^{11}	0.127	
	1100	2.26937	2.0	20 000	4.0×10^{11}	0.046	
104Zr-40Ba-40Na-536F	1300	2.31997	2.0	50 000	1.0×10^{10}	0.203	0.222
	1300	2.31997	2.0	50 000	4.0×10^{10}	0.145	
	1300	2.31997	2.0	20 000	1.0×10^{11}	0.0793	
	1300	2.31997	2.0	20 000	4.0×10^{11}	0.0365	
208Zr-80Ba-80Na-1072F	700	2.74671	2.0	50 000	4.0×10^{8}	10.6	26.2
	700	2.74671	2.0	50 000	1.0×10^{9}	8.29	
	700	2.74671	2.0	50 000	4.0×10^{9}	3.52	
	700	2.74671	2.0	50 000	1.0×10^{10}	1.24	
208Zr-80Ba-80Na-1072F	800	2.77319	2.0	50 000	4.0×10^{8}	9.40	10.8
	800	2.77319	2.0	50 000	4.0×10^{9}	2.83	
	800	2.77319	2.0	50 000	4.0×10^{10}	0.258	
	800	2.77319	2.0	50 000	4.0×10^{11}	0.036	
208Zr-80Ba-80Na-1072F	900	2.80072	2.0	50 000	4.0×10^{9}	1.19	1.45
	900	2.80072	2.0	50 000	4.0×10^{10}	0.277	
	900	2.80072	2.0	50 000	4.0×10^{11}	0.0592	

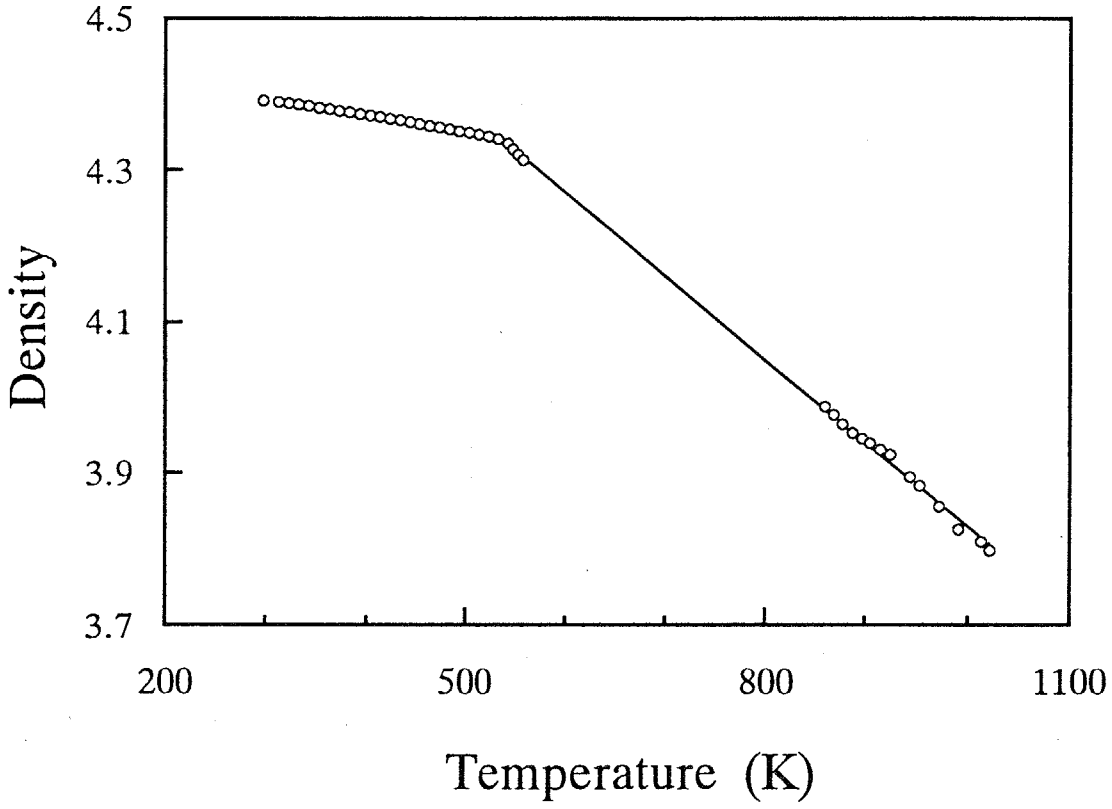

Fig. 3-2 The result of the density measurement of ZBLAN glass melt. The solid line was obtained by the least square fitting which pass through the data point at the glass transition temperature.

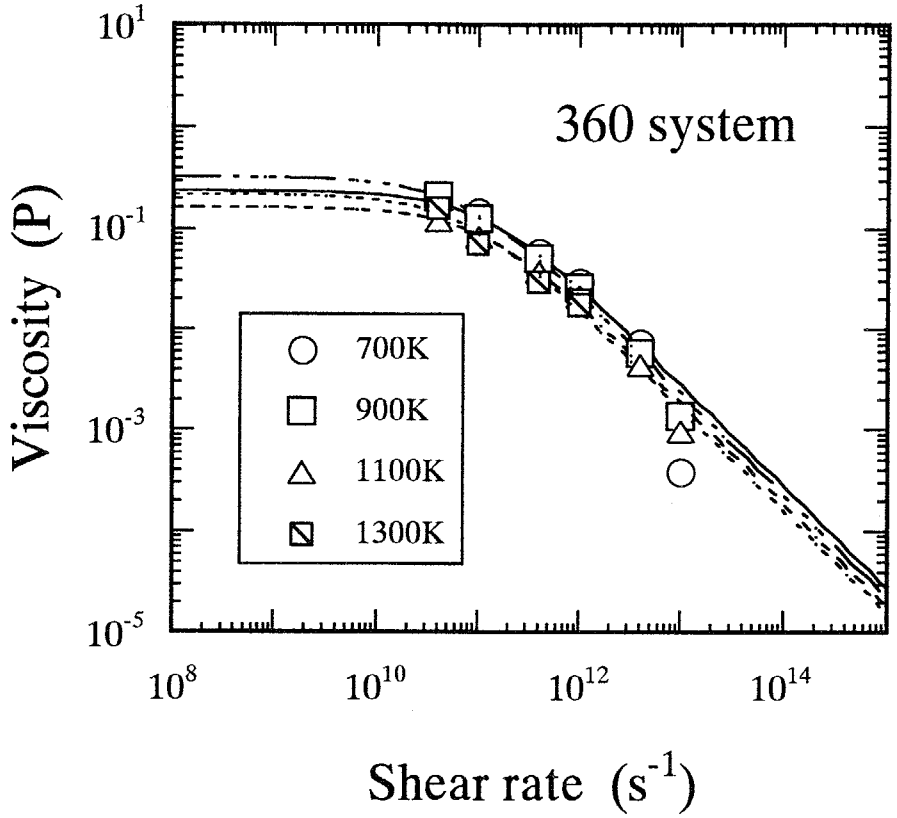

Fig. 3-3(a) The shear rate dependence of viscosity of 360 particles system at the various temperature. Thecurves were the least square fitting results into the Eq. (2-12)

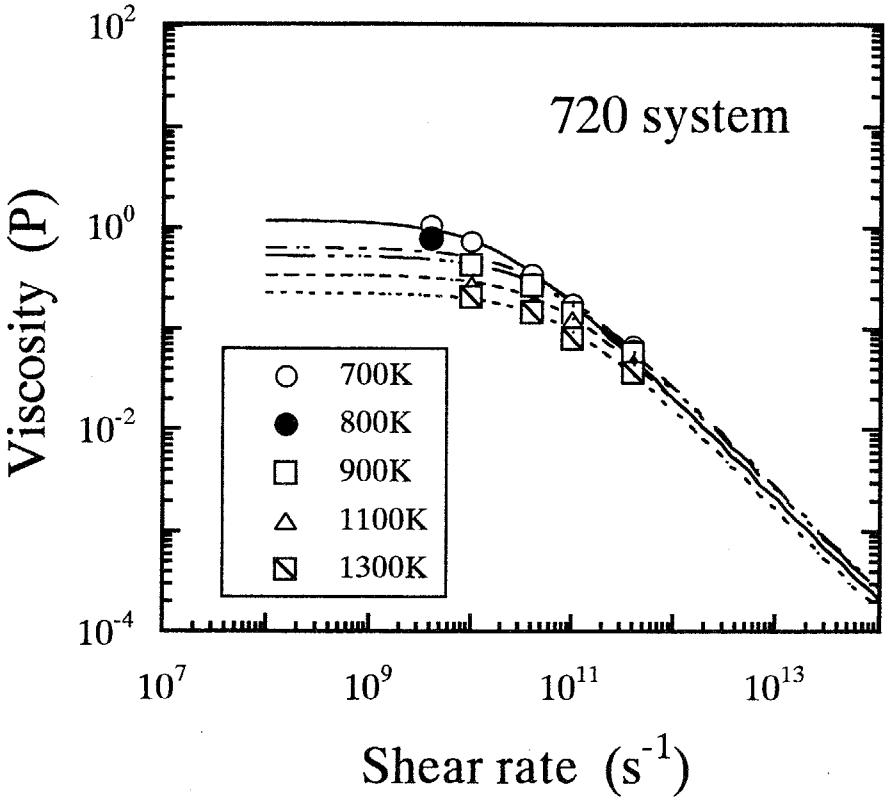

Fig. 3-3(b) The shear rate dependence of viscosity of 720 particles system at the various temperature. Thecurves were the least square fitting results into the Eq. (2-12)

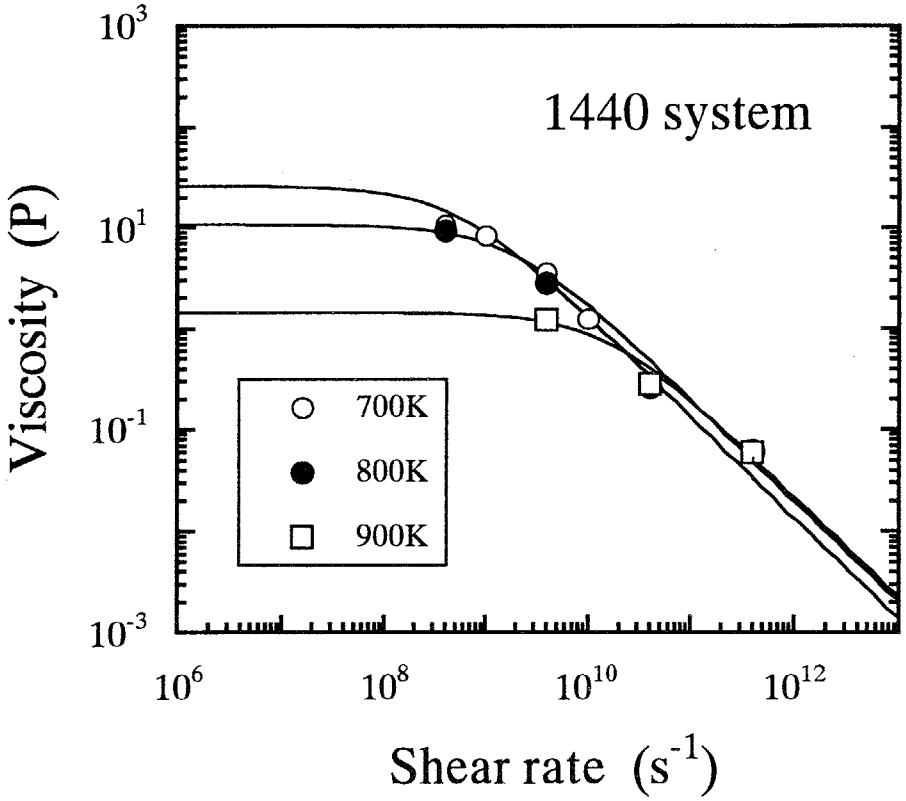

Fig. 3-3(c) The shear rate dependence of viscosity of 1440 particles system at the various temperature. Thecurves were the least square fitting results into the Eq. (2-12)

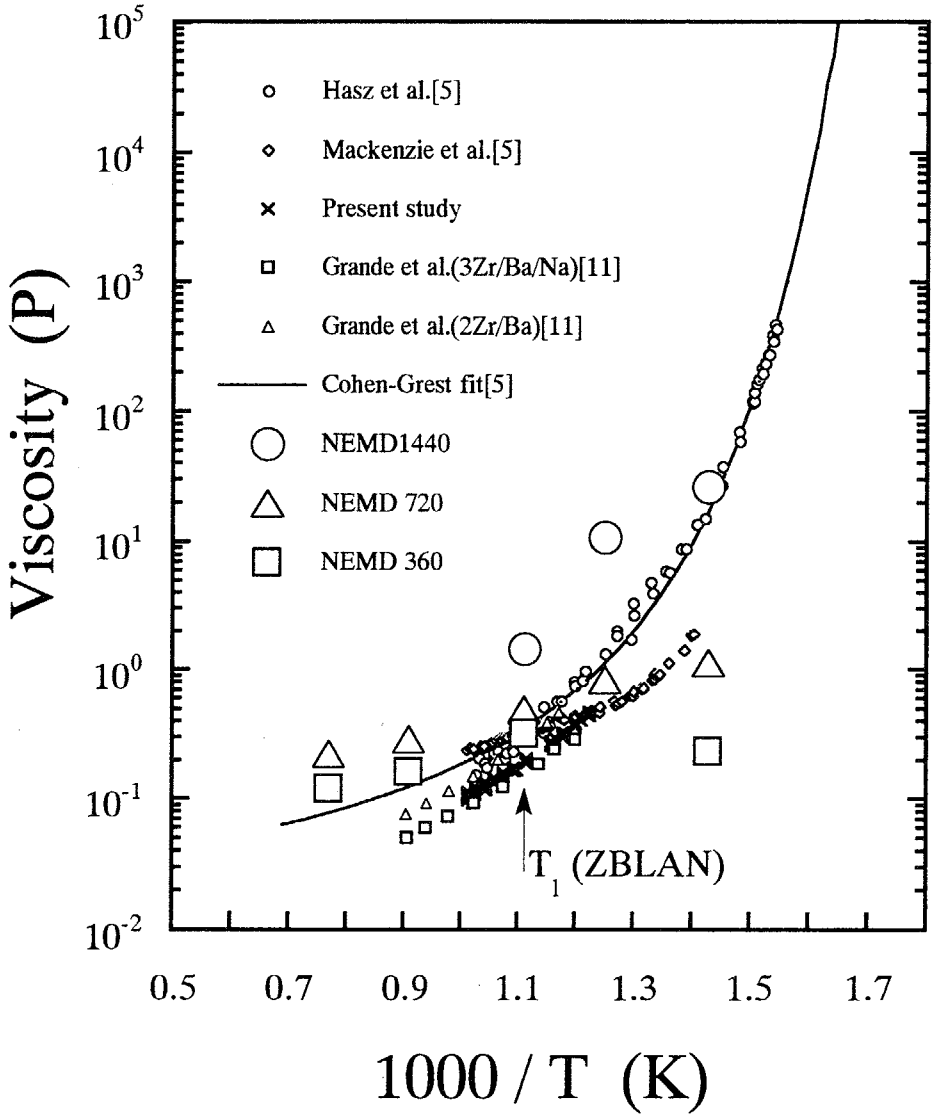

Fig. 3-4 Arrhenius plots of the calculated shear viscosity by NEMD method with the experimental values. The allow in the figure reveals the liquidus temperature of ZBLAN(53/20/4/3/20).

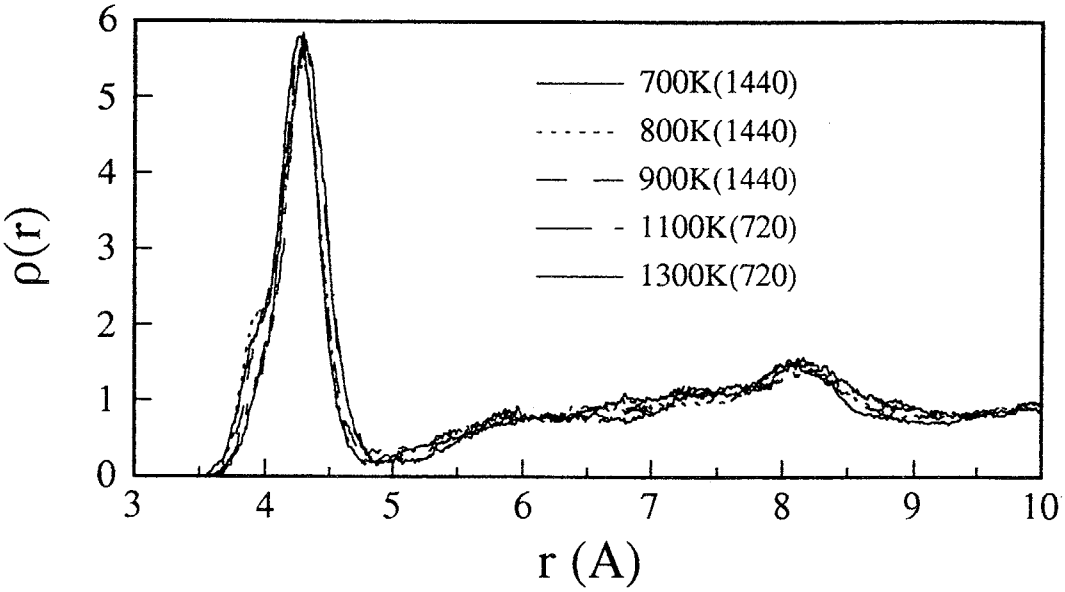

(a) Zr-Zr PairFunction

Fig. 3-5 The pair distribution functions obtained from the trajectories of particles by equilibrium conditions at the respective temperature. (a) Zr-Zr, (b) Zr-Ba, (c)Zr-Na, (d) Zr-F, (d)Ba-F, (e) Na-F, (f)F-F. (g) and (i) are the expanded representations of Zr-Zr and F-F pair, respectively.

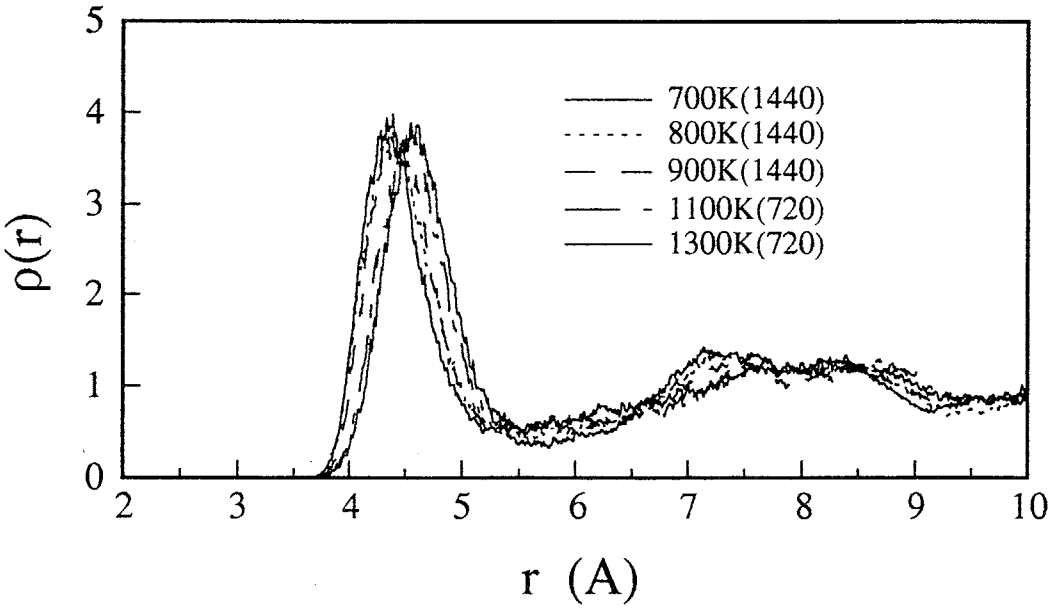

(b) Zr-Ba PairFunction

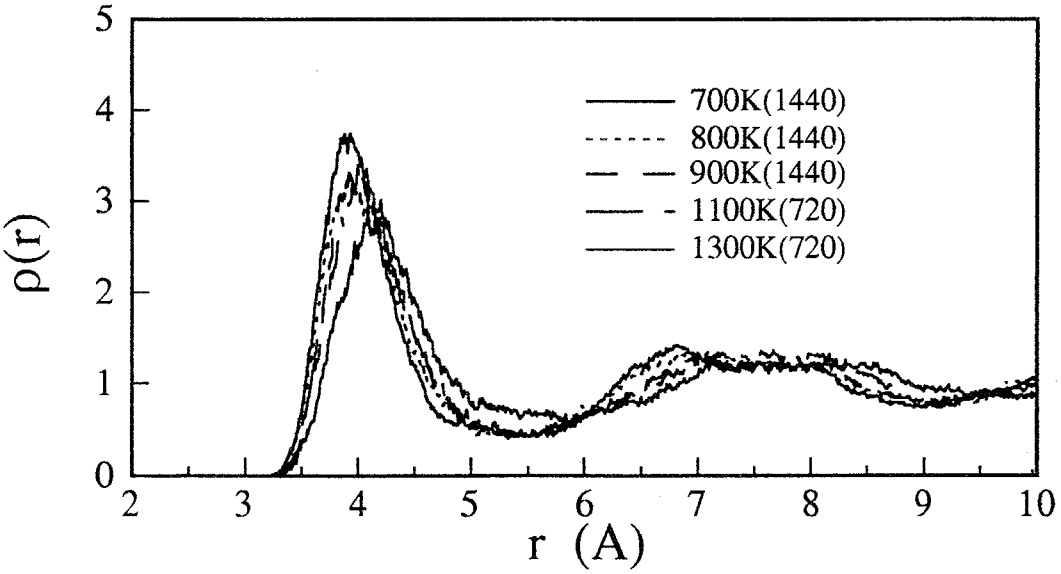

(c) Zr-Na PairFunction

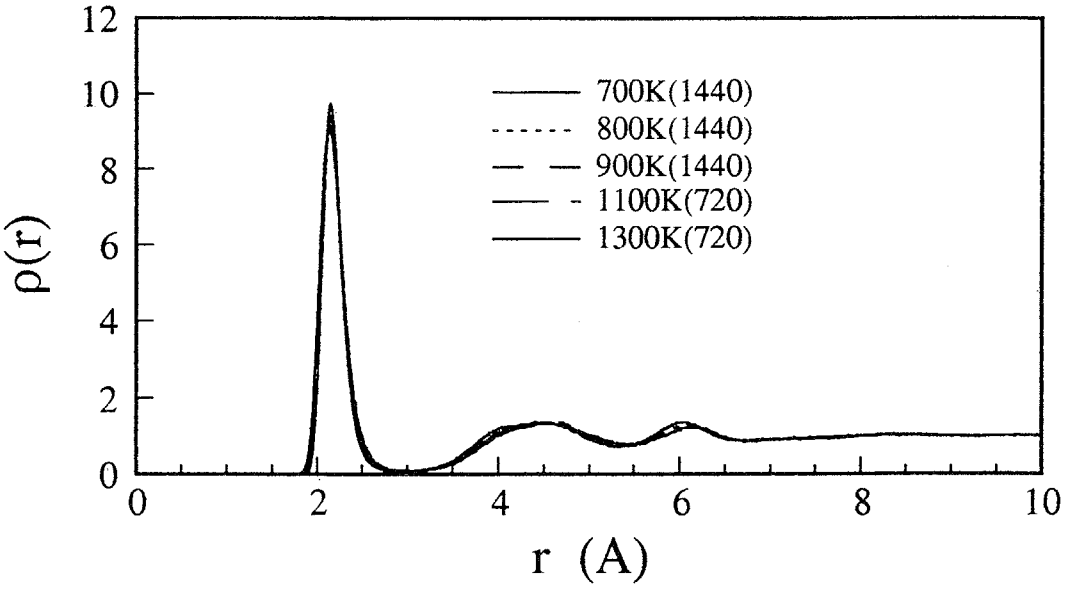

(d) Zr-F PairFunction

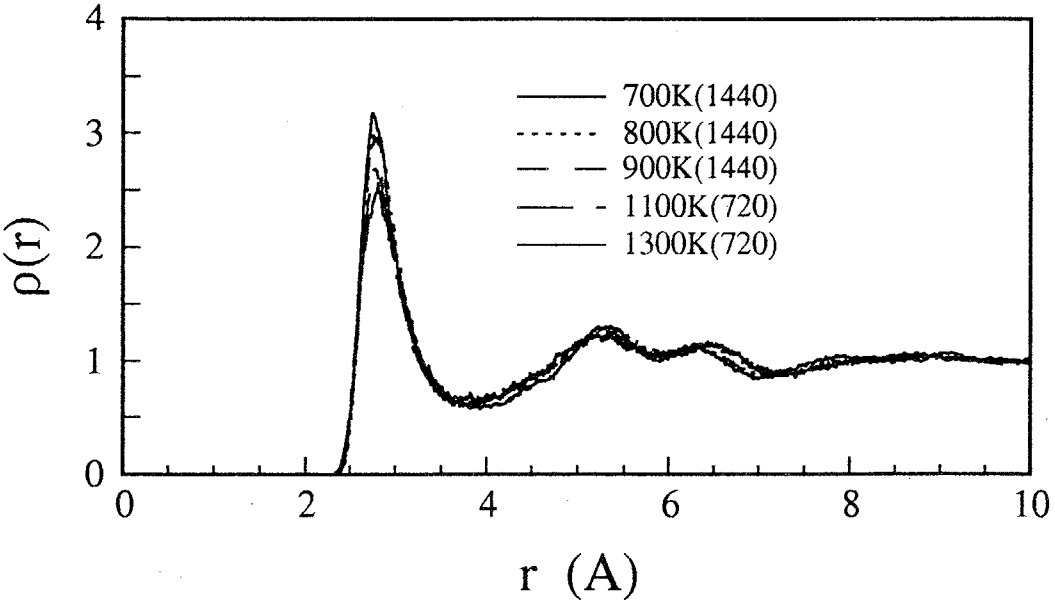

(e) Ba-F PairFunction

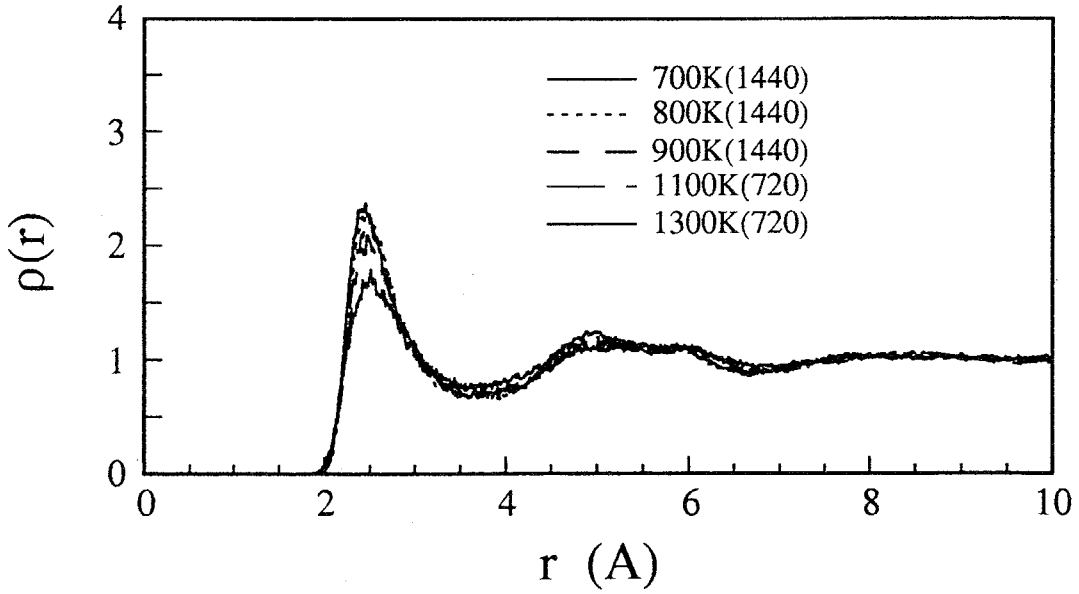

(f) Na-F PairFunction

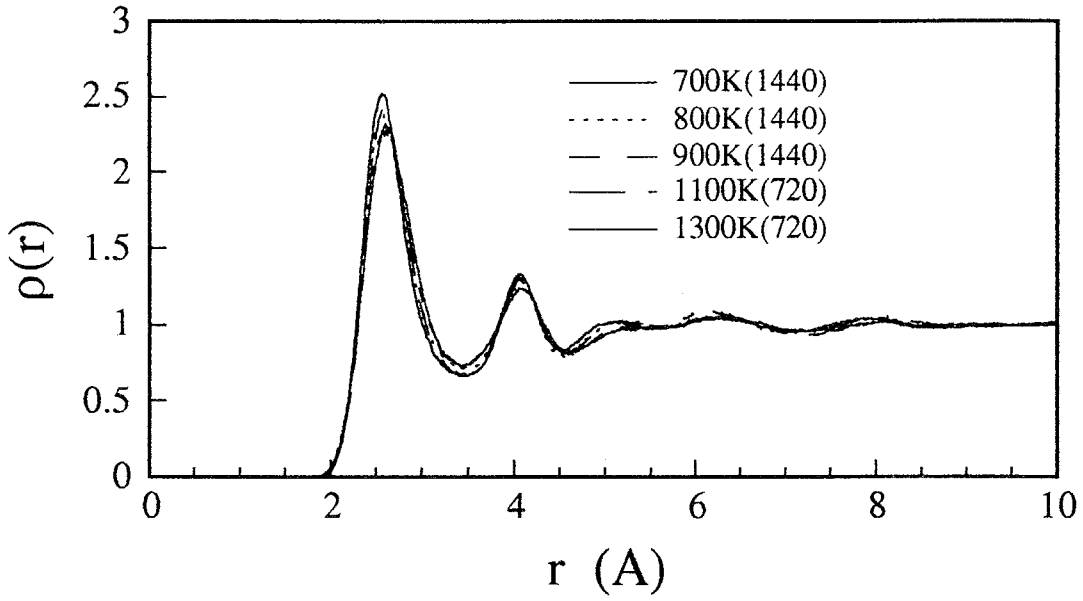

(g) F-F PairFunction

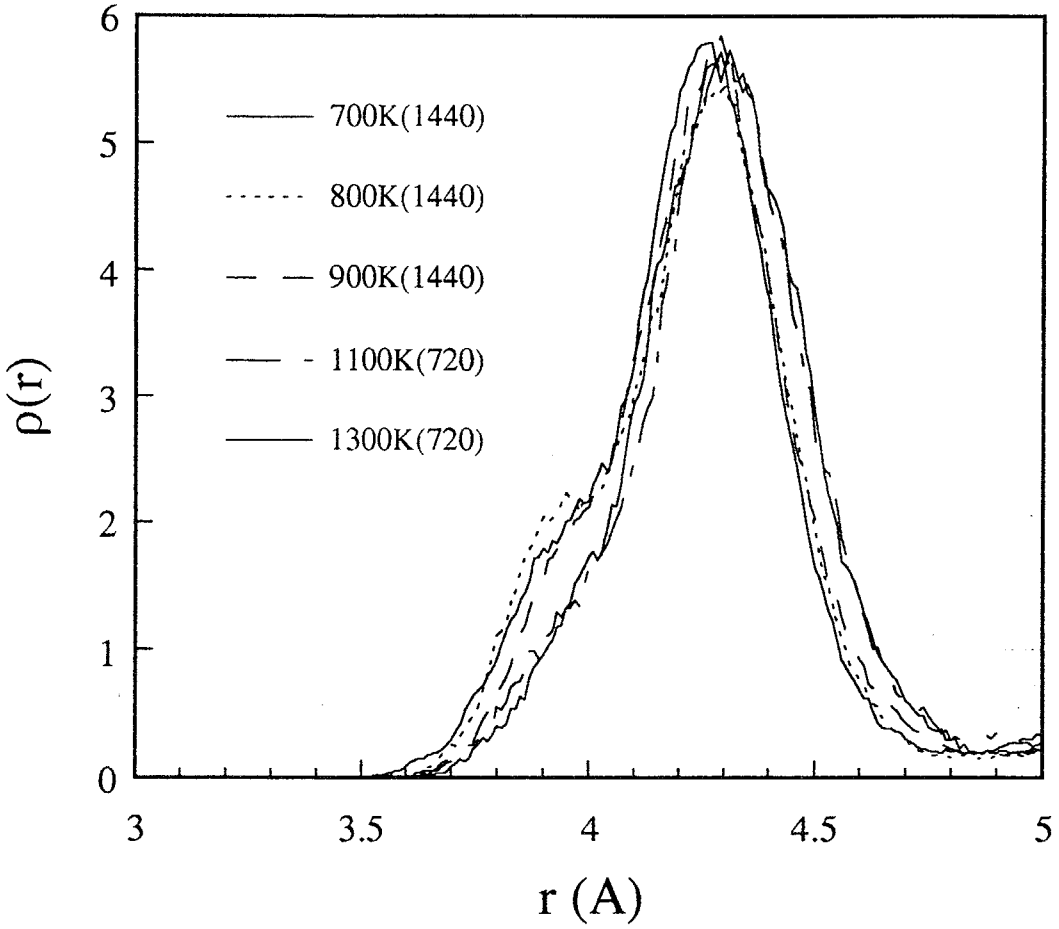

(h) Zr-Zr PairFunction

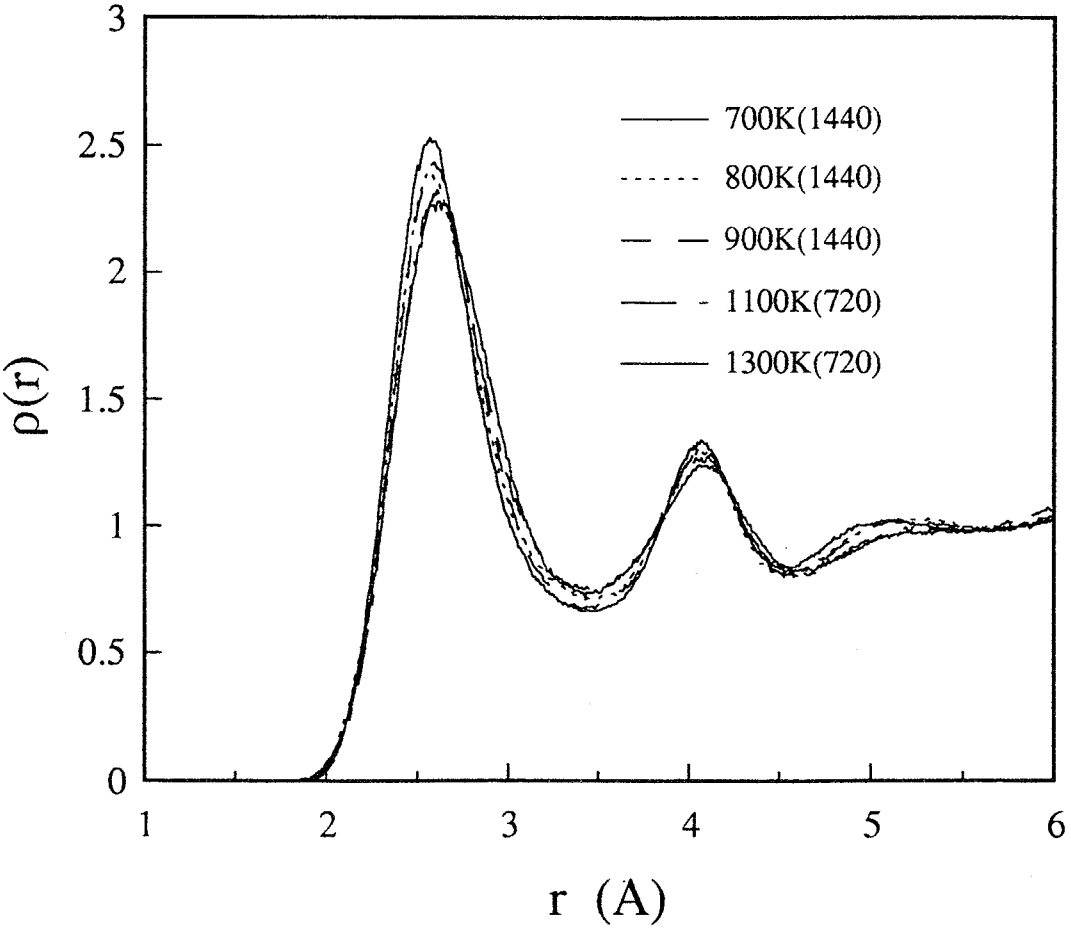

(i) F-F PairFunction

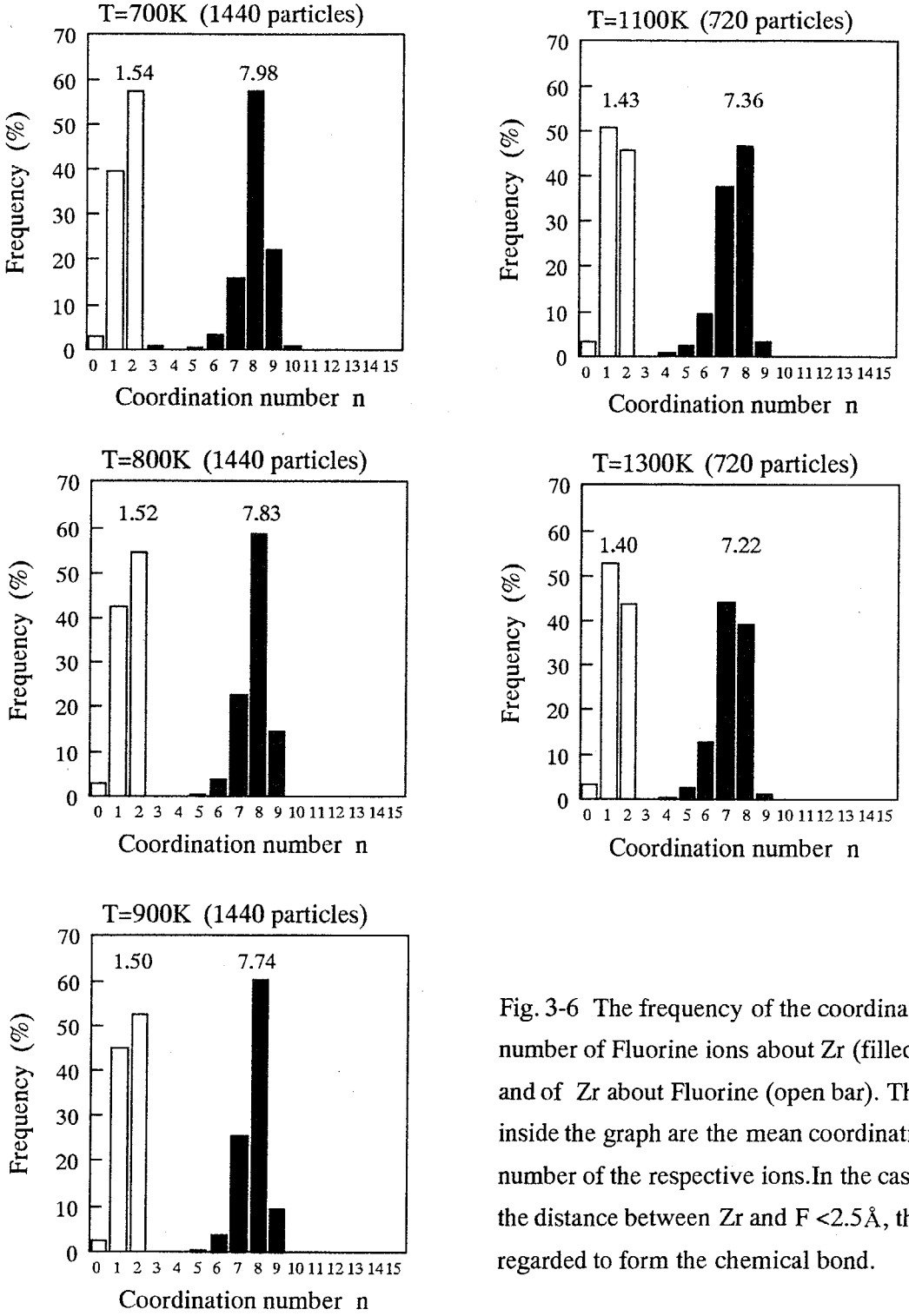

Fig. 3-6 The frequency of the coordination number of Fluorine ions about Zr (filled bar) and of Zr about Fluorine (open bar). Thevalues inside the graph are the mean coordination number of the respective ions.In the case of the distance between Zr and F <2.5Å, they are regarded to form the chemical bond.

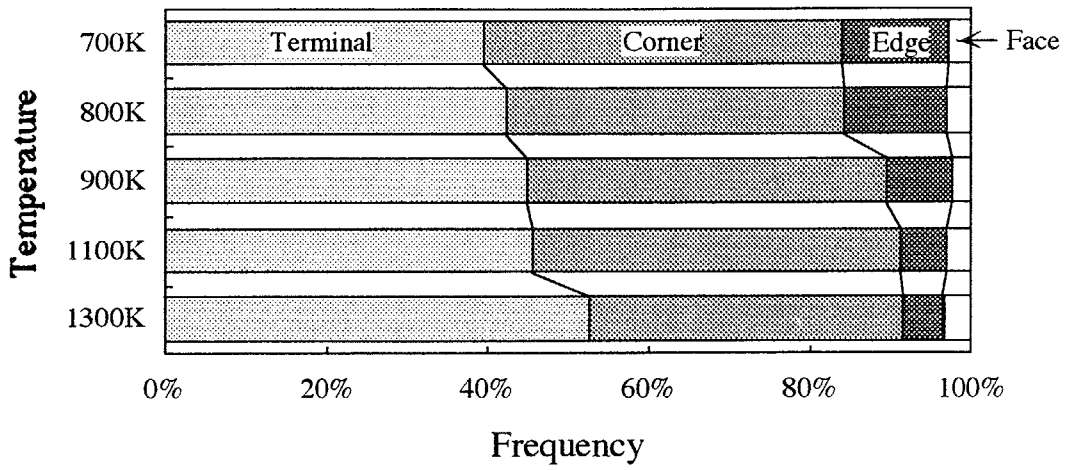

Fig. 3-7 The freqency of the bridging forms found in the simulated structures at the respective teperature. At 700, 800 and 900K, the trajectories of 1440 oarticles system were employed for the analysis. At 1100 and 1300K, the data of 720 system were used.

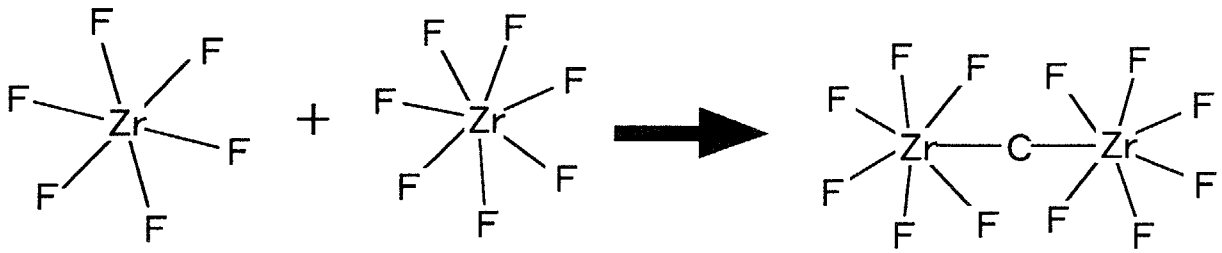

(a)

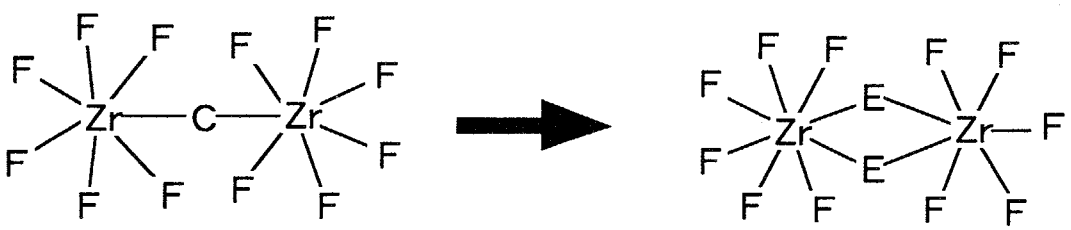

(b)

Fig. 3-8 The schematical illustration of the linkage processbetween ZrFn polthedra. (a) the formation of corner sharing, (b) the formation edge sharing from corner sharing

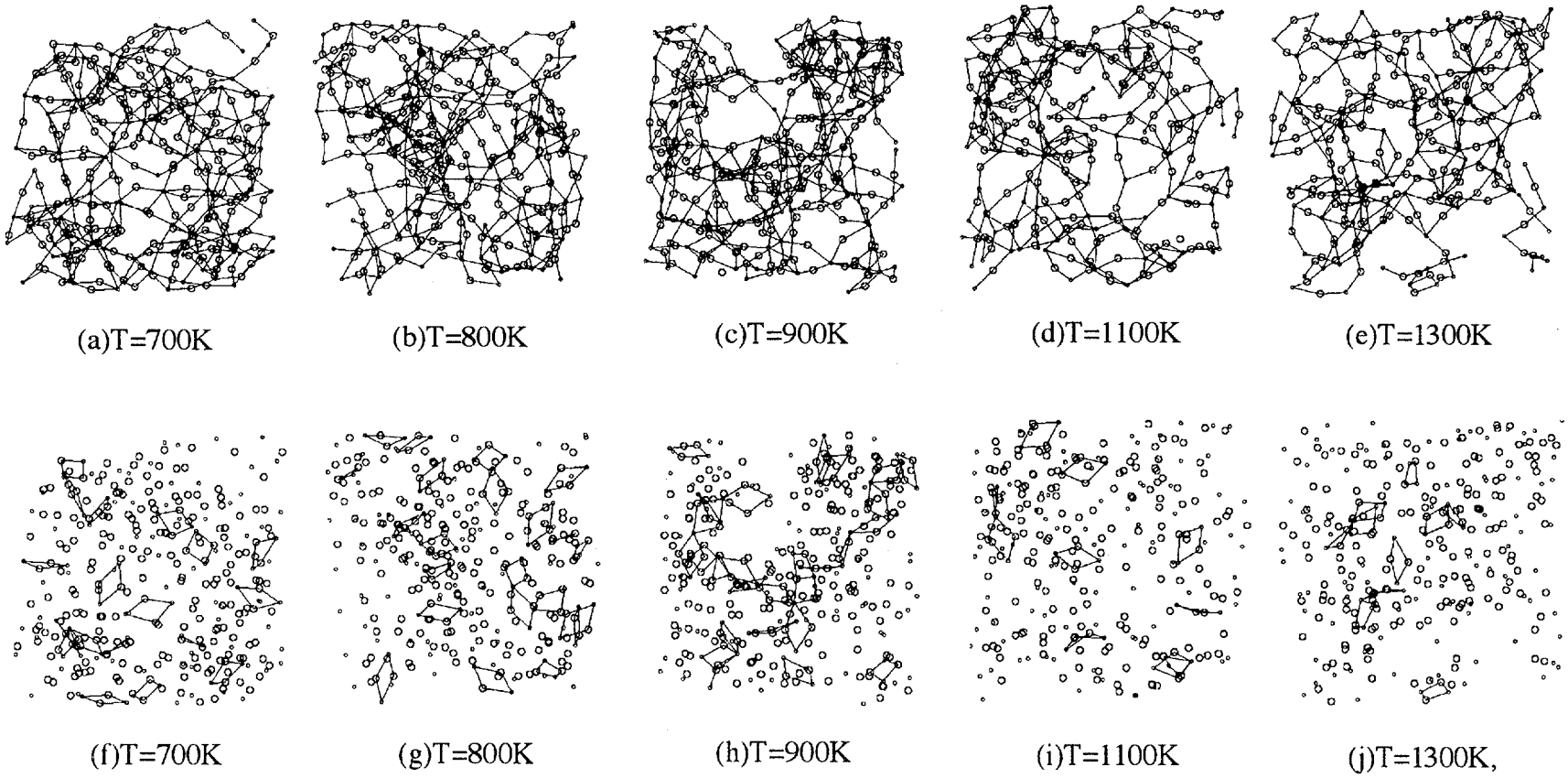

Fig. 3-9 The snap shots of the melt structures of 720 particle system at the respective temperature. (a)-(e) show only the Zr-F-Zr bridging and the other ions like modifiers of Ba and Na, the isorated Zr and the terminal F ions. (f)-(j) show only the Zr-F2-Zr edge sharing in the melts.

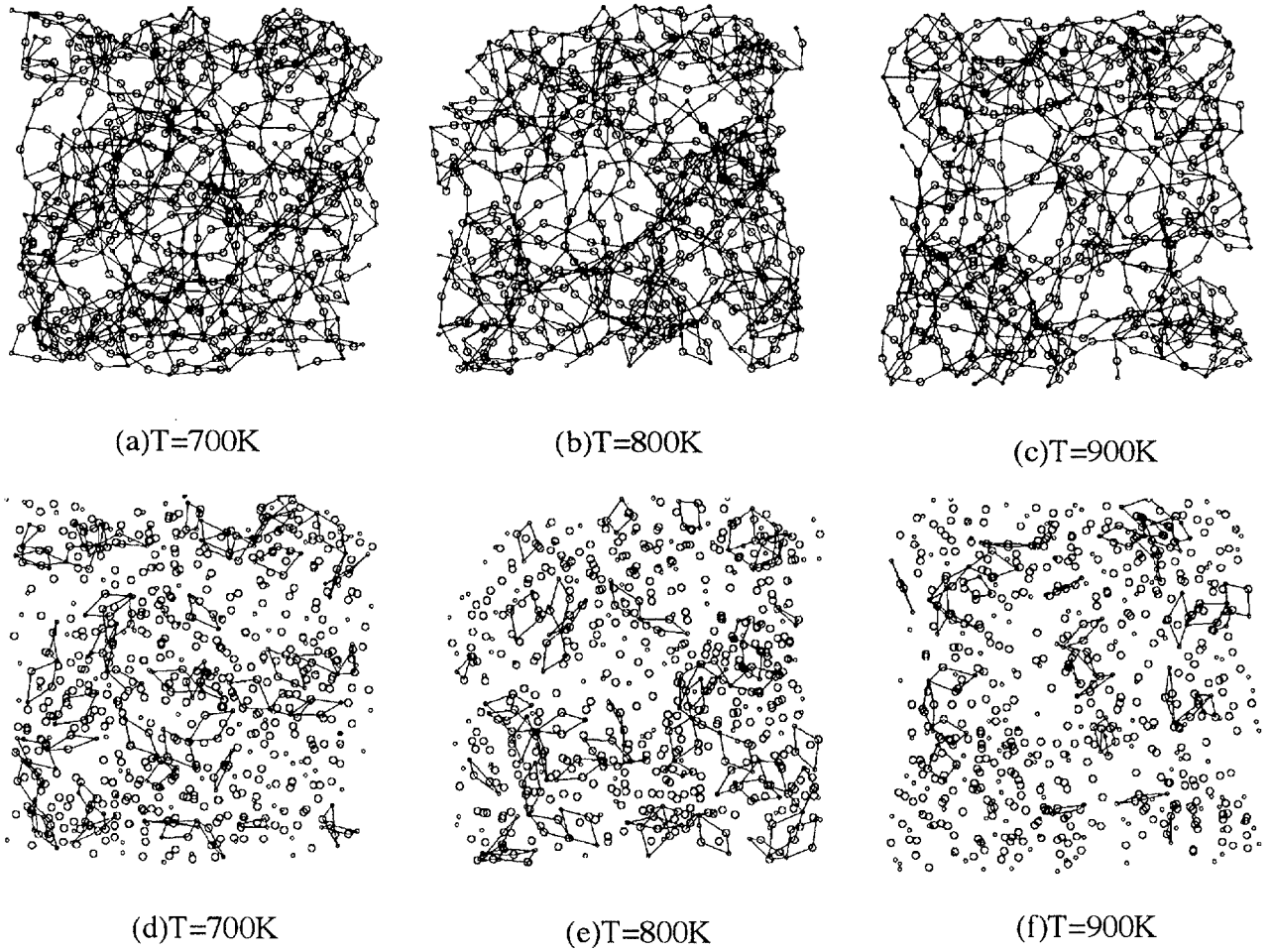

Fig. 3-10 The snap shots of the melt structures of 1440 particle system at the respective temperature. (a)-(c) show only the Zr-F-Zr bridging and the other ions like modifiers of Ba and Na, the isorated Zr and the terminal F ions. (d)-(f) show only the Zr-F2-Zr edge sharing in the melts.

CHAPTER 4

VISCOSITY OF ZBLAN MELTS WITH DIFFERENT GLASS FORMING ABILITY

4-1. INTRODUCTION

The relations between viscosity and the structural changes occurring in the melt with temperature could be depicted by employing Molecular Dynamics simulation method in last CHAPTER. The main features controlling the glass formation was found to be originated in the formation of linkages between structural units of ZrF_n polyhedra and the formation of edge sharing was one of the most representatives in fluoride glass system based on ZrF_4-BaF_2. In this CHAPTER, the steep change in viscosity under liquidus temperature (under cooling region) found in the melts with different glass forming ability was measured actually in order to clarify and prove these scheme of viscosity changes and glass forming behavior. ZrF_4-BaF_2-LaF_3-AlF_3-NaF system was also employed for the tested sample glass and the glass forming ability was changed by the compositional replacement of BaF_2 by NaF. In ZrF_4-BaF_2-based system, Ba^{2+} ions has been considered to control the edge sharing among ZrF_n polyhedra. Phifer et al. [1] proposed the structural models in the melt or glass by arranging ZrF_n polyhedra found in the fluorometalates salts to satisfy the compositions and calculated the ratio of various linkages of ZrF_n units.

The thermal stability and glass forming tendency of ZrF_4-based fluoride glasses are not very high though the glasses have great potentiality on the application for ultra low loss optical fiber. On the other hand, the structure of the melt, the height of viscosity and its

temperature relationships are closely related to the glass forming tendency. The viscosity temperature relationships of several fluoride glasses have been reported [1-8] as non-Arrhenius and/or non-Fulcher type. Angell classified several glass melts into 'strong' and 'fragile' liquid [9] and fluoride glasses seemed to belong to extremely 'fragile' liquid. This feature of fluoride glasses was thought to be arose from the structure of melt. Therefore, the investigation of the structure of the melt is very important to clarify the glass forming mechanisms in the fluoride systems. In the present study, the measurements of viscosities have been performed on the melts of ZrF_4-BaF_2-LaF_3-AlF_3-NaF system with different glass forming tendency and the viscosity-temperature relationship has been discussed from the view point of the compositional effects on the crystalline precipitation, mainly the viscosity value at liquidus temperature.

4-2. EXPERIMENTAL

A. Sample preparation

The sample glasses of ZrF_4-BaF_2-LaF_3-AlF_3-NaF system were prepared in a dry box under N_2 atmosphere as shown in Fig. 4-1. The batch for about 200g of glass prepared from high purity chemicals of ZrF_4, BaF_2, LaF_3 and from reagent grade chemicals of AlF_3 and NaF (Morita Kagaku Kogyo), were melted in a platinum crucible at 800°C for 1 hr under dry N_2 gas flow. The melt was poured into the preheated Aluminum mold and annealed at the glass transition temperature and then cooled slowly down to the room temperature. The batch composition and the results of the analysis on the glasses carried out by Energy dispersion X-ray spectroscopy (Seiko EG&G, SED8600 System) were listed in Table 4-1. The glass of ZBLAN-1 has been considered to have the most stable composition, while in the glass of

ZBLAN-2, 3 and 4, a part of BaF_2 was replaced with NaF in cation mol% in order to change intentionally the glass forming ability. Therefore the glass forming ability of the ZBLAN-4 melt was lower than those of the ZBLAN-1 melt and needed higher cooling rate by changing the mold temperature. The traces of Differential Thermal Analysis (DTA) for the sample glasses were recorded under N_2 atmosphere at the heating rate of 10K/min. The characteristic temperature, T_g (the glass transition temperature), T_x (the onset of crystallization), T_c (the first peak of crystallization), T_M (the fusion temperature), T_l (the liquidus temperature) and the values of $(T_x-T_g)/T_g$ were given in Table 4-1.

B. Viscosity measurement

The viscosity of the melts was measured by the rotating cylinder method. Fig. 4-2 shows the block diagram of the viscometer and the sketch of the carbon spindle and crucible with the dimension. The space between the inside wall of the crucible and the outside wall of the spindle was taken as 1.0 mm to measure the low viscosity less than 1 poise under low shear rate with high accuracy. The torque necessary for driving the spindle was detected with HAAKE RV12 viscotester. The infrared image furnace using halogen lamps was employed for heating sample through a transparent silica glass tube. The temperature of a melt was sensed indirectly with a thermocouple installed beneath the crucible. The calibration curves relating the output voltage of the viscotester and viscosity were prepared by measuring the viscosity of the standard oil in the range of 0.1-30 poise on various number of revolution.

The crucible including a sample glass of about 160 g was heated up to 700°C, about 150°C above the liquidus temperature under N_2 gas flow. After the spindle inserted into the

melt, the temperature of the crucible was lowered to the intended levels in steps and the torque was recorded on various numbers of revolution in each step. The number of rotation tested were 8, 16, 32, 64, 128 and 256 rpm corresponding to the shear rate of 19.2, 38.5, 77.0, 123, 3.08 and 616 s^{-1}, respectively. The evaporation from the glass melts was rarely observed during measurement and even there was little of any change of composition of the melts.

For the measurement of low viscosity region from 10^{12} to 10^{8} poise, the penetration method was employed. The apparatus was calibrated in advance by NBS710 standard glass and the measurements for the fluoride glasses were performed under dry N_2 gas flow.

4-3. RESULTS AND DISCUSSION

A. Thermal Properties

Table 4-1 showed the results of the thermal analysis by DTA measurements. The thermal stability $(T_x-T_g)/T_g$ of the obtained glass decreased with the decrease of Ba/Na ratio. As seen in Fig. 4-3, Tx and T_x-T_g decreased drastically with the decrease of Ba/Na ratio, in spite of no remarkable changes in glass transition temperature and liquidus temperature. Generally, smaller temperature difference in T_x-T_g and lower T_x mean that it needs higher cooling rate to pass through the temperature region in which the crystalline is easy to precipitate due to the high -ΔG of supercooled liquid. Fig. 4-4 showed the plots of the compositions of the sample glasses on the critical cooling rate regions of ZrF_4-BaF_2-LaF_3-AlF_3-NaF system reported by Kanamori et al. [10] with the interpolation of the plots of thermal stability against Ba/(Ba+Na) molar ratio. The substitution of BaF_2 by NaF certainly increased the critical cooling rate and lowered the glass forming ability. In addition to this, as shown in Fig. 4-3,

the complex crystallization behaviors also induced. This means that the crystalline precipitating from the melt were changed, because there were observed several endothermic peaks of the crystalline melting in the sample with low Ba/Na ratio. As reported by Parker et al. [11], sodium fluorozirconate crystalline like $NaZrF_5$, $Na_7Zr_6F_{31}$ etc. precipitated in the low Ba/Na sample in addition to barium fluorozirconate crystalline like β-$BaZrF_6$, β-$BaZr_2F_{10}$ etc. This means that the glass forming ability of the melt have to be considered from the point of view that what kinds of the melt structures are provable to suppress the precipitation of the above crystalline, which might be restricted by not only the composition, but the viscosity changes.

B. Accuracy of Viscosity Measurement

The shear rate dependence of viscosity of ZBLAN-1 glass melt was shown in Fig. 4-5. The viscosity was little dependent on the shear rate in the temperature range tested. The structural relaxation time would be quite small compared with the reciprocal value of the shear rate and this melts should behave as Newtonian liquid. The results of the independence in the shear rate mean that the high accuracy in the viscosity measurements have accomplished for this low viscosity liquid at high temperature by employing the apparatus with thin clearance between spindle outer surface and crucible inner surface. The similar results were also obtained for ZBLAN-4 melt.

C. Viscosity-Temperature Relation and Glass Forming Ability

Fig. 4-6 showed Arrhenius plots of the viscosities of the melts of ZBLAN-1 and ZBLAN-4. The viscosities and the activation energy of viscous flow for ZBLAN-1 melt were

higher than those for ZBLAN-4 melt having lower glass forming ability. The allows in this figure pointed the liquidus temperature of respective melts and the liquidus viscosity of ZBLAN-1 was about 50% higher than that of ZBLAN-4 melt and this difference was thought to originate from the different BaF_2/NaF ratio. In oxide system, a glass having higher liquidus viscosity in general has the higher the glass forming tendency. The result of this study was likely to show the empirical rule for oxide systems could be applied to fluoride systems. From the view point of nucleation and growth theory of crystallization, the rapid pass of low viscosity region of undercooling would be necessary for the vitrification of melt. As mentioned in the previous chapter, the steep viscosity change was induced by the strong correlation between structural units of ZrF_n polyhedra and that does not go on without the modifier ions like Ba^{2+}. Compared with Na^+ ion, Ba^{2+} ion has stronger field strength and the cooperativity between ZrF_n polyhedra should be enforced. Considering the linkage process of them, the repulsion between F^- ions has to be relaxed by other factors and the high coordination of F^- about Ba^{2+} was considered to play certain important role. In ZBLAN-4 melt, The liquidus viscosity is quite low and the larger supercooling would be needed to raise viscosity to suppress the crystallization. However, as pointed out by Leede and Waal [12], the liquidus viscosity would not be enough to explain fully the glass forming ability. The difference in the composition of melt should change the crystallizing phase and the other factor that what kind of crystalline phase is easy to precipitate can not be ignored. As mentioned in section A, the DTA traces of the samples with different Ba^{2+}/Na^+ ratio showed the complex crystallization behaviors. This mean that the precipitation conditions of crystalline was also changed depending on Ba^{2+}/Na^+ ratio. The differences in the connectivity between ZrF_n polyhedra caused by

Ba/Na ratio is also considered to have much influence on the precipitation of crystalline, because the various metal fluorozirconate crystals are known to be consisted of the characteristic linkages of ZrF_n polyhedra.

4-4. CONCLUSIONS

In this chapter, the viscosity of ZBLAN melts with different glass forming ability was measured by employing the rotation method, which designed to be able to measure low viscosity with high accuracy. The difference in the liquidus viscosity was found and it was concluded that the melt with higher glass forming ability had higher viscosity value at this point. This means that higher liquidus viscosity is required to avoid the crystallization easily. In such a meaning, the ordinary rule in oxide glasses would be applicable to the fluoride glasses. However, the relatively better glass forming ability in spite of quite low liquidus viscosity suggested that there are some another potential in the melt structure to suppress the crystallization. The characteristic structural changes in the melt would be deeply related in causing unprovable situation of the crystalline precipitation and the bridging formula found in metal fluorozirconate crystals would offer information.

REFERENCES

[1] C. C. Phifer and J. Lucas, Mater. Sci. Forum, **19&20** (1987), 111

[2] A. J. Bruce, C. T. Moynihan, R. Leehr, M. Opalka, R. Mossageph, N. P. Bansal, R. H. Doremus and M. G. Drexhage, Opt. Engin., **24** (1985) 522

[3] H. Hu and J. D. Mackenzie, J. Non-Cryst. Solids, **54** (1983) 522

[4] J. M. Shelby, C. G. Pantano and A. A. Tesor, J. Am. Ceram. Soc., (1984), C164

[5] C. T. Moynihan, R. Mossadegh, P. K. Gupta and M. G. Drexhage, Mater. Sci. Forum, (1985) , **6**, 655

[6] H. Hu and J. D. Mackenzie, J. Non-Cryst. Solids, (1986), **80**, 495

[7] S. N. Crichton, R. Mossadegh, C. T. Moynihan, P. K. Gupta and M. G. Drexhage, Mater. Sci. Forum, (1987), **19&20**, 435

[8] W. C. Hasz, S. N. Crichton and C. T. Moynihan, Mater. Sci. Forum, (1988), **32&33**, 589

[9] C. A. Angell, J. Non-Cryst. Solids, **73** (1985) 1

[10] T. Kanamori, Mater. Sci. Forum, **19&20** (1987) 363

[11] J. M. Parker, G. N. Ainsworth, A. M. Seddon and A. Clare, Phys. Chem. Glasses, **27** (1986) 219

[12] G. De Leed and H. de Waal, J. Non-Cryst. Solids, **104** (1988) 45

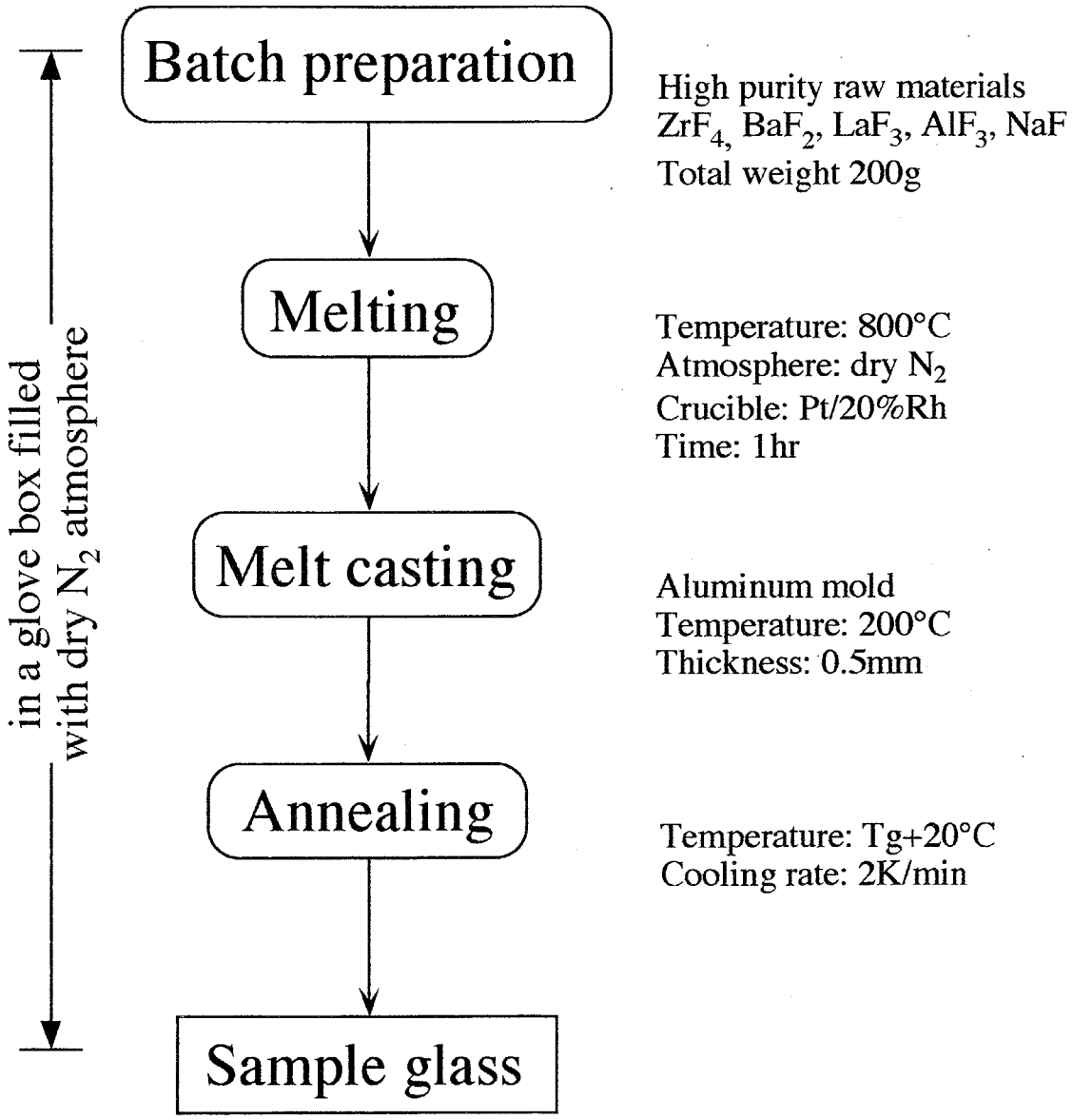

Fig. 4-1 Flow chart of the sample preparation.

Table 4-1 lists of the glass compositions, their characteristic temperatures and the thermal stabiolity factors.

Sample	ZrF_4	BaF_2	LaF_3	AlF_3	NaF	Glass Transition Tg (℃)	Onset of Crystallization Tx (℃)	Liquidus temperature Tl (℃)	Stability factor (Tx-Tg)/Tg
ZBLAN-1	53 (49.9)	20 (19.8)	4 (6.5)	3 (6.8)	20 (17.0)	296	377	643	0.210
ZBLAN-2	53 (59.5)	5 (3.9)	4 (2.9)	3 (4.1)	35 (29.6)	242	328	652	0.164

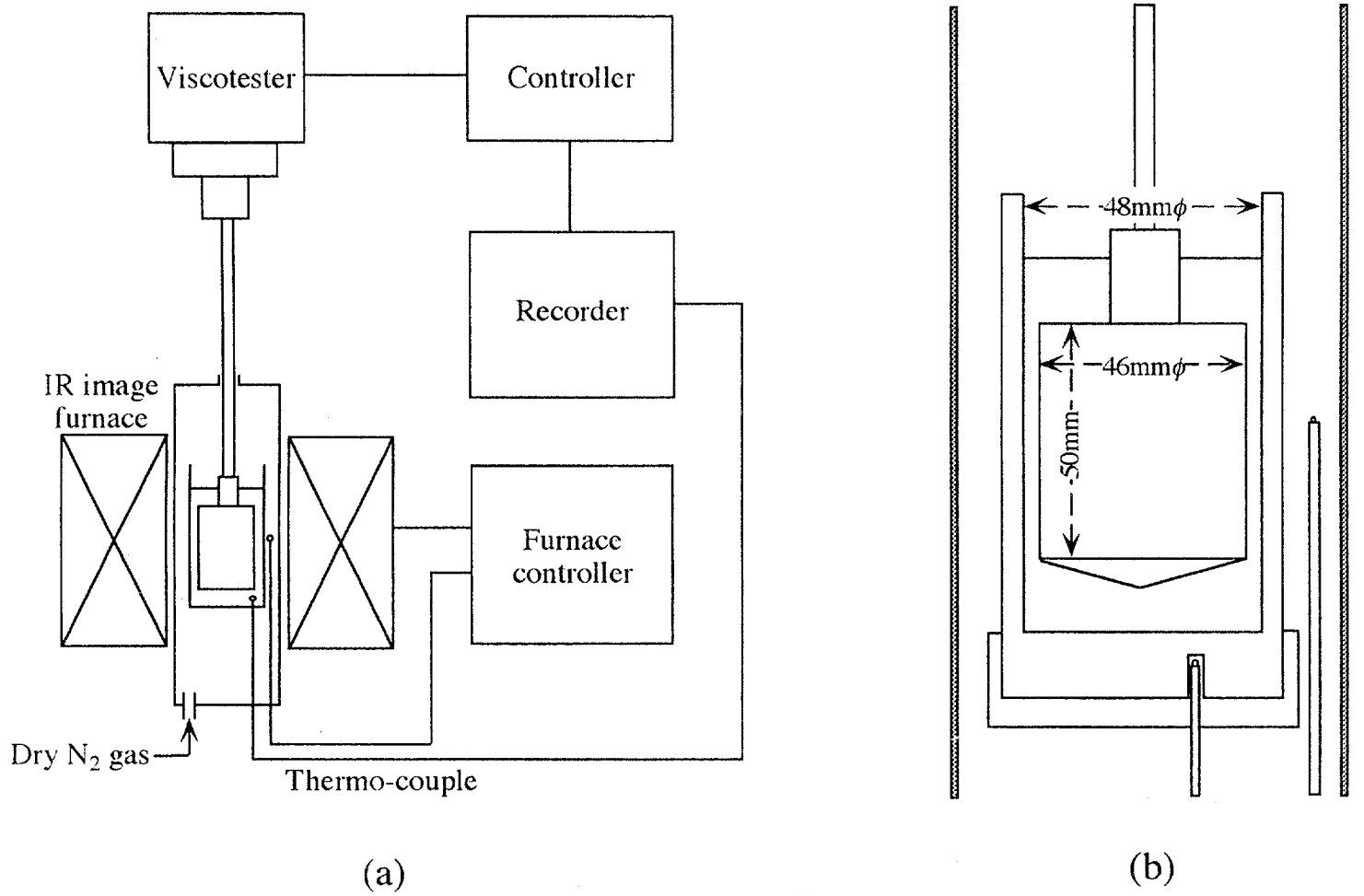

Fig. 4-2 The block diagram of the employed viscometer (a) and the sktch of the carbon spindle and crucible with dimension (b).

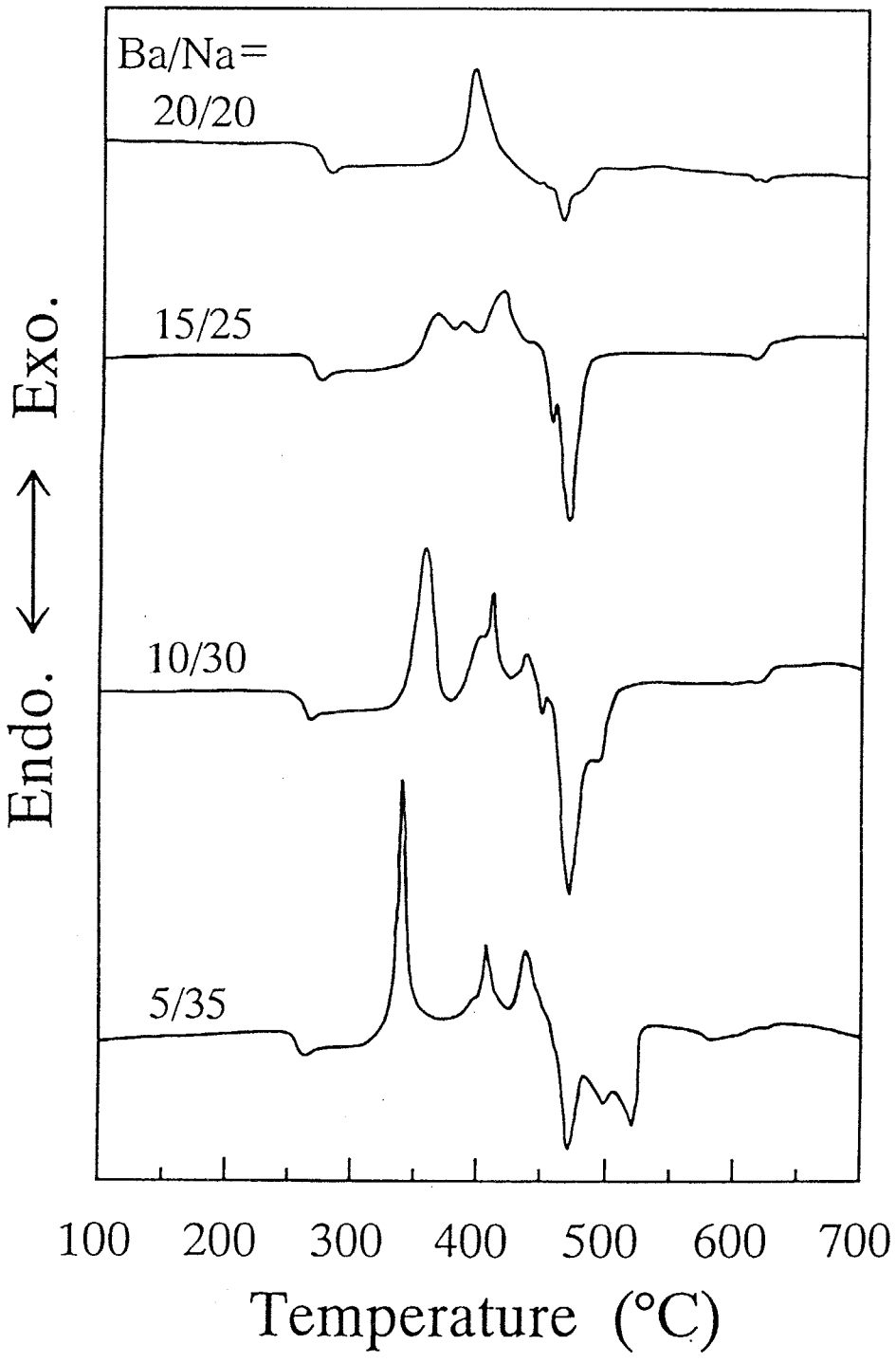

Fig. 4-3 DTA traces of ZBLAN glass samples with different Ba/Na molar ratio. The heating rate was 10K/min and the atmosphere was controlled by N_2 gas flow.

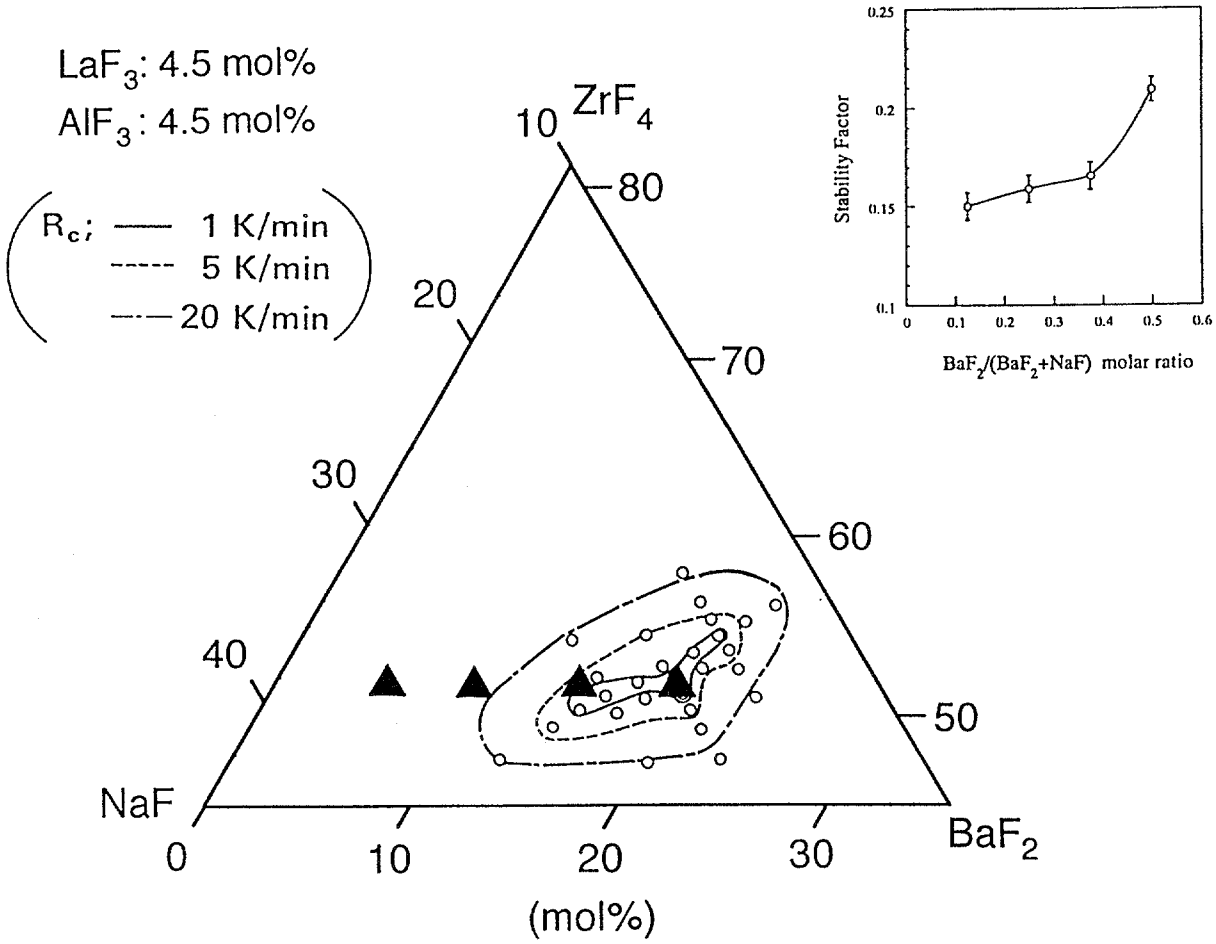

Fig. 4-4 The plots of the glass compositions studied in this chapter. The triangle diagram reveals the critical cooling rate region reported by Kanamori [10]. The figure of upper-right side is the plots of the thermal stability factor (Tx-Tg)/Tg against Ba/(Ba+Na) ratio.

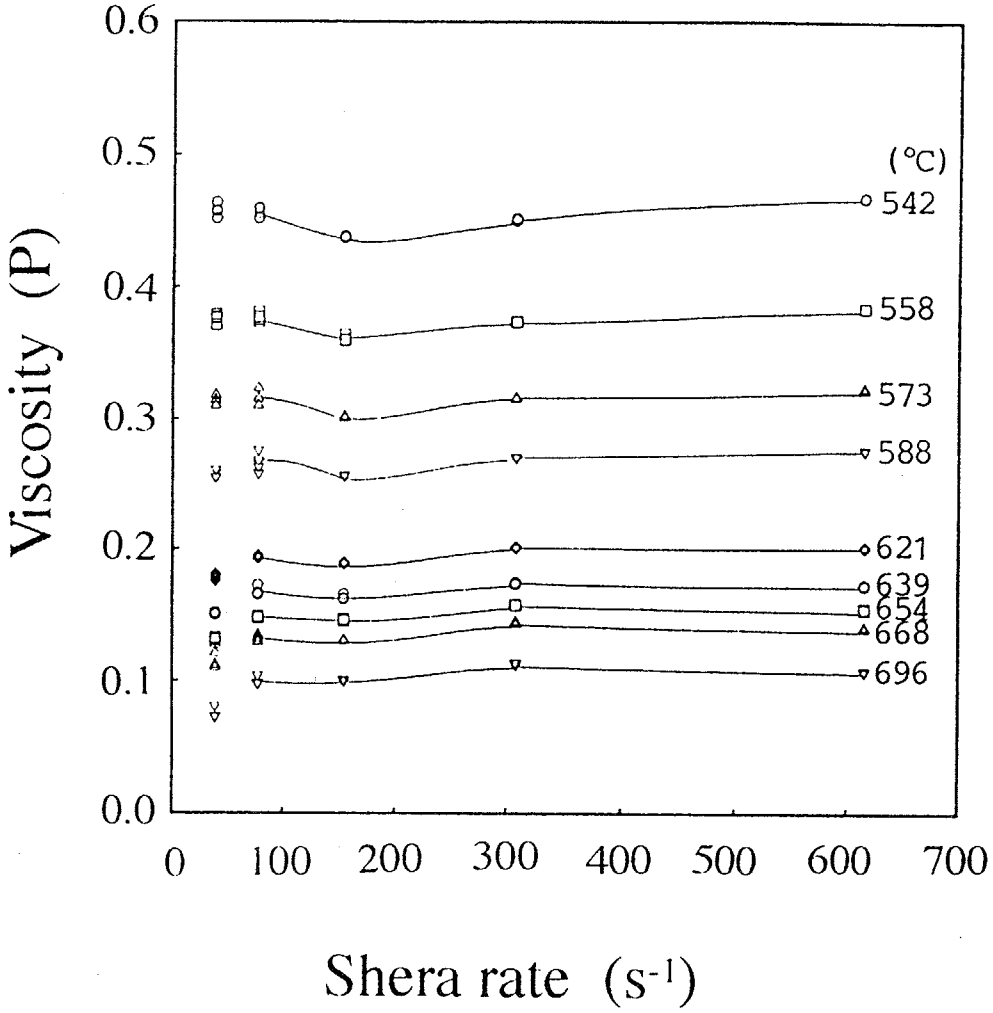

Fig. 4-5 The rotational speed (shear rate) dependence of the measured viscosity of ZBLAN-1 (Ba/Na=20/20) glass melts.

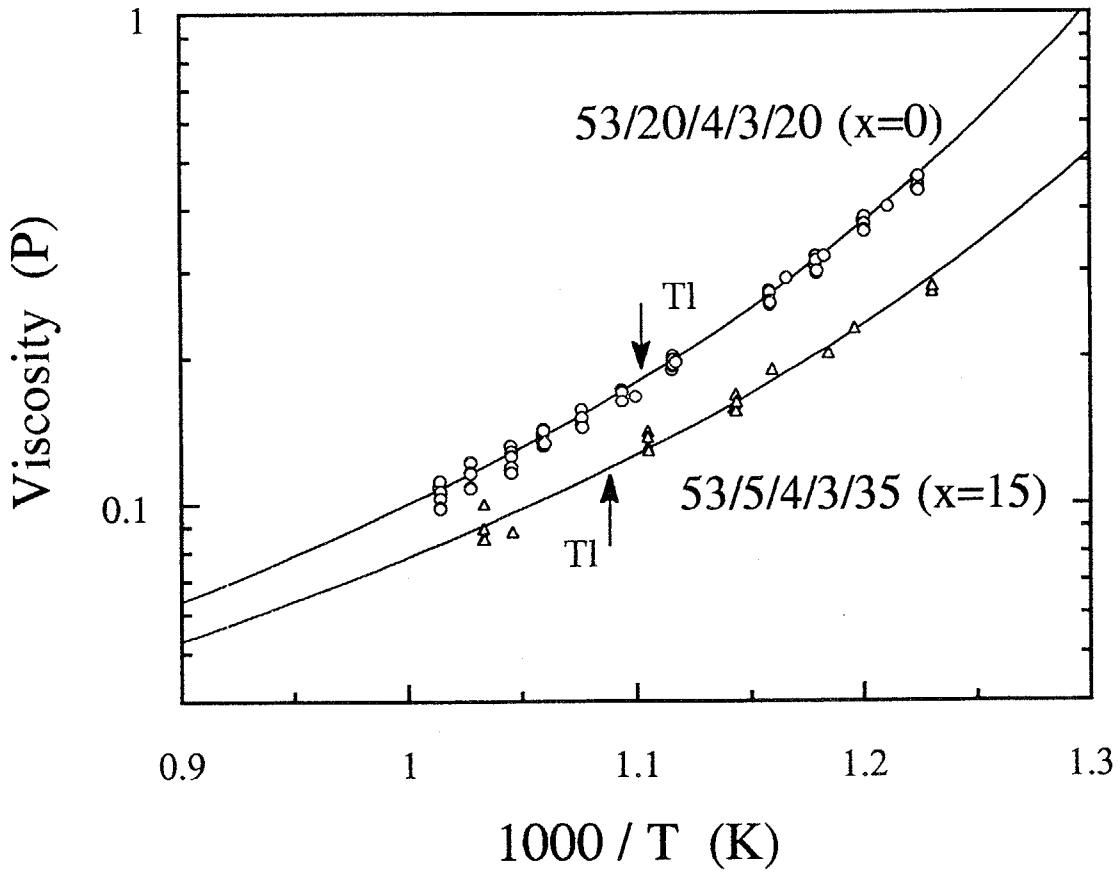

Fig. 4-6 Arrhenius plots of viscosity at high temperature region. The allows inside the graph reveal the liquidus temperature obtained from DTA measurement of the respective glass.

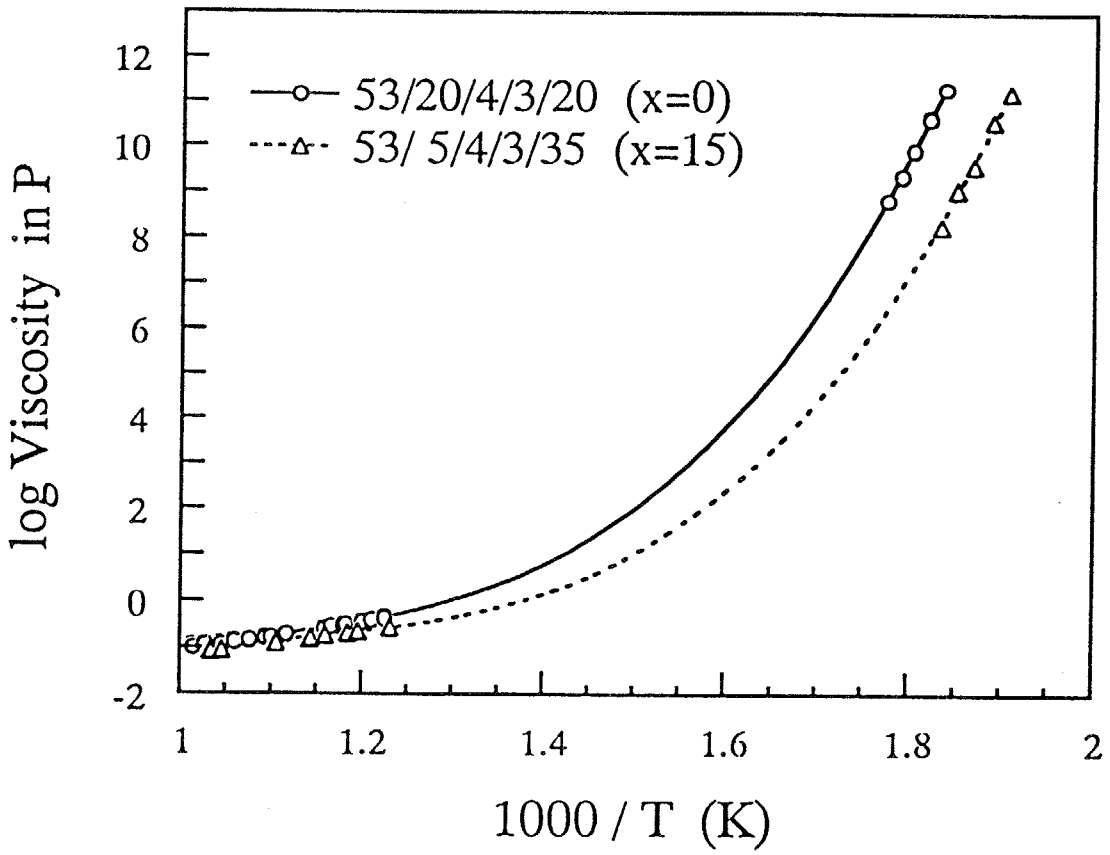

Fig. 4-7 Arrhenius plots of viscosity combining data of viscosity at high temperature with those measured at low temperature region by the penetration method. The curves are obtained by the polynomial fitting.

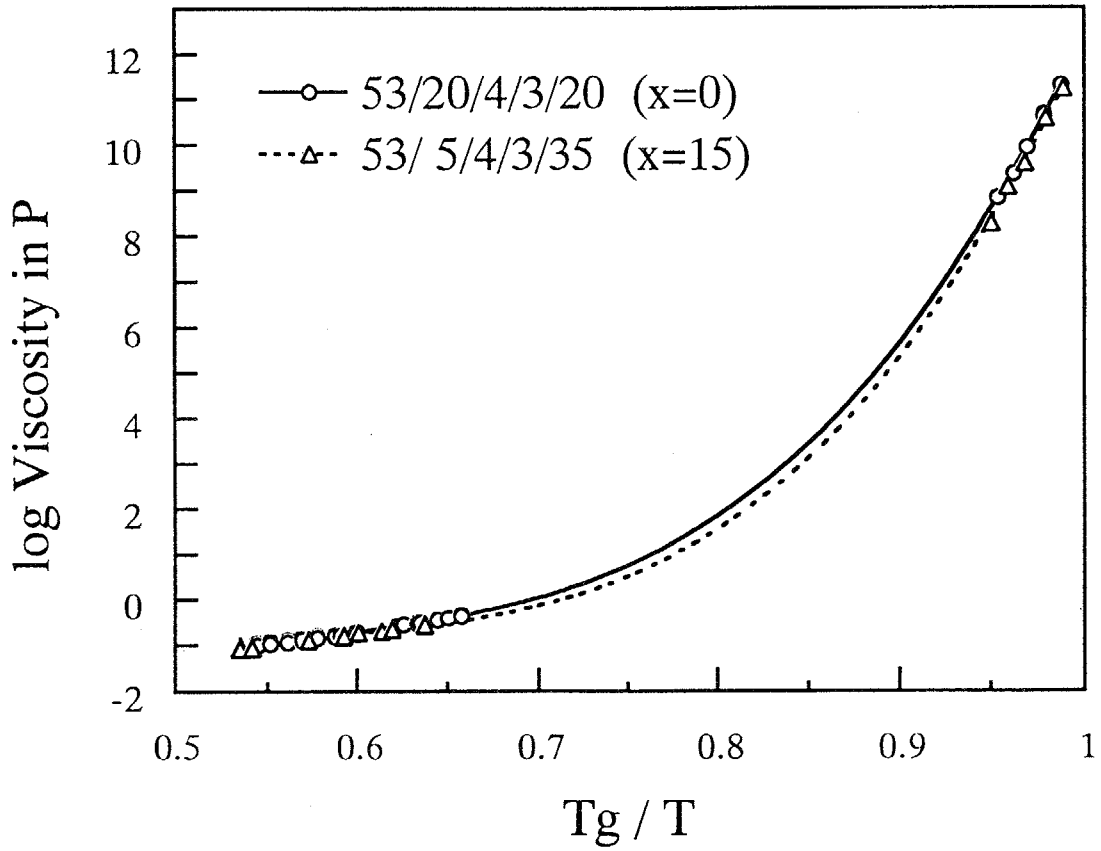

Fig. 4-8 Arrhenius plots of viscosity. Temperature are normalized by the glass transition temperature of the respective sample glasses.

CHAPTER 5

THE EFFECTS OF NON-FLUORINE ANIONS ON THERMAL STABILITY AND CRYSTALLIZATION BEHAVIOR OF ZBLAN MELTS

5-1. INTRODUCTION

In the previous CHAPTERs, the structural changes occurring in the cooling process were investigated to originate from the linkages between ZrF_n polyhedra represented by the formation of edge sharing. These structural change was considered to be efficient especially under the supercooling condition, in which the crystallization is easy to occur. Considering the glass forming ability of fluoride melt, the precipitation behavior of crystalline is one of the most important factors to be taken into account, and the crystalline structures of the precipitated crystalline informs much about the melt structures, because it is considered to be understandable that the crystalline with similar structure to the melt is provable to firstly appear. In such a meaning, the crystallization behavior is worth investigating the glass forming ability of fluoride melt. The crystallization study on ZrF_4-BaF_2-based fluoride glasses have been enormously reported. The most representative features can be summarized as follows;

(1) Main crystallizing phases are β-$BaZrF_6$ and β-$BaZr_2F_{10}$. The former are known to precipitate from the interface like the glass surface and troublesome to cause the loss of the optical quality in the glass forming process like the fibre drawing.

(2) Many kinds of crystalline phases were detected. Even in the ZrF_4-BaF_2 binary system, several crystallines appear. In the case of the multicomponent glass

like ZBLAN, more phases precipitate.

(3) The crystallization behavior are known, empirically, to be sensitive to the melting history like the melting temperature, melting period, its atmosphere, the crucible, fining temperature, the mold temperature, etc.

Especially, the last feature has revealed some conjugation of understanding the crystallization behavior and prevented improving the melting process in order to obtain the glass with higher quality. The reasons are considered to exist in the contamination, especially of anions, incorporated into the melt during melting. Table 5-1 summarizes the anion impurity effects on the glass forming and the crystallization behavior of several fluoride glass systems. The most impressive facts that only a small amount of impurities of the order of 10^2 ppm heavily influenced those properties. For instance, Oxygen doping increased the critical cooling rate in the order of magnitude [1], and chlorine induced another crystalline that is usually observed in the chlorine-free glass sample [3-5]. These features about the impurity effects on the glass forming ability and the crystallization behavior should have much relation to the melt structures and the relatively high glass forming ability of ZrF_4-based system might originate in their features.

In this CHAPTER, the detailed crystallization behaviors of ZrF_4-based fluoride glass ZBLAN with different amount of anion impurities of OH^- and Cl^- are investigated. The precipitations of crystallines are evaluated by drawing the crystalline phase developing curves*

*They are different with ' Time-Temperature-Transformantion (TTT) curve ' in the strict meaning. TTT-curve is defined to be used only in the case that only one crystalline precipitates from the melt. In the case of this study, several kinds of crystallines precipitate and there would be some interactions between them in their nucleation and growth process and the word of 'TTT curve' is inappropriate.

for the respective crystalline phases and the relation between the glass forming ability and the crystallization behavior of ZrF_4-based fluoride glass melt is discussed.

5-2. EXPERIMENTAL

A. Glass preparation

The base glass chosen was typical ZBLAN (53mol% ZrF_4-20BaF_2-4LaF_3-3AlF_3-20NaF) glass prepared from reagents ZrF_4 (optical fiber grade), BaF_2 (OFG), LaF_3 (4N), AlF_3 (4N), and NaF (4N, Rare Metallic Co.). In order to obtain the glass samples including different amount of anion impurities, the various preparation methods were used for the respective glass samples. Table 5-2 summarized the glass preparation conditions. The preparation of the glass with low OH^- content was produced by melting the fluoride batch mixtures under dry N_2 atmosphere. Melting was carried out at 850°C for 1 h. In preparing a high OH^- content glass (Glass B), treatment of reagents mixture with NH_4HF_2 and NF_3 was employed according to Braglia et al. [6]. In this study, NF_3 (99.9%) gas was introduced into the furnace only at high temperatures in order to leave a high amount of OH^- concentration in the glass, because NF_3 acts to reduce the amount of oxygen relating species at low temperature treatment. 5 wt% NH_4HF_2 to the batch was added to the batch mixture and heated up to 450°C at the rate of 5°C/min and held for 1 h. After that, temperature raised up to 850°C at the rate of 4.5°C and kept for 1 h. In preparing Cl^- doped glasses, 2.5 mol% (Glass C) and 5 mol% (Glass D) of $BaCl_2$ (3N, Rare Metallic Co.) was substituted for BaF_2. Glass melting was carried out under dry N_2 atmosphere prepared by passing N_2 gas through a liquid N_2 trap. Each reagent mixture was heated to 900°C for 1 h at 5K/min. All the melt were casted into a preheated mold at

250°C (in case of Glass C and D, 200°C) and cooled to room temperature without annealing. Gold crucible was used to prepare Glass B, and Pt/20%Rh crucible was used to prepare the other glasses.

B. Composition Analysis

Glass composition was analyzed by the method of inductively coupled plasma emission spectroscopy (Shimazu ICPS-1000). Chlorine concentration was determined by ion chromatography (Dionex 4520i). Hydroxide content was analyzed from infrared spectroscopy. The molar absorption coefficients of the OH^- stretching mode at 2.9μm in the fluoride glasses was taken from ref[7].

C. Thermal Analysis

In order to determine whether surface crystallization was dominant, differential thermal analysis (DTA) curves were determined for each glass at following ranges of particle size: 45-150, 150-300, 300-500 and >500μm (bulk). Care was taken in crushing the glass in the dry box to avoid surface modification by moisture in the atmosphere. Thermal analysis was done at 10K/min under dry N_2 atmosphere using an Al_2O_3 reference.

D. Procedures for Crystallization Study

Time-temperature relations of the precipitation of crystallines were obtained for all glasses for the first exothermic peak of the DTA curve located in the range 300-400°C. About

0.3-0.4g of each glass was remelted at 750°C for 3min in a small glassy carbon crucible (8mm I.D. 0.4ml). The remelted glass was quickly transferred into another furnace for crystallization in the range 300-400°C for 1-80 min, followed by rapid cooling to room temperature. All procedures for investigating crystallization were done under dry N_2 atmosphere. The crystallized samples were crushed into powders less than 50μm. The amounts of crystallized phases were determined by internal standard method of powder X-ray diffraction (XRD) where NaCl was used as the standard, and calibration curves for each crystalline phase were determined in advance by using the standard crystals. The preparation of the standards of the precipitated crystalline phases are mentioned in APPENDIX.

5-3. RESULTS

Table 5-3 summarizes the impurity concentration and characteristic temperatures for each glass. Glass A had approximately five times lower OH^- content than Glass B which was prepared with NH_4HF_2 and NF_3. Glasses C and D contain 0.95 and 1.95 wt% Cl^-, respectively, as well as some OH^- impurities naturally introduced. Glass transition T_g, onset of crystallization T_x, crystallization peak T_p, and the calculated stability factor $(T_x-T_g)/T_g$ were determined for the first exothermic peak of the DTA curve (see Fig. 5-1) for each bulk glass (>500μm).

Curves for each glass at the various particle sizes are also shown in Fig. 5-1. For Glass A, the first crystallization peak is due to surface crystallization, because the peak increased in intensity and shifted towards lower temperatures as sample surface area increased. For Glass B with five times higher OH^- content, the T_g and the shape of the exothermic peak were similar to those of Glass A. However, the first peak appeared at a lower temperature, and the

particle size effect on surface crystallization was larger. Glasses C and D containing Cl^- ions exhibited different behaviors from those of Glasses A and B. The T_g decreased with increasing Cl^- content. The stability of Glass C was larger than that of Cl^--free Glass A. With increasing surface area, T_x for Glass C decreased due to the appearance of a new peak at a lower temperature, as shown in Fig. 5-1(c). On the contrary, compared to Glass C, the first crystallization peak of Glass D was located at a lower temperature and the peak was almost independent of particle size.

Table 5-4 summarizes the XRD analysis for each glass heat-treated isothermally. The crystalline phases were α- and β-$BaZrF_6$(BZ), disordered β-$BaZrF_6$(β-BZ_d), α- and β-$BaZr_2F_{10}$(BZ_2), and $Na_7Zr_6F_{31}$(N_7Z_6). Some peaks were unidentifiable, but they have very weak intensities. The degree of shading in Table 5-4 represents the magnitude of the relative intensities of the diffraction peaks. For Glass A, the strongest peak came from the β-BZ_2 phase, followed by the α-BZ_2, β-BZ and β-BZ_d phases in decreasing order of intensities. In Glass B with high OH^- content, the β-BZ_d phase was the dominant crystalline phase. Contrary to Glass A, the β-BZ_2 phase was not detected in Glass B at the lower temperatures. With the addition of Cl^-, the crystallizing phases drastically changed as follows. In Glass C, the α-BZ_2 phase was dominant, and the crystallization of β-BZ and β-BZ_2 phases which were more dominant in Glass A was retarded. In Glass D with about twice the Cl^- content, the α-BZ and β-BZ phases crystallized, while neither the α-BZ_2 nor β-BZ_2 phase were not detected.

Fig. 5-2 shows examples of the XRD powder patterns of the respectively heat-treated sample. From the peak intensities of the precipitated crystallines, the crystalline growth curves were obtained as shown in Fig. 5-3. The time-temperature combination required for

each of the various crystalline phases to grow to 10vol% is depicted in the curves of Fig. 5-4. In Glass A, the β-BZ_2 phase appeared first and defined the nose position of the time-temperature curve at T~370°C and τ_N~9min. The α-BZ_2 and β-BZ phases also developed but not as readily. In Glass B, the α-BZ_2 and β-BZ (or β-BZ_d) phases appeared faster than β-BZ_2 in the low temperature region. Nose position was located at T~360°C and τ_N~9min. In Glass C, Cl^- addition suppressed the growth rates of the β-BZ_2 and β-BZ phases to one-fifth times that observed in Glasses A and B, as shown by Fig. 5-4(c). However, the development of the α-BZ_2 phase was less sensitive to Cl^- addition, leaving the nose position unchanged at T~370°C and τ_N~8min. In Glass D, new transformation curves of the α-BZ and β-BZ phases occurred at shorter times and lower temperatures than the former glasses, as shown in Fig. 5-4(d). Nose position defined by the α-BZ phase was T~350°C and τ_N~3min. The β-BZ phase always appeared after the formation of the α-BZ phase. Longer heat-treatment times in this temperature region have not yet been carried out at present.

5-4. DISCUSSIONS

A. The effects of OH^- ion

Comparison of the time-temperature relations for the development of crystalline phases in Glasses A and B reveals that OH^- impurity enhances crystallization of the β-BZ and α-BZ_2 phases but affects to a lesser degree the development of the β-BZ_2 phase. Furthermore, enhancement of surface crystallization by OH^- impurity was manifested in the shifting of the exothermic peak of the DTA curves, therefore, formation of the β-BZ and β-BZ_d phases somehow plays a role in surface crystallization. In addition, OH^- impurity influences the

growth of the α-BZ_2 phase, thereby leading to the reduction of the β-BZ_2 phase. The crossing of the time-temperature curves of the α-BZ_2 and β-BZ_2 phases in Fig. 5-4(b) suggests that the α phase did not grow through transformation from the β phase, but that it nucleated independently. As discussed in the next section, the α-BZ_2 phase is considered to exhibit bulk crystallization. More detailed and qualitative studies are needed in order to understand these phenomena.

B. The effects of Cl^- ion

The results shown in Table 5-3 agree with reports by Poulain et al. [8] and Parker et al. [9] regarding the effect of Cl^- on thermal stability. Thermal stability was maximum when Cl^- concentration was about 0.95wt%. However, excess Cl^- over this percent decreased the stability against crystallization.

In Glass C, the α-BZ_2 phase appeared first, and the crystallization of both the β-BZ and β-BZ_2 phases were remarkably retarded, despite the large OH^- content. The suppression of surface crystallization of the β-BZ phase was in contrast to Glass A. From the time-temperature curves and the particle size dependence of the DTA curves for Glass C, it is known that the α-BZ_2 phase develops by bulk crystallization so that nucleation is independent of the β-BZ_2 phase. Chlorine acted as a restraint against surface crystallization of the β-BZ phase in ZBLAN. In addition, the α-BZ_2 phase grew slowly and became saturated at about 30 vol.% at the nose temperature. This fact that the α-BZ_2 phase was the only crystalline phase which developed in this sample is the reason for both good thermal stability and glass forming ability.

As shown in Fig. 5-4(d), excess addition of Cl^- induced crystallization of a new phase,

α-BZ, at a lower temperature region. Compared with the DTA results, the α-BZ phase nucleates in the bulk before the β-BZ phase develops at this Cl^- concentration. Although we have not investigated at the intermediate Cl^- content, it is considered that the α-BZ phase, which is not observed in Glass C, will become appreciable as Cl^- content increases and will become dominant after exceeding a certain concentration.

The structural relations between the melts and the precipitating crystallines

Fig.5-5 illustrated the fundamental structural units of ZrF_n polyhedra found in metal fluorozirconate crystals. Metal ions have been omitted for clarity. The most representative features are their coordination number of fluorine ions and the connectivity among them. These structural flames found in the crystals are much informative to understand the crystallization behavior observed in ZBLAN glass melts, because it would be reasonable to think that the crystalline with the structure similar to those of the melt tends to precipitate easily; the potential barriers for change in the structural flame and for diffusion to compensate the difference in the composition are lower than the other. As discussed in CHAPTER 3, the structural changes in the melt occurs remarkably below liquidus temperature and its characteristics exist in their linkage forms. The rapid formation of edge sharing under supercooling condition plays an important role in the increase of viscosity. This temperature region consists with the temperature region in which the crystalline nucleation and growth rate shows maximum. Therefore, the structural linkage forms in the melt would efficiently influence to determine the crystalline phase that appears first.

As represented by Fig. 5-4, only a small amount of non-fluorine anions changed the

crystallization behaviors, especially chlorine could play the role to improve the stability against the crystallization in the appropriate concentration. Different from the operation of the composition of metal fluoride compounds, the incorporation of other anion is considered to be able to influence the structural unit directly unless that anion does not bond the metal ion composing the structural flame of the glass melt. At the present, there is no evidence that reveals chlorine directly bonds with zirconium ions. However, the linear decrease in glass transition temperature with chlorine content [10] could be understood to say that chlorine are introduced uniformly into ZrF_4-BaF_2-based glass melt. The crystalline phases which were suppressed to develop in Glass C contain their characteristic structures respectively. As shown in Fig. 5-5, β-$BaZrF_6$ has the chain-like structure consisting from octahedral ZrF_8 polyhedra, which connect by two edge sharing in trans position. β-$BaZr_2F_{10}$ has the three-dimensional connection of sheet-like structures which include pentagonal bipyramids of ZrF_7 units. They have one edge and one corner bridging in the sheet plane and another one corner bridging plays a role to connect the neighbored sheet structures. As known from the stereochemical studies, 7-coordinates and 8-coordinates structures can take the various type of polyhedra, which are easily influenced by the anions (in the field of stereochemistry, anion are treated as ligands) Chlorine ion has the much different characteristics from fluorine ions; larger ionic radius, weaker electric field strength and higher covalency in chemical bond. These differences would be enough to change the stability of coordinates and the population of the stereochemistries existing in the melt would be influenced.

α-$BaZrF_6$ phase which precipitated easily in Glass D has the discrete dimer units of $[Zr_2F_{13}]^{5-}$ in the structure. Two ZrF_7 monocapped trigonal prisms connect in the corner sharing

manner. Compared with the structure of β-$BaZrF_6$, β→α transformation means that one side of the edge sharing in chain structure disconnects into the discrete dimer units. The decline of the precipitation of β-$BaZrF_6$ phase in Glass C and the appearance of α-$BaZrF_6$ in Glass D suggested that it was difficult to form the two edge sharing in trans position in the melt by the incorporation of chlorine and α-$BaZrF_6$ phase would like to precipitate easily.

As shown in Fig. 5-5, in β-$BaZr_2F_{10}$ phase crystalline structure, the top of one side of bipyramids is the bridging site and the other is terminated. In order to construct these three-dimensional structures, the former bridging site would play an important role. From the stereochemical study about [MX_6X'] coordinates, it is predicted that a different ligand X' (chlorine) takes the position of the top of bipyramids. This suggested that the different characters of chlorine ion would change the connectivity of the sheet structure and affect the formation of the three dimensional structure of β-$BaZr_2F_{10}$ phase. From the above considerations, chlorine ion would act to change the structural units of ZrF_n polyhedra and their connectivity. The excess incorporation, in turn, would induce the other provable structure in the melt, which are favorable to the crystalline precipitation like α-$BaZrF_6$. Concerning oxygen relating anion of OH^-, there is not be able to propose any explanation, because it is clear that OH^- plays some role as the precursors, but no evidence that OH^- directly act as the trigger of the precipitation of β-$BaZrF_6$ phases. There is another provability that oxides caused from the reaction of OH^- spices act as the site of the nucleation.

5-5. CONCLUSIONS

The effects of OH^- and Cl^- impurities on the crystallization behavior of the ZBLAN

($53ZrF_4$-$20BaF_2$-$4LaF_3$-$3AlF_3$-20NaF in mol%) glass system were investigated. The OH^- ions play the role of enhancing surface crystallization of the β-$BaZrF_6$ phase, while the Cl^- ions suppress the development of β-$BaZrF_6$ and β-$BaZr_2F_{10}$ phases and improve the thermal stability of the ZBLAN glass at the appropriate concentration.

Only a small amount of incorporation changed the glass forming ability and the thermal stability of ZBLAN glass melt. 10^2 ppm order of OH^- enhanced the development of the surface crystallizing phase of β-$BaZrF_6$ and the reduced heavily the stability against the crystallization of the melt. On the other hand, Chlorine showed the characteristic behaviors of the crystallization. 0.95wt% introduction declined the development of β-$BaZrF_6$ and β-$BaZr_2F_{10}$ phases, which are the dominant crystallines to decide the glass forming ability of ZrF_4-BaF_2-based melt. These crystallization behaviors improved the thermal stability, because the surface crystallization was suppressed and the onset temperature of the crystallization increased. More incorporation, in turn, induced another crystalline phase of α-$BaZrF_6$ and lowed the glass forming ability.

The structural investigation about the precipitated crystallines suggested that the structural units of ZrF_n polyhedra were heavily influenced by chlorine. There are various type of coordinates of ZrF_7 and ZrF_8 polyhedra and the precipitated crystallines consist of the respectively different coordinates of ZrF_n units. From the consideration based on the stereochemistry, their stability are easy to be changed by the surrounding anions and their linkages and chlorine can affect directly the coordination structure of ZrF_n, because chlorine has much different characters from fluorine. The chlorine changed the population of the existing ZrF_n polyhedra in the glass melt and determine the first developing crystalline phase

from the melt. Their valances in the melt are sensitive to the small amount of anion impurities and the appropriate amount of chlorine could act as the additive to control the developing crystalline phases from the melt.

REFERENCES

[1] S. Mitachi and P. A. Tick, Mat. Sci. Forum, **67&68** (1991)169

[2] T. Nakai, N. Norimatsu, and Y. Noda, Opt. Laser Tech., **19** (1987) 271

[3] M. C. Weinberg, G. F. Neilson, and G. L. Smith, J. Non-Cryst. Solids, **56** (1983) 45

[4] G. F. Neilson, G. L. Smith, and M. C. Weinberg, Mat. Res. Bull., **19** (1984) 279

[5] G. F. Neilson, G. L. Smith, and M. C. Weinberg, J. Am. Ceram. Soc., **68** (1985) 629

[6] M. Braglia, M. Ferraris, G. Grego, G. Parisi, and F. Taiariol, Mat. Res. Bull., **24** (1989) 661

[7] S. Mitachi, S. Sakaguchi, and S. Takahashi, Phys. Chem. Glasses, **27** (3) (1986) 144

[8] M. Poulain and A. Elyamani, Mat. Sci. Forum, **32&33** (1988) 143

[9] J. M. Parker, A. G. Clave, A. B. Seddon, J. Morris, and N. Pitt, Mat. Sci. Forum, **19&20** (1987) 475

[10] M. Tatsumisago, Y. Akamatsu and T. Minami, Solid State Ionics, **31** (1988) 41

Table 5-1 The previous studies on the effects of impurities on the glass forming ability and the crystallization behavior of various fluoride glass systems.

Impurity	Glass System	Effects on the glass formation and the crystallization	Authers
O	ZBLA ZBLAN	Critical cooling rate R_c increases with oxygen content	Mitachi et al. [1]
	HBLA,YABC CLAP	Optimum concentration for the minumum Rc value	
OH	ZBLAN	induce the surface crystallization at fiber drawing temperature.	Nakai et al. [2]
Cl	ZBLA	cause the development of α-$BaZrF_6$ phase.	Weinberg, Neilson et al. [3-5]
	ZB, ZBSr	enlarge the glass forming region. improve the thermal stability.	Poulain et al. [8]
	ZBLAN	improve the thermal stability of $(T_x-T_g)/T_g$.	Parker et al. [9]

Table 5-2 The preparation conditions of ZBLAN sample glasses.

Base Glass: $53ZrF_4$-$20BaF_2$-$4LaF_3$-$3AlF_3$-$20NaF$ (in mol%)

Glass A	Chemical additive free process in dry N_2 atmosphere	low OH content
Glass B	Reactive atmosphere process by using NH_4HF_2 and NF_3/N_2 atmosphere	high OH content
Glass C	Chlorine dope by the replacement of 2.5mol%BaF_2 with $BaCl_2$	low Cl content
Glass D	Chloride dope by the relpacement of 5.0mol%BaF_2 with $BaCl_2$	high Cl content

Table 5-3 The impurity concentrations and the characteristic temperatures of sample glasses.

	OH^- (ppm)	Cl^- (wt%)	Tg (℃)	Tx (℃)	Stability factor (Tx-Tg)/Tg
Glass A	103	-	260	349	0.182
Glass B	519	-	260	338	0.148
Glass C	210	0.95	250	353	0.196
Glass D	343	1.95	241	325	0.163

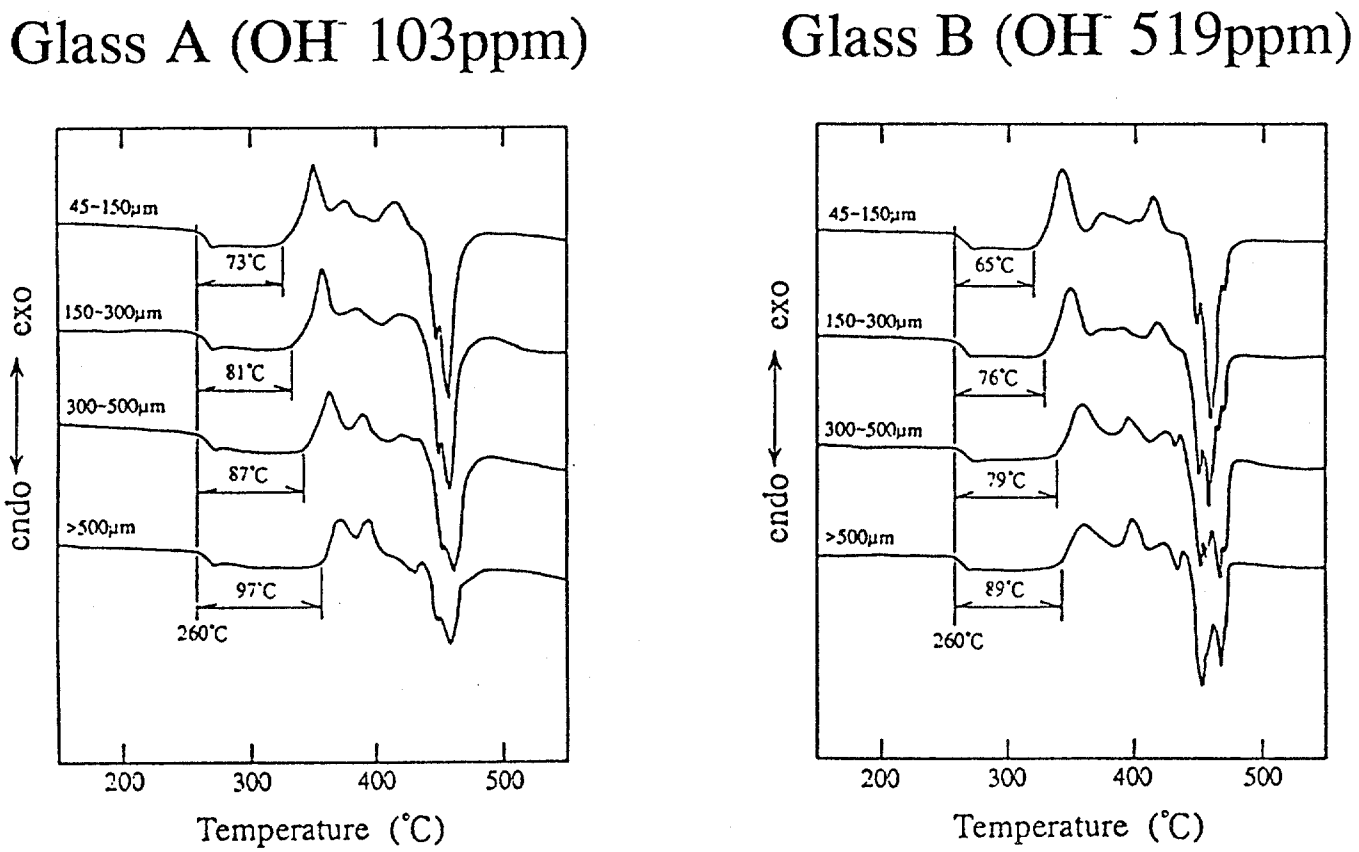

Fig. 5-1 DTA traces of the sample glasses with different grain size. The heating rate was 10K/min and the atmosphere was controlled by dry N_2 gas flow.

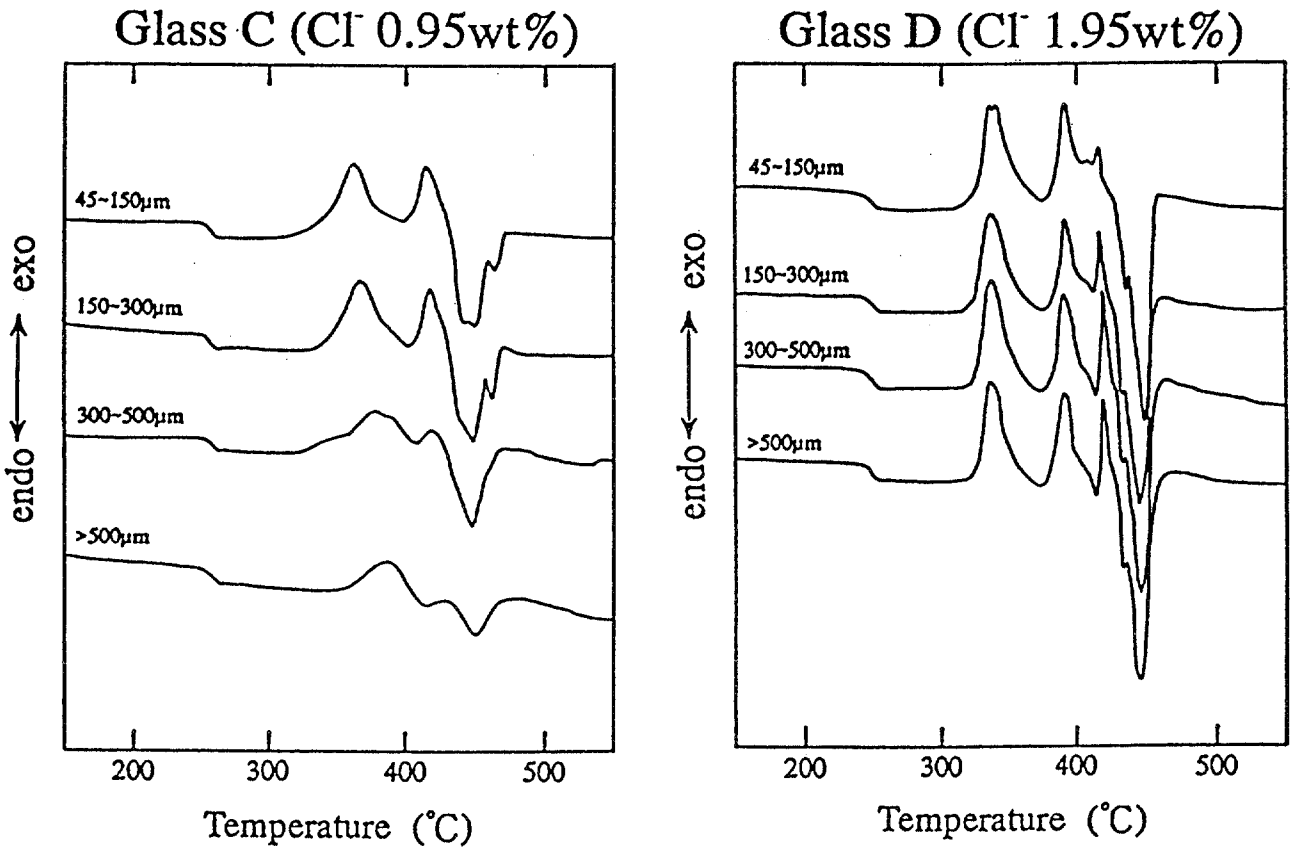
Glass C (Cl⁻ 0.95wt%)
45~150μm
150~300μm
300~500μm
>500μm
endo
exo
200
300
400
500
Temperature (°C)
Glass D (Cl⁻ 1.95wt%)
45~150μm
150~300μm
300~500μm
>500μm
endo
exo
200
300
400
500
Temperature (°C)

Table 5-4 The summary of the crystalline phases detected in heat-treated samples.

Glass A (OH^- 103ppm)

Temp	α-BZ	β-BZ	β-BZd	α-BZ2	β-BZ2	N7Z6
340℃	ND	D	D	D	D	D
350℃	ND	D	D	D	D	ND
360℃	ND	D	ND	D	D	ND
370℃	ND	ND	D	D	D	ND
380℃	ND	ND	D	D	D	D

Glass B (OH^- 519ppm)

Temp	α-BZ	β-BZ	β-BZd	α-BZ2	β-BZ2	N7Z6
330℃	ND	D	D	D	ND	ND
340℃	ND	D	D	D	ND	ND
350℃	ND	D	D	D	ND	ND
360℃	ND	D	D	D	ND	ND
370℃	ND	D	D	D	D	D
380℃	ND	D	D	D	D	D
390℃	ND	D	D	D	D	D
400℃	ND	D	D	D	D	D

α-BZ :α-$BaZrF_6$

α-BZ_2:α-$BaZr_2F_{10}$

N_7Z_6 :$Na_7Zr_6F_{31}$

β-BZ :β-$BaZrF_6$

β-BZ_d:disordered phase of β-BZ

β-BZ_2: β-$BaZr_2F_{10}$

Table. 5-4 The summary of the crystallinephases detected in heat-treated sample

Glass C (Cl^- 0.95wt%)

Temp	α-BZ	β-BZ	β-BZd	α-BZ2	β-BZ2	N7Z6
340℃	ND	D	D	D	D	D
350℃	ND	D	D	D	D	D
357℃	ND	D	D	D	D	D
363℃	ND	D	D	D	D	D
381℃	ND	D	D	D	ND	D
390℃	ND	ND	D	D	ND	D

Glass D (Cl^- 1.95wt%)

Temp	α-BZ	β-BZ	β-BZd	α-BZ2	β-BZ2	N7Z6
305℃	D	ND	D	ND	ND	ND
314℃	D	D	ND	ND	ND	ND
320℃	D	D	ND	ND	ND	ND
333℃	D	D	ND	ND	ND	ND
349℃	D	D	D	ND	ND	ND
370℃	D	D	ND	ND	ND	ND

α-BZ :α-$BaZrF_6$

β-BZ :β-$BaZrF_6$

β-BZd:disordered phase of β-BZ

α-BZ_2:α-$BaZr_2F_{10}$

β-BZ_2: β-$BaZr_2F_{10}$

N_7Z_6 :$Na_7Zr_6F_{31}$

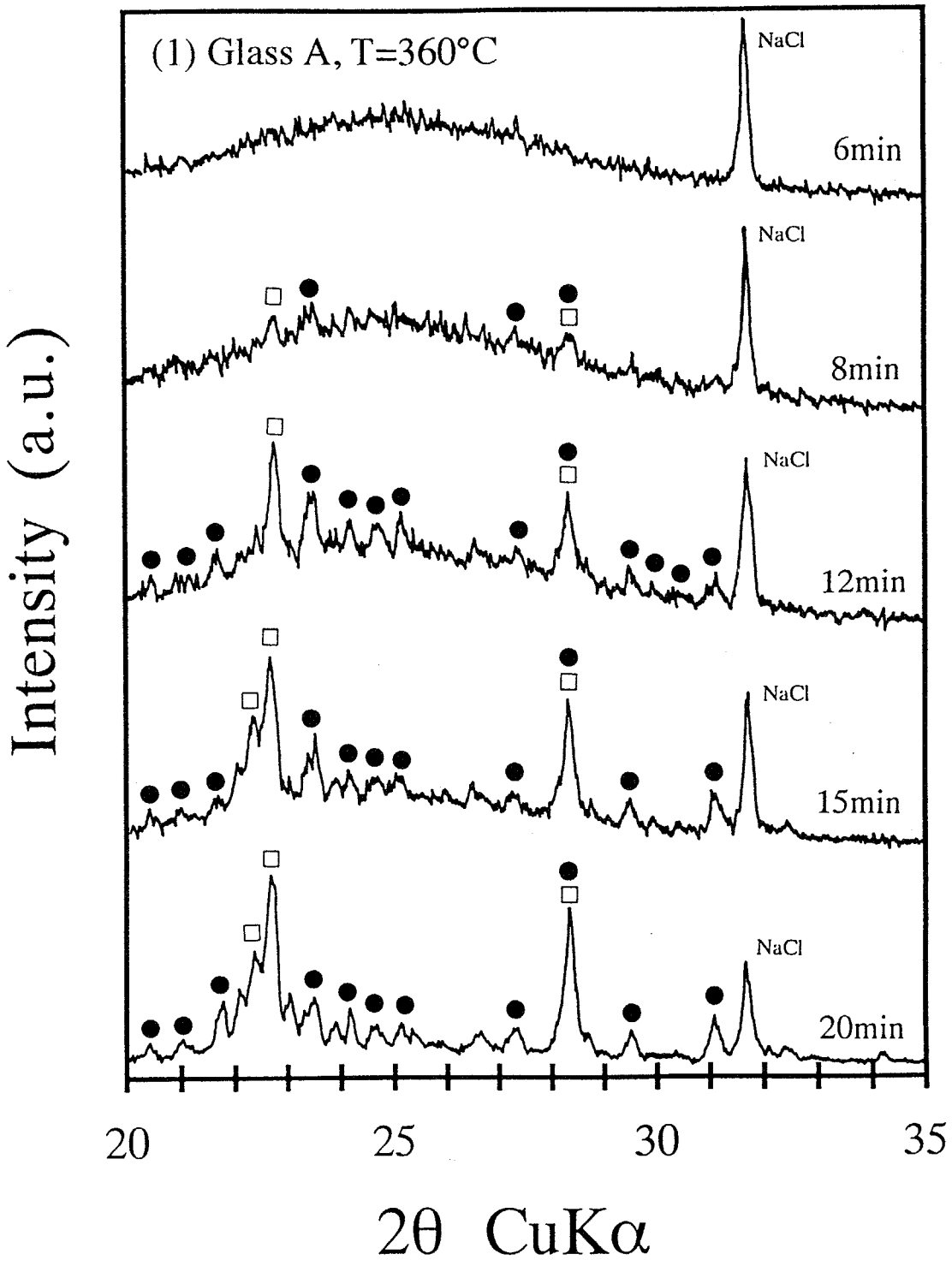

Fig. 5-2 The examples of XRD powder patterns obtained for the heat-treated samples of the respective glasses of (1) Glass A, (2) Glass C and (3) Glass C, respectively.

■: α-$BaZrF_6$, □: β-$BaZrF_6$, ○: α-$BaZr_2F_{10}$, ●: β-$BaZr_2F_{10}$, △: $Na_7Zr_6F_{31}$

×: Unknown

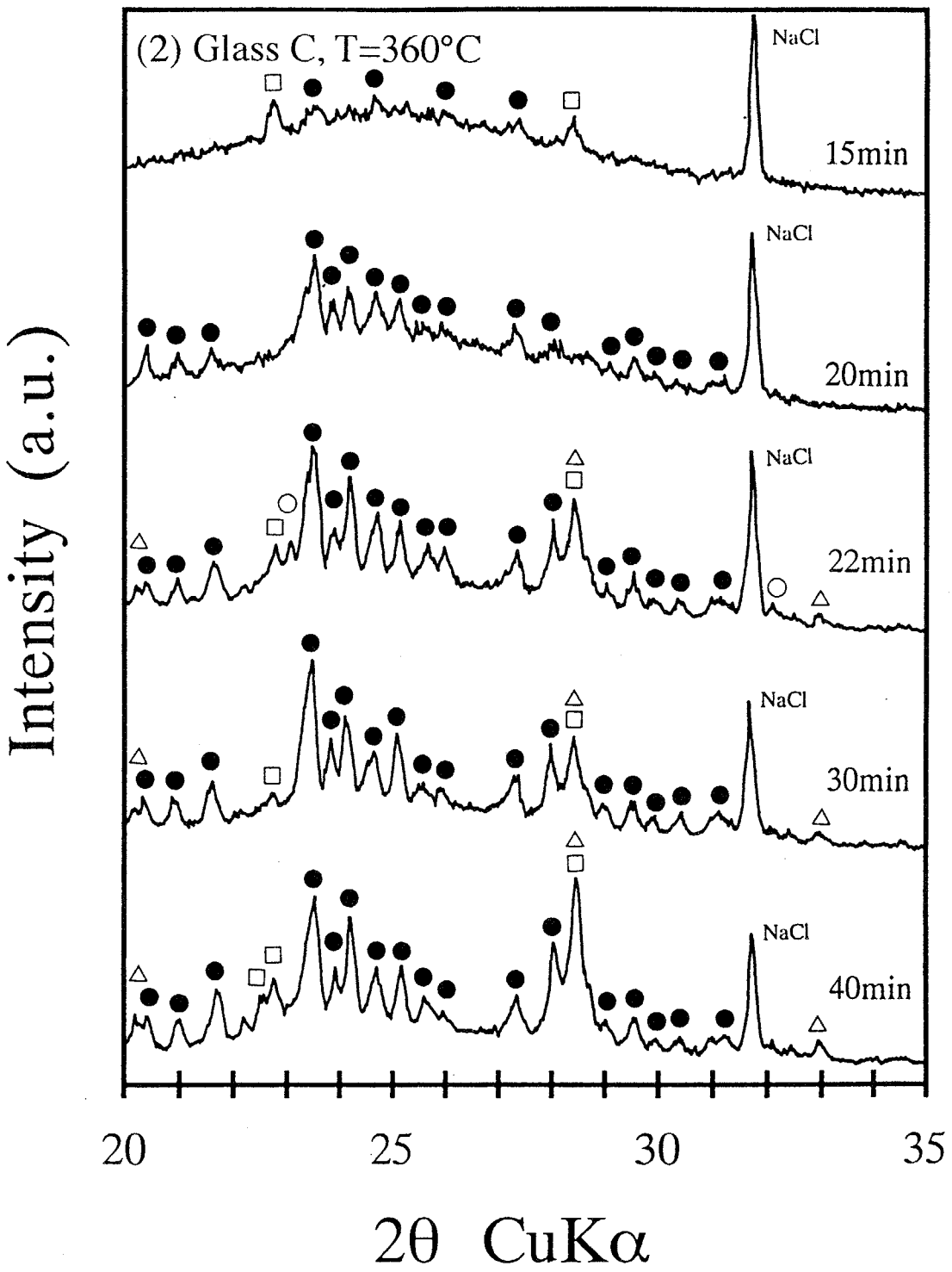

■: α-$BaZrF_6$, □: β-$BaZrF_6$, ○: α-$BaZr_2F_{10}$, ●: β-$BaZr_2F_{10}$, △: $Na_7Zr_6F_{31}$

×: Unknown

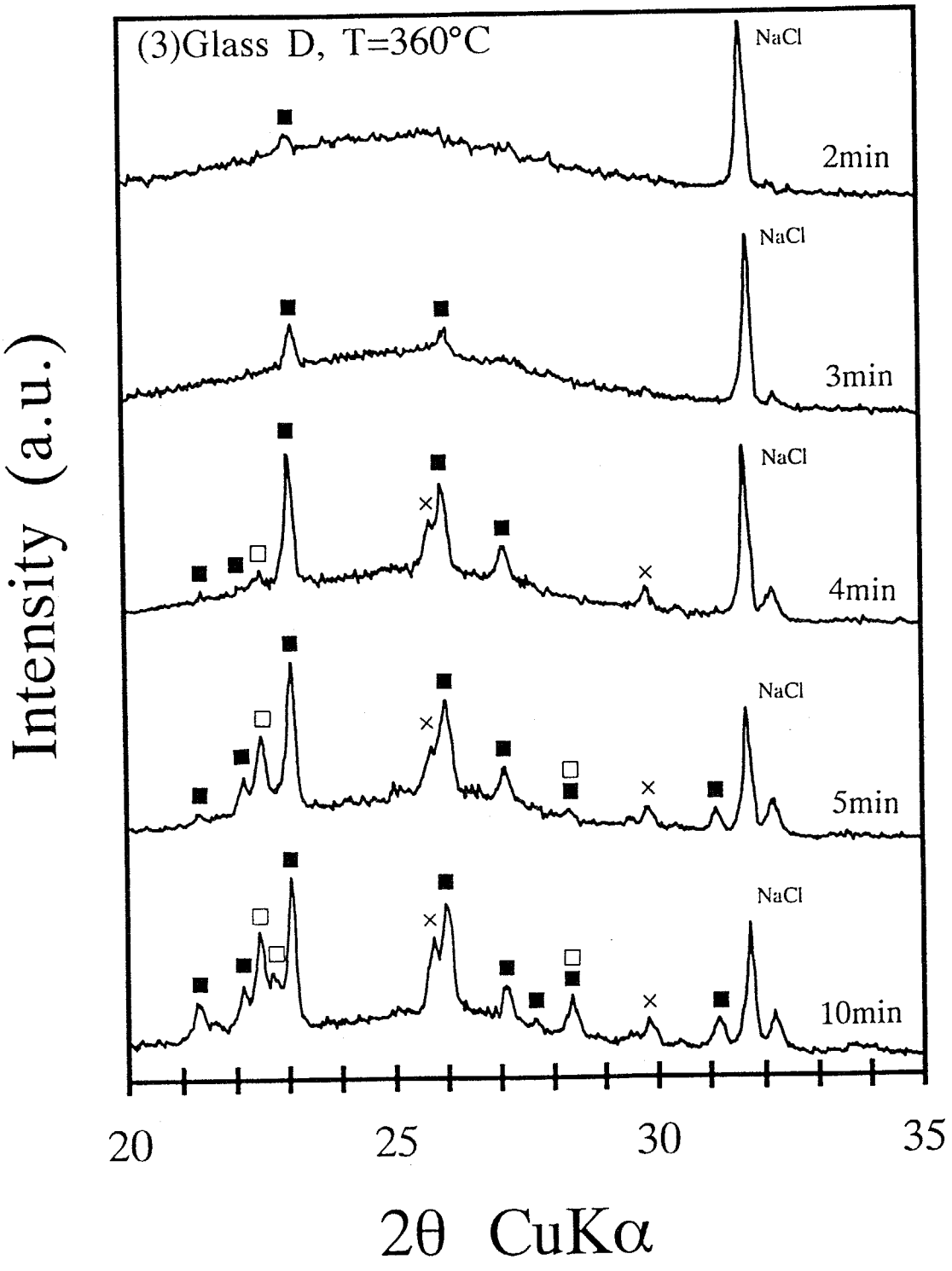

■: α-$BaZrF_6$, □: β-$BaZrF_6$, ○: α-$BaZr_2F_{10}$, ●: β-$BaZr_2F_{10}$, △: $Na_7Zr_6F_{31}$

×: Unknown

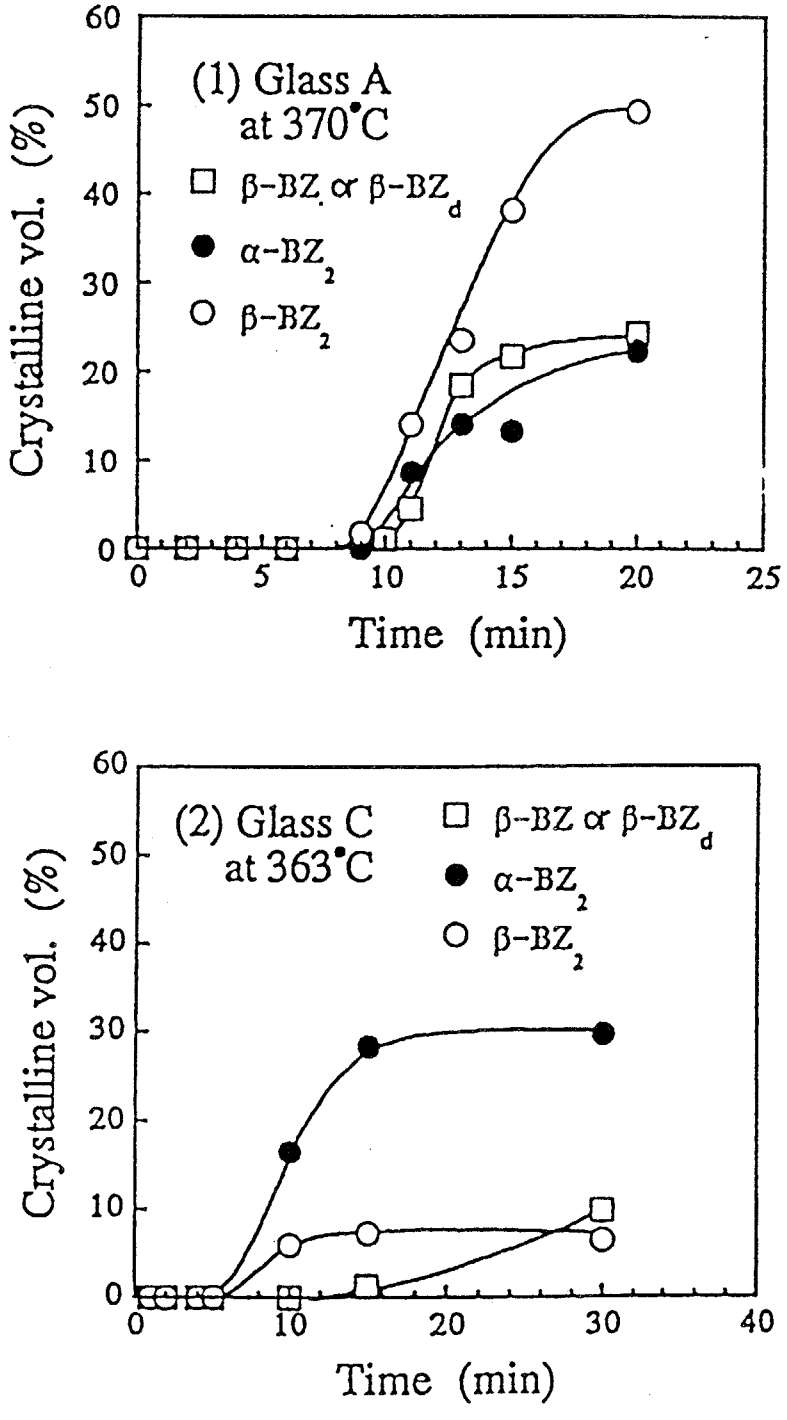

Fig. 5-3 Examples of the crystalline growth curves of (1) Glass A and (2)Glass C, respectively.

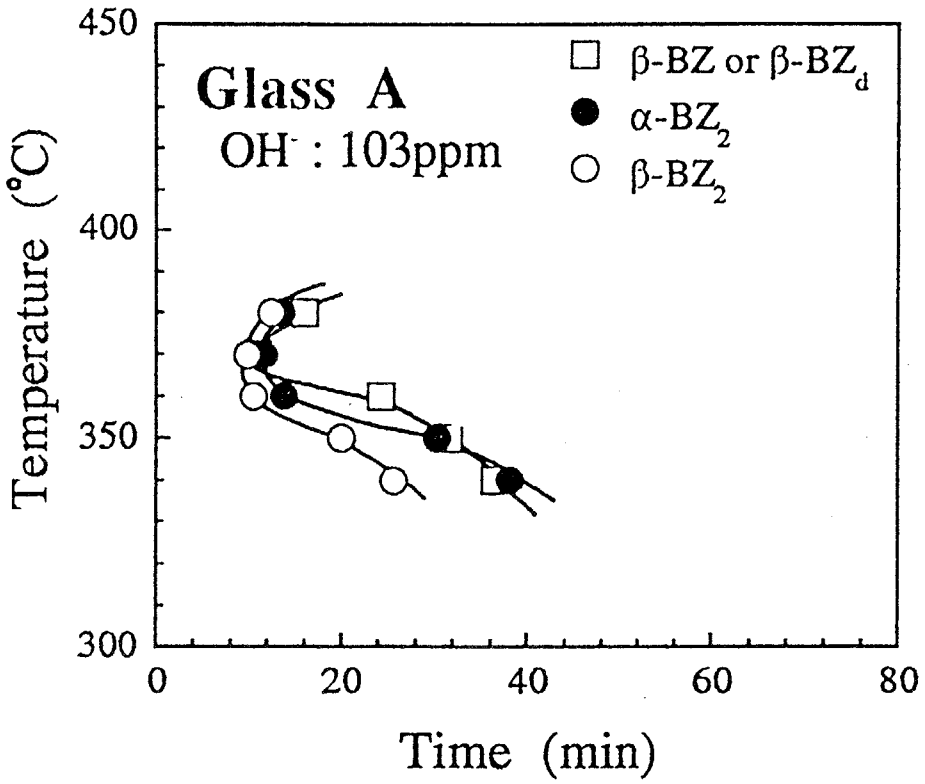

(1)

Fig. 5-4 The time-temperature relation of the development of the precipitating crystalline phases. (1)Glass A, (2)Glass B, (3) Glass C and (4)Glass D.

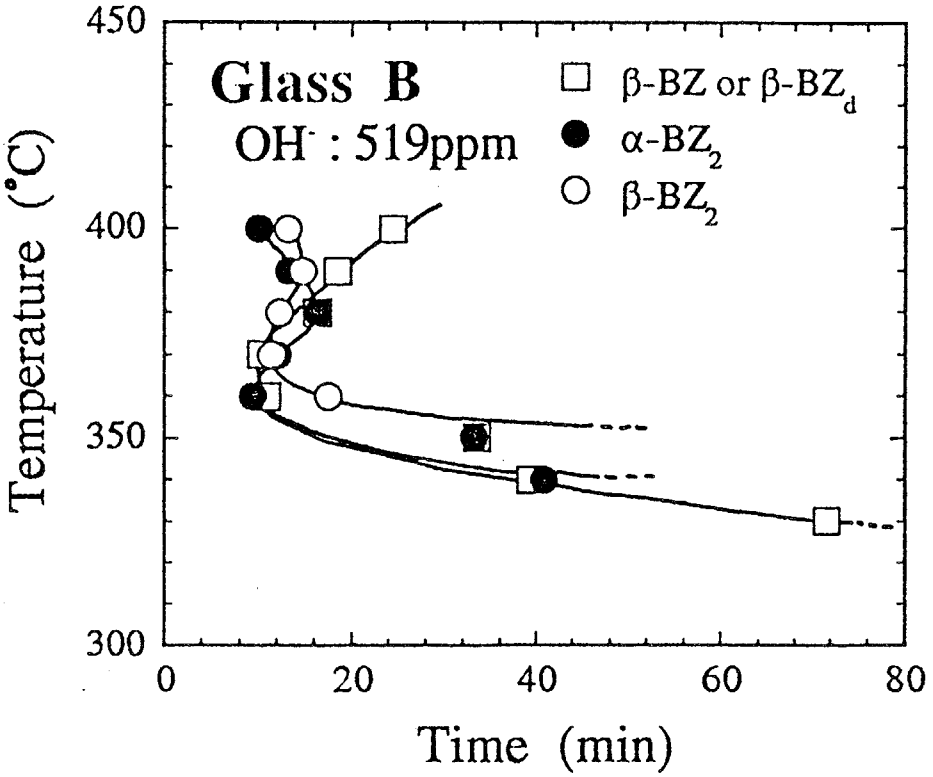
Glass B
OH⁻ : 519ppm
β-BZ or β-BZd
α-BZ2
β-BZ2
Temperature (°C)
450
400
350
300
0
20
40
60
80
Time (min)

(2)

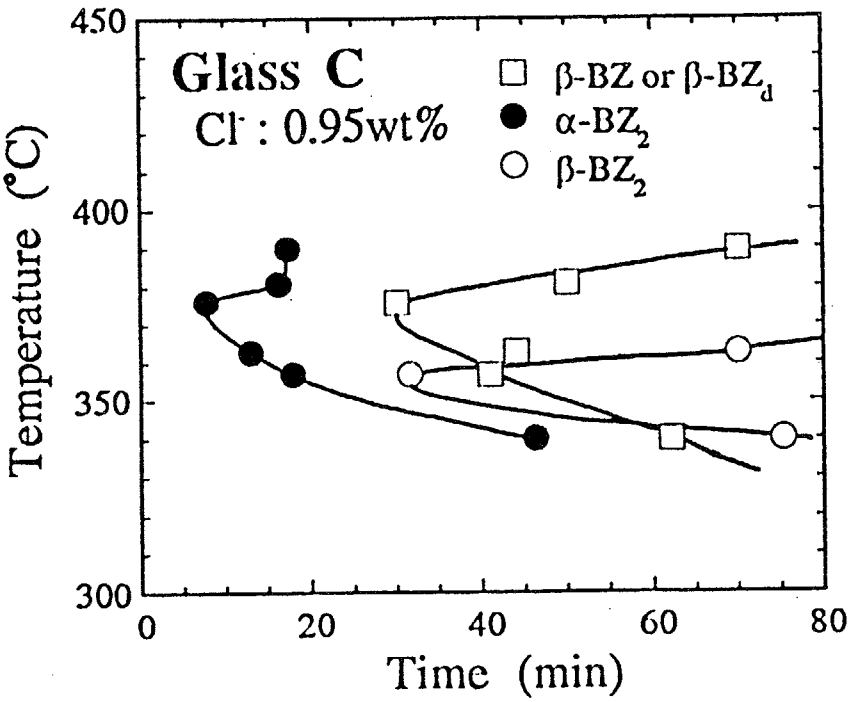
Glass C
Cl⁻ : 0.95wt%
β-BZ or β-BZd
α-BZ2
β-BZ2
Temperature (°C)
Time (min)
450
400
350
300
0
20
40
60
80

(3)

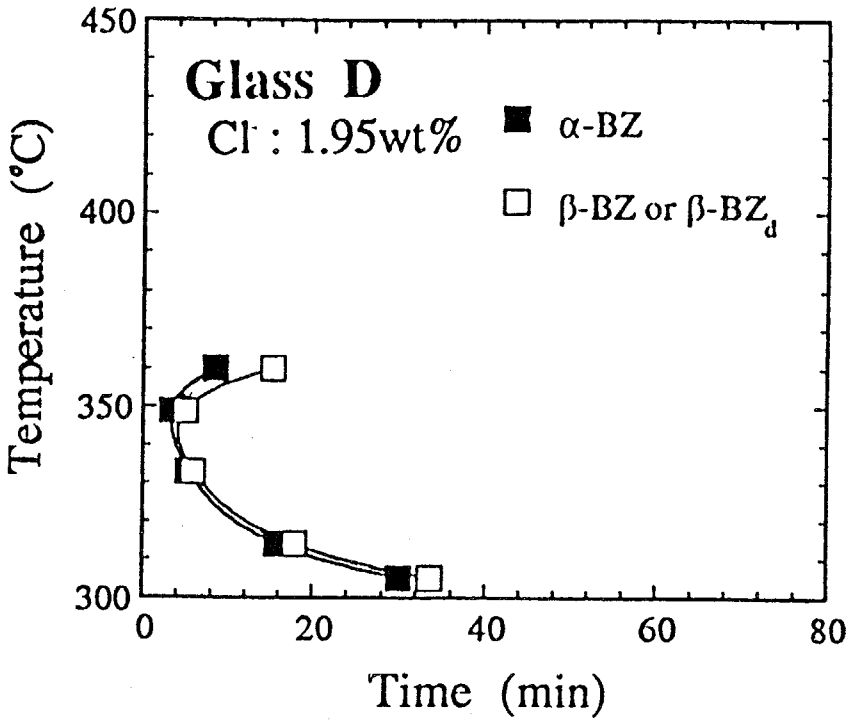
Glass D
Cl : 1.95wt%
α-BZ
β-BZ or β-BZd
Temperature (°C)
450
400
350
300
0
20
40
60
80
Time (min)

(4)

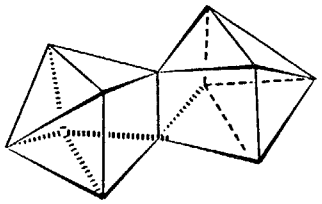

α-$BaZrF_6$

mono-capped trigonal prism

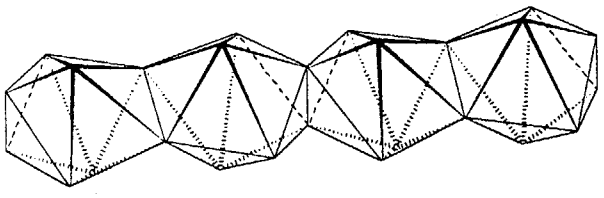

β-$BaZrF_6$

dodecahedron

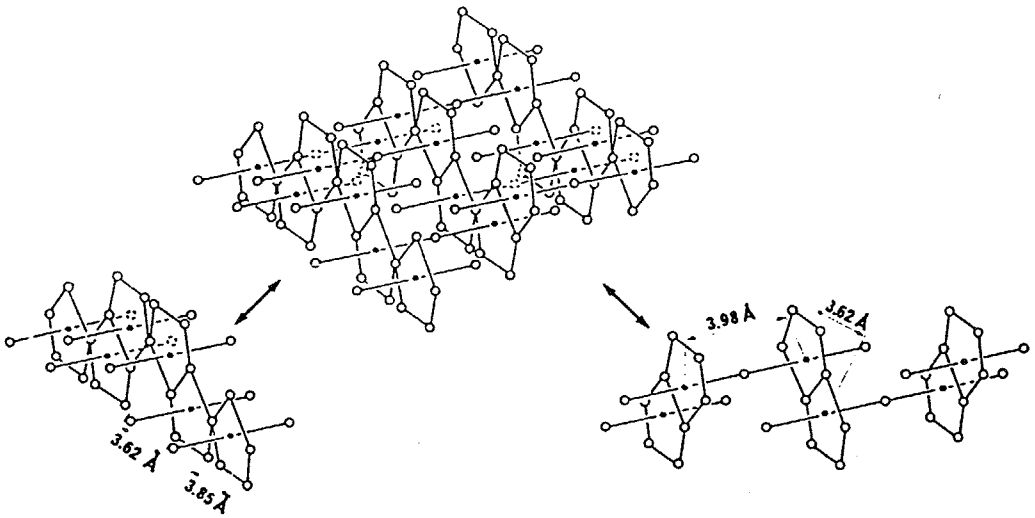

β-$BaZr_2F_{10}$

pentagonal-bipyramid

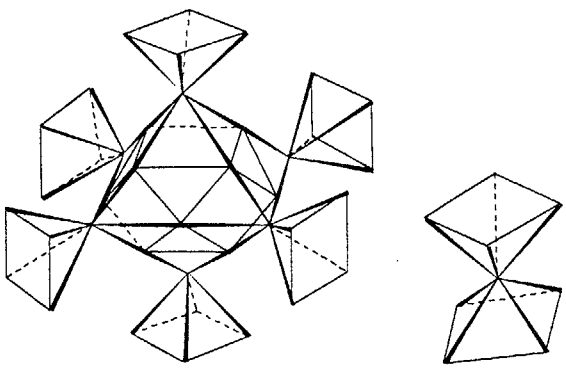

$Na_7Zr_6F_{31}$

square anti-prism

Fig. 5-5 The flame structures ZrF_n polyhedra found in the respective crystals. In case of a-$BaZr_2F_{10}$, there is no strict data of its structure.

CHAPTER 6

THE EFFECT OF CHLORINE ION ON GLASS FORMING ABILITY AND THERMAL STABILITY OF YABC MELT

6-1. INTRODUCTION

AlF_3-based fluoride glass systems like YF_3-AlF_3-BaF_2-CaF_2, are known to show some characteristic properties that are not observed in ZrF_4-based system; higher optical transparency in UV region, low refractive index and low dispersion, low non-linear refractive index, and the higher chemical durability [1]. The last one was reported to be 3 orders of magnitude higher than that of ZrF_4-BaF_2-based glasses like ZBLAN system. This feature is considered to be fascinating to apply this material to the optical devices. However, difficulties to prepare the glass with large dimension and high optical quality have prevented its developments in the optical application. Compared with ZrF_4-based system, the efforts to improve the glass forming ability of AlF_3-based systems have been made by only a few researchers. YF_3-AlF_3-MF_2 system is one of the most representative, where M means the alkaline earth ions. Kanamori et al. [2] extensively investigated this glass system and reported the wide glass forming region in YF_3-AlF_3-BaF_2-CaF_2 components. However, the glass forming ability was considered to be not high enough to apply it in the practical use even at the central point of its region. The most easy way to improve it is the addition of the other glass forming progenitors like ZrF_4, HfF_4, ThF_4 etc., but they have some negative factors like lower chemical durability, radioactivity,

and so on. In addition to the glass forming ability, the thermal stability should be one of the most important factors in the glass preparation. For instance, in the forming process of the fibre preform and the fiber drawing process [4], the higher thermal stability is indispensable to realize the highest optical properties. In order to improve the glass forming ability and thermal stability, the multiplication of the fluoride compounds have been carried out in almost of fluoride glass systems, but as shown in CHAPTER 5, chlorine introduction improved the thermal stability and dynamically changed the crystallization behaviors of ZBLAN glass system. This results revealed that chlorine could play as the additives to control the precipitating crystalline phases and their behaviors. In this CHAPTER, the incorporation of chlorine into YF_3-AlF_3-BaF_2-CaF_2 system are carried out and its effects on the glass forming ability and the thermal stability of melts are investigated. The several properties are discussed from the view point of the connectivity of the structural units of the melt.

6-2. EXPERIMENTAL

A. Glass Preparation

The based glass composition was $20YF_3$-$40AlF_3$-$xBaCl_2$-$(20-x)BaF_2$-$20CaF_2$ in mol%, where x was varied from 0 to 10 as shown in Table 6-1. Fig. 6-1 shows the flow of the sample preparation. The 20 g raw materials from YF_3, AlF_3, $BaCl_2$, BaF_2, and CaF_2 (>99.9% purity, Rare Metallic co.) were mixed and melted with a glassy carbon crucible at 1000°C for 2 h under dry Ar atmosphere (>99.9995%). The melts was poured into the pre-heated carbon mold, annealed for 30 min at glass transition temperature and then cooled down to the room temperature at a rate of 2 K/min. The sample thickness in the mold was changed from 5 mm

to 10 mm depending on the glass forming tendency. In the survey results, other chloride starting compound, $CaCl_2$ was also used but any difference could not be observed with in the case of $BaCl_2$. The chlorine content remaining in the glass was analyzed by Ion-electrode measurement.

B. Density, Thermal Expansion Coefficient and Refractive Index measurements

The glass density values were obtained the weight and the dimension of the cubic glass samples. Thermal expansion coefficients were measured by using the sample with dimension of 3x3x10mm at the heating rate of 5 K/min. Refractive index at Na-d line (587.56 nm) were measured by Pluflich method (CARL ZEISS JENA, PR2).

C. Thermal Properties and Critical Cooling Rate Measurements

The thermal stability and the glass forming ability were evaluated by using thermal analysis. Differential thermal analysis (DTA) was carried out against bulk samples of the obtained glasses at the heating rate of 10 K/min under dry N_2 flow. The thermal stability factor was calculated from glass transition temperature T_g, and onset temperature of the first crystallization T_x.

$$S=(T_x-T_g)/T_g$$

The glass forming ability was estimated from the critical cooling rate obtained by the rate cooling method of DTA measurement. Fig. 6-2 shows the example traces for C-0.0 samples. The critical cooling rate, R_c was obtained from the equation,

$$\ln R = \ln R_c - B/\Delta T^2$$

where R is the cooling rate, B is a constant and ΔT is the temperature difference between liquidus temperature T_l and onset temperature of crystallization under cooling T_c.

D. Viscosity Measurement

Viscosity near glass transition temperature ranging 10^8-10^{12} poise was measured by using penetration method. The apparatus was calibrated in advance by NBS710 standard glass and the measurements for the fluoride glass samples were carried out under dry N_2 gas flow.

E. Heat Treatment for Crystallization

In order to observe the changes in the crystallization behavior, DTA measurement against the glass samples and X-ray Diffraction measurement for the isothermally heat-treated samples at the peak temperature of the first crystallization. In DTA measurements, the surface crystallization effect was estimated by using the sample glasses with various grain size. The heating rate was 10 K/min and the dry N_2 gas was flowed during measurement. In the later measurement, the sample glasses were cut and polished into the size of 5x5x2mm^3 and introduced directly into the furnace held at T_p under dry N_2 atmosphere. After 4-6 min heat-treated, the sample glasses were quenched down to the room temperature. X-ray diffraction patterns were recorded against the powder of the samples of which the surface crystallized parts were removed in advance by polishing, because the surface crystallization is efficiently influenced by the pre-treatment history and that prevents the investigation of the intrinsic crystallization behavior. Secondary Electron Microscopy (SEM) observation was also carried

out for the fractured surface, which was etched by 0.1N HNO_3 Aquarius solution for 90 sec.

F. Vibrational Spectroscopy Measurements

The IR spectra were recorded for the range of 400-4000 cm^{-1} and 10-500 cm^{-1} by using KBr pellet method (JASCO A-202 IR spectrometer) and Nujolle method (BIORAD FT-FIR spectrometer), respectively. Raman scattering measurement was also carried out for the bulk samples. 488 nm Ar^+ ion laser was used for the excitation. The scattered light was introduced into the 50 cm double-monochromator (JASCO CT-25ND) and detected by the photo-multiplier (Hamamatsu Photonics, R-446). The obtained spectra were corrected with the Bose-Einstein factor.

6-3. RESULTS AND DISCUSSION

A. Thermal Properties and Thermal Stability

Table 6-1 showed the composition of the starting batches and the resulted glass samples with the characteristic temperatures taken from DTA traces for bulk sample (>500 μm). In all samples, most of chlorine over 94% in the starting batch was remained in the glass in spite of 2 h melting at 1000°C. The dependence of the starting materials of chloride introduced was also examined by using $CaCl_2$, but any remarkable deference in the thermal properties was not observed. Generally, for the introduction of chlorine into the fluoride glasses, we have to take much care of its loss during melting. In all cations included in YABC glass, aluminum chloride compound has extremely higher vapor pressure; i.e. $AlCl_3$ sublimates

at 180°C [6]. This data predicts that most of chlorine should be lost during melting at 1000°C. However, the quite high chlorine content in the resulted glass is considered to be explained by the fact that $AlCl_3$ sublimates as Al_2Cl_6 dimer molecule. Even if $AlCl_4$ tetrahedra could be formed, dimerization would not easily occur, because the low concentration of chlorine. Furthermore, it is well known that the incorporation of chlorine into ZrF_4-based system is quite difficult, because the sublimation from the melt heavily occurs even in the case of low chlorine concentration. This reveals that chlorine would like to bond easily to Zr^{4+} ion, but Al^{3+} ions. The chlorine effects on the glass structure will be discussed later in detail, but the in AlF_3-based YABC glass, chlorine could be introduced with high controllability compared with ZrF_4-based systems. Fig. 6-3, 4 and 5 show the plots of density, refractive index n_d and thermal expansion coefficient, respectively. They revealed the linear dependency and the thermal expansion coefficients kept almost constant. Fig. 6-6 and 6-7 plotted the characteristic temperatures and the thermal stability factor, $(T_x-T_g)/T_g$ against chlorine concentration, respectively. The addition of chlorine decreased glass transition temperature T_g monotonously and showed minimum at near 4 anion%. More chlorine introduction in turn increased glass transition temperature showing another small minimum at 6.5 %. Generally, Metal-Chlorine bond strength is considered to be lower than those of M-Fluorine and the chlorine introduction would be expected to decrease glass transition temperature monotonously. In fact, according to the results about chlorine in ZrF_4-BaF_2-MF systems by Tatsumisago eta l. [7], T_g decreased with the chlorine introduction. In such a meaning, the addition of 4 anion% chlorine into YABC system would be critical point to change the glass structures. On the other hand, the onset temperature of 1st crystallization, T_x, and its peak temperature, T_c, showed maximum at

near 1 anion% chlorine incorporation and after that decreased linearly up to 7 anion%. This behavior about T_g and T_x reflected to the relation of thermal stability factor as shown in Fig. 6-7. The thermal stability maximized up to 0.18 at near 2.5 anion% chlorine addition. This value was comparable or higher than one of most stable fluoride glasses of ZBLA and ZBGA and ZBLAN which have $(T_x-T_g)/T_g$=0.10, 0.16 and 0.17-0.19, respectively [8]. This revealed that the appropriate incorporation of chlorine play a role of additive to improve the thermal stability of the glass against the crystallization. The large temperature difference of T_x-T_g~130K makes it easy to prepare the glass with larger dimension.

B. Critical Cooling Rate

Fig. 6-8 showed the results of the critical cooling rate measurement of the samples glasses of C-0.0, C-2.5, C-5.0 and C-7.5, respectively. The critical cooling rate was obtained from the interception of the linear fitting with ln R_C axis and is considered to be one of the most realistic index to evaluate the glass forming ability of melt. Fig. 6-9 plots R_C values against the concentration of chlorine incorporated. R_C value showed the remarkable chlorine concentration dependence having a minimum at near 2.0 anion% and resembles well with the thermal stability-chlorine relation. The obtained minimum values was under 30 K/min and lower than ZBGA of 40-70 K/min and ZBLA of 55 K/min glasses [8], which have been actually drawn into fibre. This means that the addition of the same amount chlorine established to maximize both of thermal stability and glass forming ability in this YABC glass system. According to the chlorine doping study in fluoro-zirco-aluminate glasses by Miura et al., [9] the thermal stability was maximized at the chlorine concentration different from one in R_c

minimum. Considering these results with the crystallization study for ZBLAN in CHAPTER 5, the critical chlorine concentration against ZrF_4 and AlF_3 systems are thought to be different in various properties.

C. Viscosity and Fragility Factor

Fig. 6-10 showed the viscosity-temperature relations of C-0.0, C-2.5, C-5.0 and C-7.5. samples in the region between 10^8 to 10^{13} poise. The plots of respective samples were well expressed by Arrhenius type equation in this narrow range. The activation energy of viscous flow E_η and normalized activation energy E_η/T_g were plotted in Fig. 6-11. The activation energy values showed slightly decreased up to 3.0 anion% and increased at 6 mol%. As mentioned in Sec. A, glass transition temperature showed the unique changes against chlorine concentration ; T_g turned to increase as chloride replacement exceeded about 4.0 anion%. The similar change in activation energy of viscous flow was considered to be related to this T_g changes and suggested that the structural change would occur in 4.0 anion% chlorine concentration range. On the other hand, E_η/T_g value showed the minimum at 2.0 anion% and had strong correlation with the critical cooling rate and the thermal stability. According to Angell's classification [10], E_η/T_g value has been considered as the fragility factor, which means the bending or steepness degree of the normalized viscosity-temperature relation. Although the changes in the fragility factor in chlorine doped YABC glass was small, only a small amount of chlorine certainly decreased the fragility of this glass melt and improved the glass forming ability. Such a same kind of behavior has been reported in the study of the comparison of ZBLA and ZBLAN glasses and also in CHAPTER 4. The decrease of the

fragility of the melt increases the liquidus viscosity and has some effect to suppress the nucleation and the growth of the crystallization.

E. Crystallization behavior

Fig. 6-12 showed DTA traces of the sample glasses, which was crushed into various grain size, respectively. The first exothermic peak due to the crystallization changed in both of peak position and broadness in different way depending on chlorine concentration. C-2.5(1.92 anion%) sample revealed the broadest and efficiently grain size dependent peak. The other feature was found in the changes of the endothermic peaks by crystalline melting. The chlorine addition induced one another endothermic peak at lower temperature ~670°C and the temperature range in which liquid and solid phase coexist was enveloped. The lower melting point was thought to deduce the under cooling of the melt during quenching and prevent the nucleation and growth of crystallization. As mentioned previous section, the fragility factor in C-2.5(1.92 anion%) glass was lowest and the liquidus viscosity was considered to become higher value. This seems to enhance the glass forming ability of melt and lower the critical cooling rate to vitrify. Figs. 6-13 and 6-14 showed the results of SEM observation and XRD measurements for the partly crystallized samples heat-treated at T_x, respectively. The SEM microphotographs reveal that the bulk crystallization rate was different among the samples while almost of the same amount of the surface crystallized. In the glass with highest glass forming ability and thermal stability, the nucleation of the crystallization was heavily suppressed and coincided very well with the results in DTA measurement. As shown in Fig. 6-14, the crystallizing phases inside the glass were changed by the chlorine incorporation. In the

sample C-2.5(1.92 anion%), the diffraction peaks relating to the AlF_3-based crystals disappeared or decreased. Different with ZBLAN glass treated in CHAPTER 5, it was too difficult to obtain the crystalline growth curves for the respective phases, because the diffraction peaks were very complex and several main peaks overlapped. However, qualitatively speaking, the chlorine has effects on the development of major phases of AlF_3 containing crystalline, and improved the glass forming ability of the melt. Fig. 6-15 illustrates the structural flames of AlF_6 units found in the metal-fluoroaluminate crystals. Their features are (i) only AlF_6 octahedra were found, (ii) the connection forms are efficiently dependent on metal ions and their amount, (iii) there is not found any edge sharing form. The former is quite different with those in ZrF_4-based systems, in which ZrF_n polyhedra can take 7 and 8 coordinates and the respective coordinate can also take the various stereochemistry. In contrast to them, AlF_3-based systems, aluminum ion can take only one stereochemistry and is considered to have lower degree of freedom in the structural unit. However, represented by feature (ii), they can construct various types of the structural flames and their connection forms are dependent on the metal of alkarine earth ions. In case of calcium ions, AlF_6 octahedra connect in the corner sharing manner of trans position, while in case of barium ions, the cis-corner bridging is dominant. In case of strontium ions, which is considered to be located at intermediate between calcium and barium ions, both of the trans-corner bridging and cis-corner branching are observed. These variations in the bridging manner would exist in the melt and reflect on the crystallization behaviors. According to the structural investigation of YAC glass system by X-ray diffraction and Molecular Dynamics simulation method by Akasaka et al. [11], there were some amount of isolated AlF_6 polyhedra in the glass and YF_n units play the role to

segregate AlF_6 units and prevent the formation of the larger flames. The observed chlorine effect on the crystallization behavior would be related well with the connectivity of AlF_6 polyhedra in the melt.

F. The Effect of Chlorine on the Glass Structure

Fig. 6-16 showed IR spectra of the glass samples by using KBr pellet method. The absorption at near 600 cm^{-1} could be assigned to the absorption by the stretching mode of Al-F bonds in AlF_6 octahedra and the most of aluminum ions were considered to form the octahedral units in every sample glasses. Any remarkable chlorine dependence was not be observed in their peak position, but their FWHM were slightly increased with the chlorine content. Fig. 6-17 showed the FIR absorption spectra and showing some chlorine dependences. The 370 cm^{-1} band became to show a clear peak with the chlorine content and there were small shoulders near 230 cm^{-1} and 150 cm^{-1}. Fig. 6-17 also included the absorption spectra of raw materials of AlF_3, $AlCl_3$ YF_3, and YCl_3 as standards. The measurements for chloride compounds especially taken care of the corroded by the moisture. As shown in their spectra, both Al-F and Y-F have the absorption peak at the same frequency range near 370 cm^{-1}. Comparing these spectra, the peak of AlF_3 compound was located at very similar wavenumber and AlF_n polyhedra seemed to be influenced apparently. However, as illustrated in Fig. 6-15, there should be a lot of terminated F ions in the glass and Al-F vibration frequency would be shifted to higher wavenumber, because the bond length of Al-F would be shorter than the bridging ones. These differences were also observed in ZrF_4-based glasses, revealing that the peaks can not be easily assigned by the comparison of the spectra of raw materials, i.e., in

AlF_3 compound, there is no terminated F ions in the structure and all Al-F bonds have the equal bond length of 1.79Å. However, little dependence in the absorption band at 600 cm^{-1} suggested that YF_n polyhedra were mainly affected by chlorine ions. Fig. 6-18 showed Raman spectra of the respective glass samples. They also revealed some dependence on the chlorine content. The peak at about 580 cm^{-1} broadened and shifted to lower frequency with the chlorine content. The relative peak intensity between 580 cm^{-1} and 410 cm^{-1} also changed with the chlorine incorporation. As same as IR spectra (Fig. 6-16), the peak at 570 cm^{-1} was mainly due to the Al-F stretching mode, but from selection rules, this Raman peak are mainly correlated with Al-F_{nb} vibrations. According to the Raman measurements of various alkaline earth fluoroaluminate crystals by Kawamoto et al. [12], this Raman peak around 580 cm^{-1} could be deconvoluted into three bands, one AlF_{nb} in $[AlF_6]^{3-}$ and two Al-F_{nb} in $[AlF_5]^{2-}$. The disagreement of the peak position with in IR spectra might be induced from the selection rules relating to the symmetry of the vibrational mode of AlF_n polyhedra and caused some complexity in the peak assignments as well as IR spectra. However, the consideration of the YF_n polyhedra would help to understand the changes in the Raman spectra. As reported by Zalkin et al. [13], YF_3 compound includes tricapped trigonal prism structure, in which one fluorine located at one of the three capped site has the longer Y-F bond length of 2.6Å compared with other 8 fluorine (2.3Å). This fact suggested that YF_n polyhedra would like to be influenced firstly and AlF_6 octahedra would not be directly affected by the chlorine ions. However, Y^{3+} ions play the important roles to segregate the AlF_n polyhedra linkages and to form the edge sharing with them, the appropriate chlorine could act to increase the potential barrier to the precipitation of AlF_3-based crystalline.

6-4. CONCLUSIONS

The chlorine effects on the glass forming ability and the thermal stability in the glass of $20YF_3$-$40AlF_3$-$20BaF_2$-$20CaF_2$ (in mol%), were investigated. Both of the glass forming ability and the thermal stability have been improved at the same chlorine incorporation. The critical cooling rate was reduced to under 30 K/min, and the thermal stability $(T_x-T_g)/T_g$ was improved up to 0.18. These values were equal or superior to ZrF_4-based glass systems, ZBLA (55 K/min, 0.16) and ZBGA (40-70 K/min, 0.10), which have been actually drawn into fibre. These values suggested that the chlorine doped YABC glass has much potential to the practical use.

The viscosity measurement revealed that the fragility of the melt was also improved by the appropriate chlorine incorporation. The steep change in the viscosity-temperature relation was relaxed and the liquidus viscosity increased, meaning that chlorine enforced the cooporativity of the structural flames in the glass melt.

The crystallization study revealed that the bulk crystallization was heavily suppressed, mainly the metal fluoroaluminate phases like β-$BaAlF_5$, β-$CaAlF_5$, γ-$BaAlF_5$. This mean that the additional potential barrier to form the characteristic structures of chain consisting from AlF_6 octahedra were induced by the chlorine and resulted in the higher glass forming ability.

The structural investigation by spectroscopic measurements suggested that the chlorine mainly affected YF_n polyhedra, which have the roles to segregate AlF_6 polyhedra to form chain structure and are linked with them by the edge sharing manner. The improvement found in the glass formation was considered to be caused by some indirect effect of chlorine on the network flame of AlF_6 units through Y^{3+} ions.

REFERENCES

[1] e.g., H. Hefang, L. Fengying, G. Donghong and L. Min, Mater. Sci. Forum, **5** (1985) 145 ; M. R. Shahriari, T. Iqbal, G. H. Sigel, Jr. and G. Merberg, Mater. Sci. Forum, **32&33** (1988) 99

[2] T. Kanamori, K. Oikawa, S. Shibata and T. Manabe, Jpn. J. Appl. Phys., **20** (1981) L326

[3] C. J. Simmons, J. Am. Ceram. Soc., **70** (1987) 295

[4] S. F. Carter, P. W. France, M. W. Moor, J. R. Williams and J. M. Parker, 91st Annual meeting of the Am. Ceram Soc., Indianapolis (18989)

[5] e.g., P. A. Tick reviewed about the non-Zr fluoride glasses in Mater. Sci. Forum, **32&33** (1988) 115

[6] K. Wade and J. Banister; in *Comprehensive Inorganic Chemistry*, vol. (19) p993

[7] M. Tatsumisago, Y. Akamatsu and T. Minami, Solid State Iones, **31** (1988) 41

[8] S. Mitachi and P. A. Tick, Mater. Sci. Forum, **32&33** (1988) 197 ; T. Kanamori and S. J. Takahashi, J. Appl. Phys, **24** (1985) 1758

[9] K. Miura, I. Masuda, M. Tokida and T. Yamashita, Mater. Sci. Forum, **32&33** (1988) 367

[10] C. A. Angell; in *Relaxations in Condensed Systems* , ed. K. Ngai and G. B. Wright, National Technical Information Service, U. S. Department of Commerce, Springfield, VA 22161 (1985) 1

[11] Y. Akasaka, T. Nanba, H. Inoue, T. Osuka and I. Yasui, J. Non-Cryst. Solids, **140** (1992) 249

[12] Y. Kawamoto and A. Kono, J. Non-Crysta. Solids, **85** (18986) 335

[13] A. Zalkin and D. H. Templeton, J. Am. Chem. Soc., **75** (1953) 2453

Table 6-1 The lists of the chlorine contents and the characteristic temperature of YABC glass samples. The blank means there is no available data.

Sample	Cl content in Batch (anion%)	Cl content in Glass (anion%)	Glass Transition Tg (℃)	Onset of Crystallzatiion Tx (℃)	Onset of Endotherm Tm (℃)	Liquidus Temperature Tl (℃)	ΔT= Tx-Tg
C-0.0	0.0	0.0	440	543	713	814	103
C-1.5	1.15	---	428	546	---	---	118
C-2.5	1.92	1.86	423	548	656	824.3	125
C-3.5	2.69	---	417	538	---	---	121
C-5.0	3.84	3.60	412	529	644	849	117
C-6.5	5.00	---	426	506	---	---	80
C-7.5	5.77	5.48	430	504	650	869	74
C-8.5	6.54	---	422	496	---	---	74
C-10	7.69	---	438	495	---	---	57

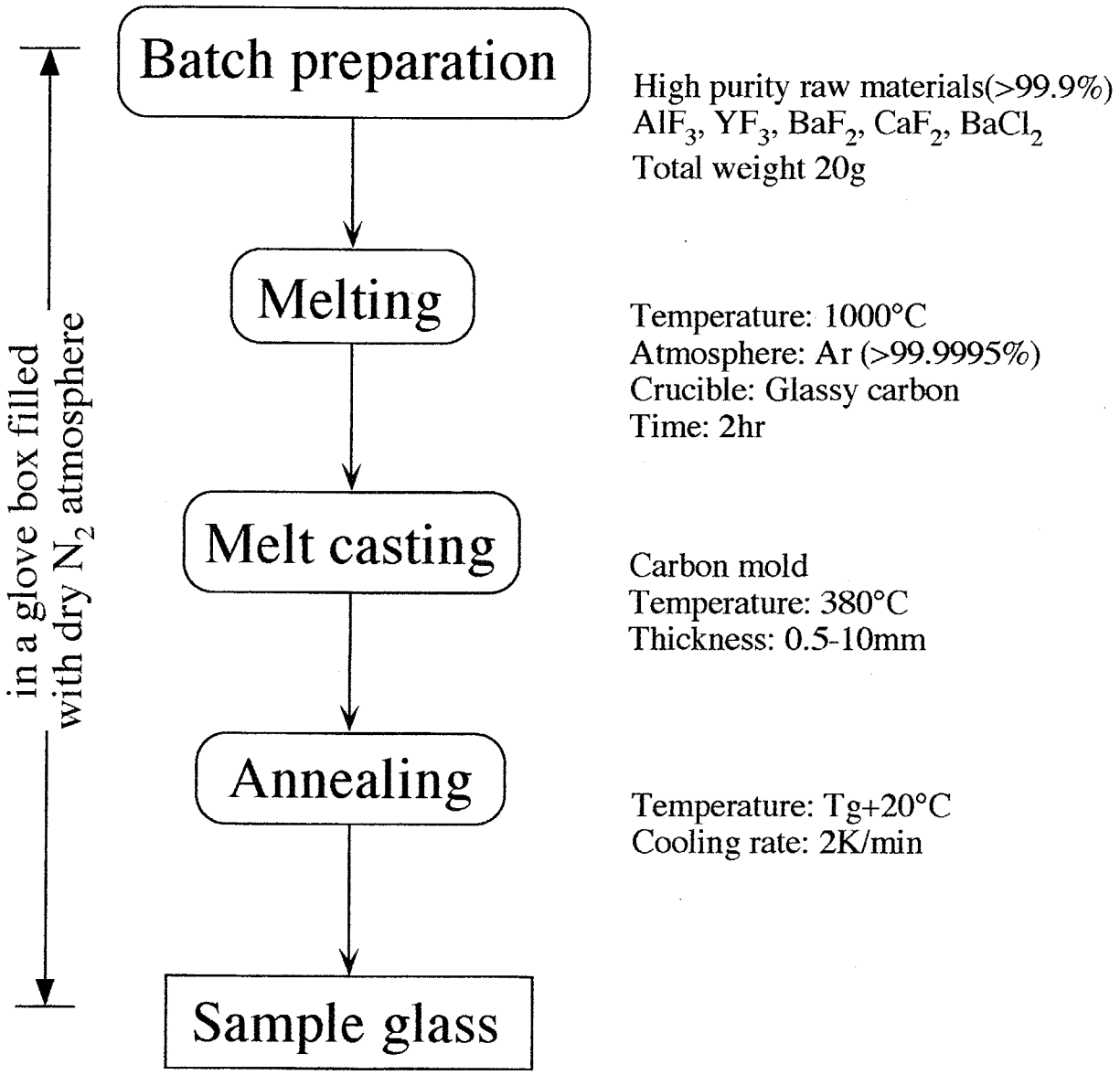

Fig. 6-1 Flow chart of the sample preparation.

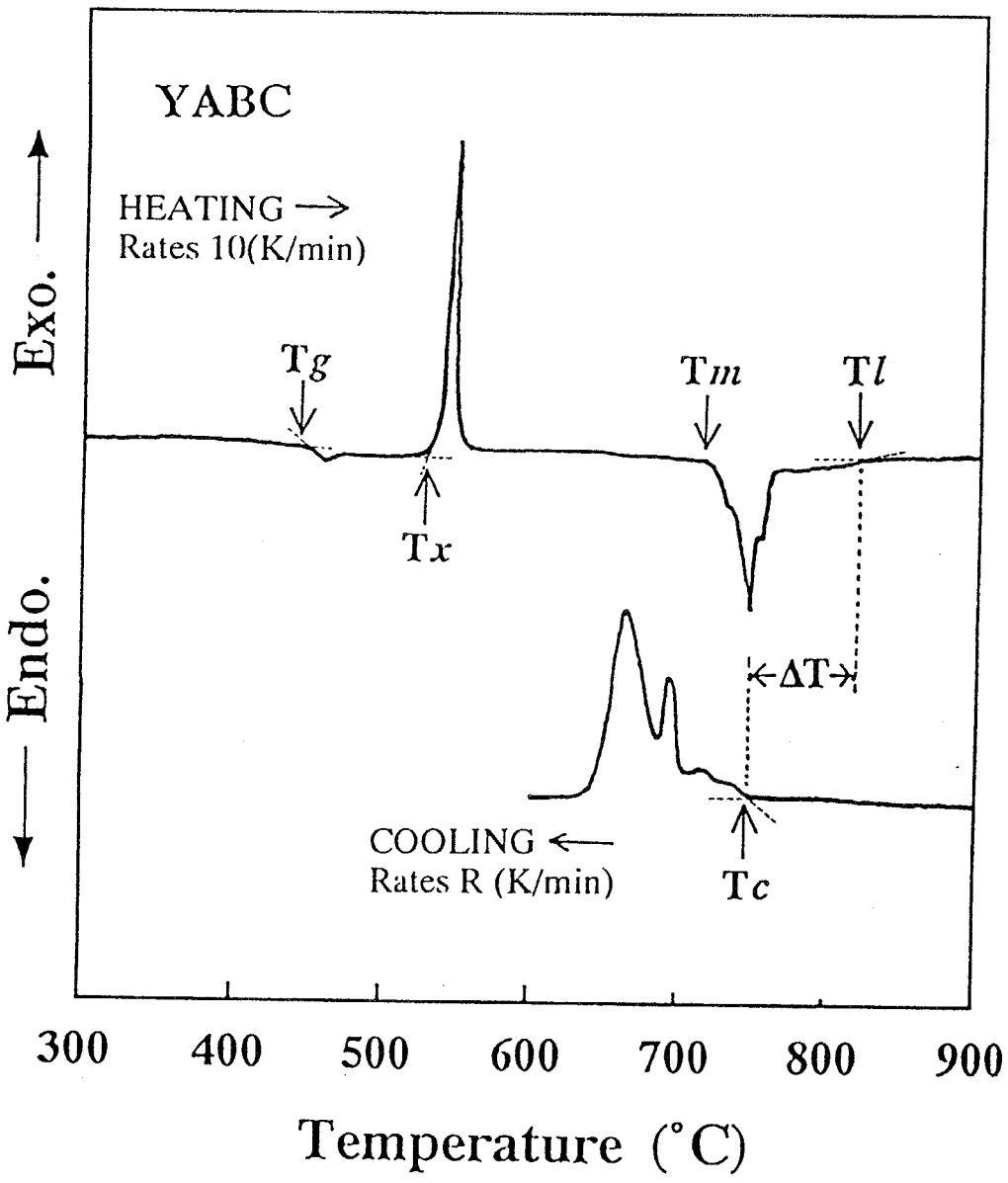

Fig. 6-2 Example of DTA traces used in the evaluation of the critical cooling rate R_c. Liquidus temperature was determined at the heating rate of 10K/min.

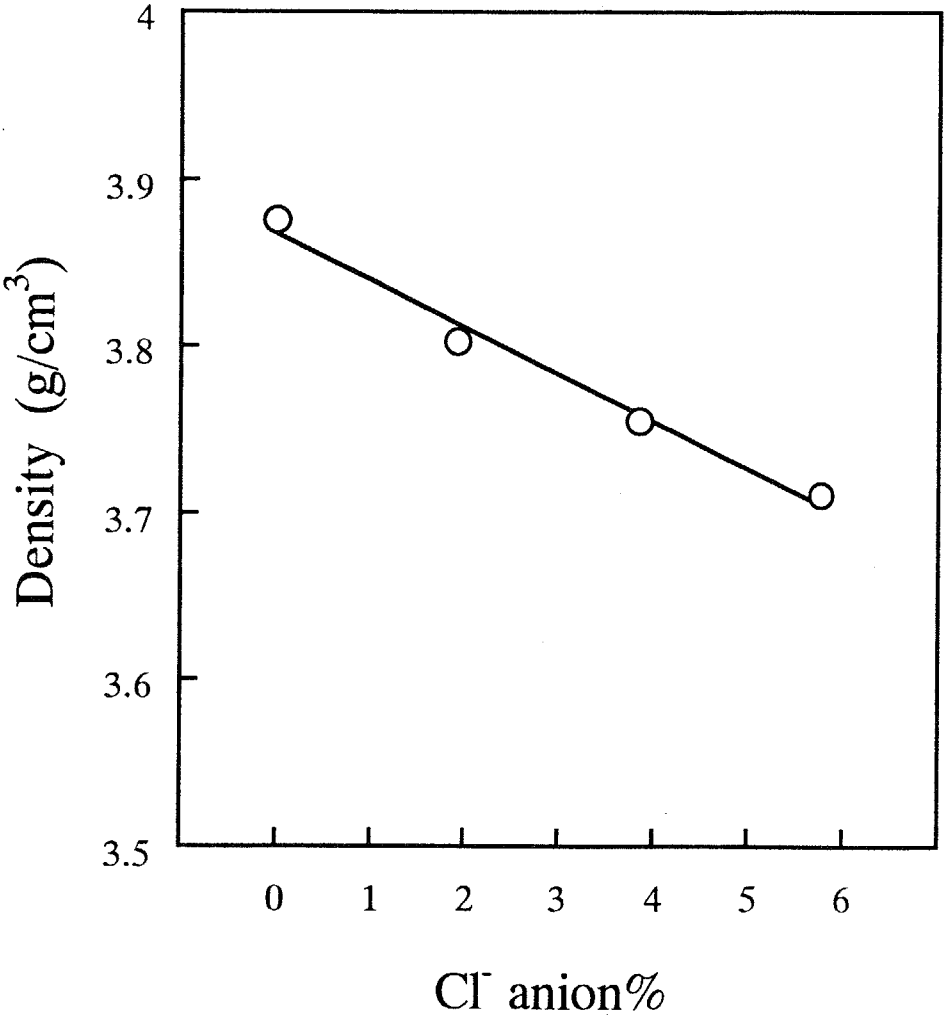

Fig. 6-3 The relation betwwn the glass density and the chlorine concentration.

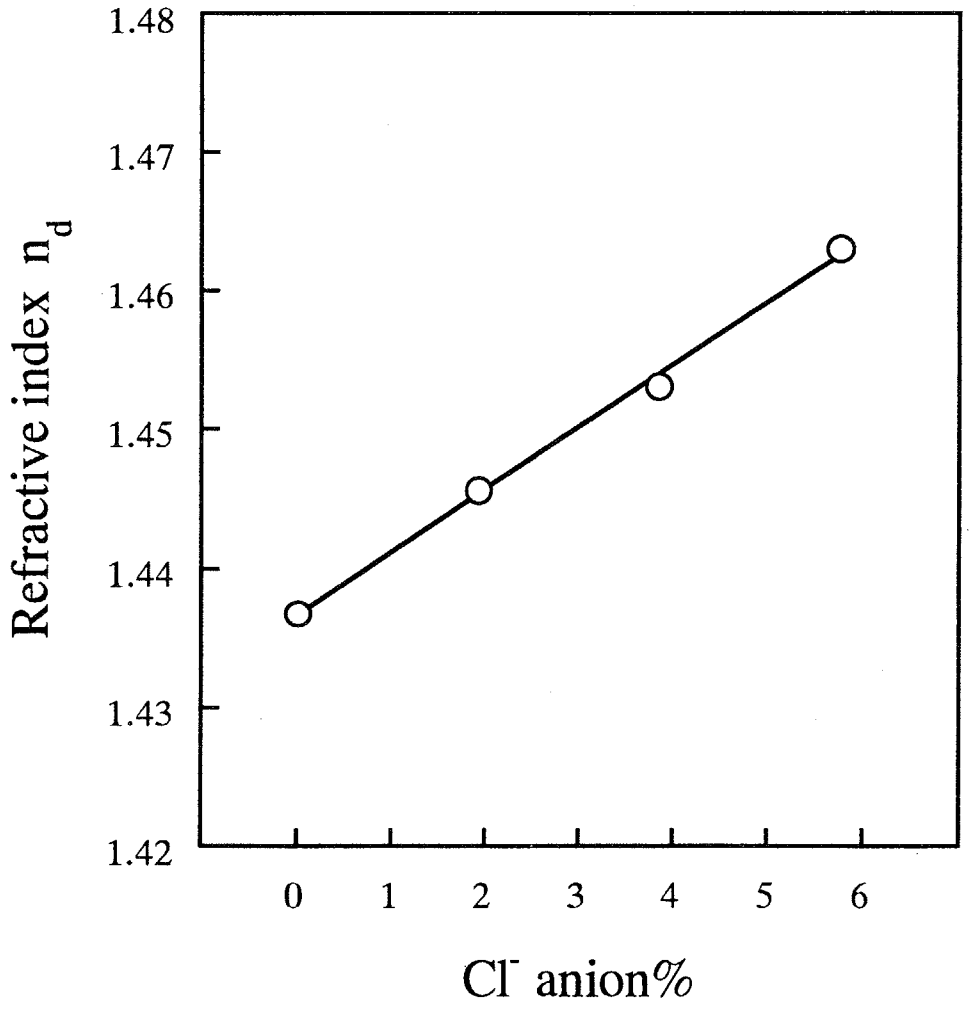

Fig. 6-4 The relation betwwn the refractive index n_d and the chlorine concentration in YABC glass.

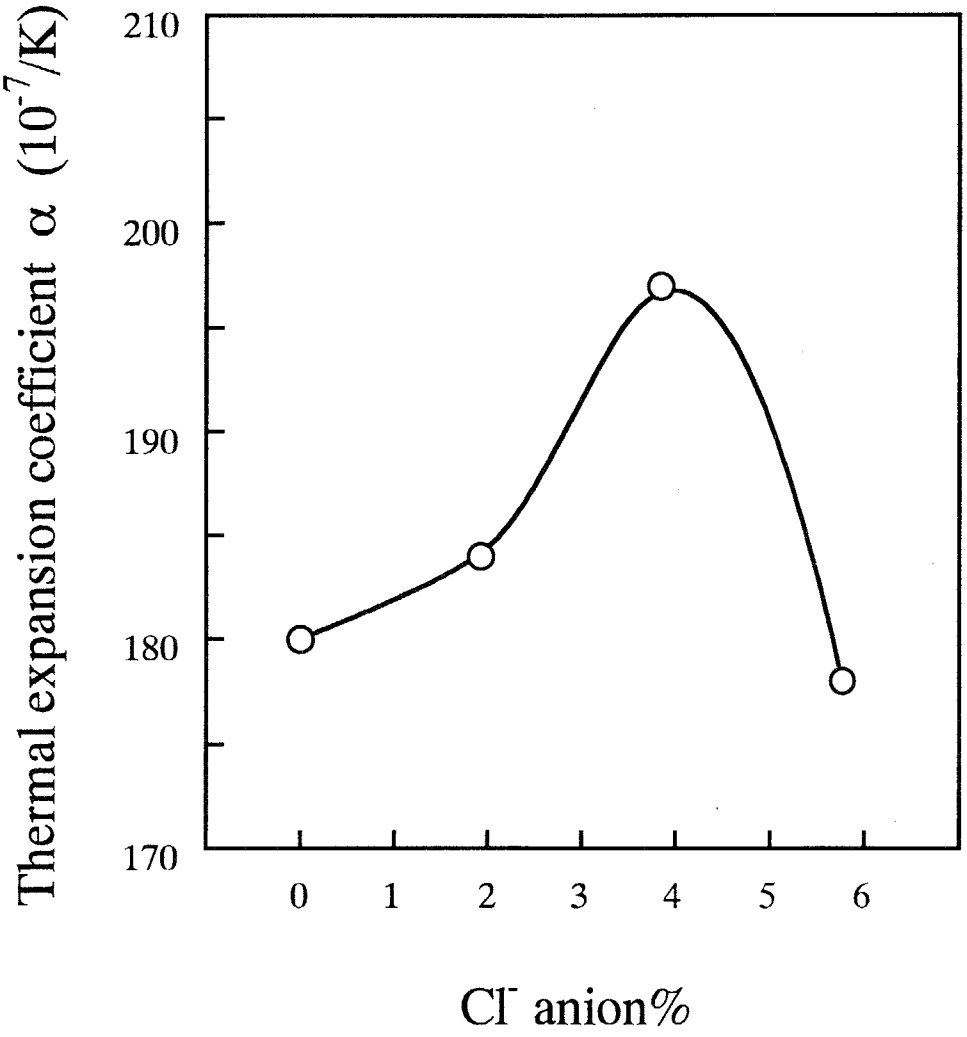

Fig. 6-5 The relation betwwn the thermal expansion coefficient and the chlorine concentration in YABC glass.

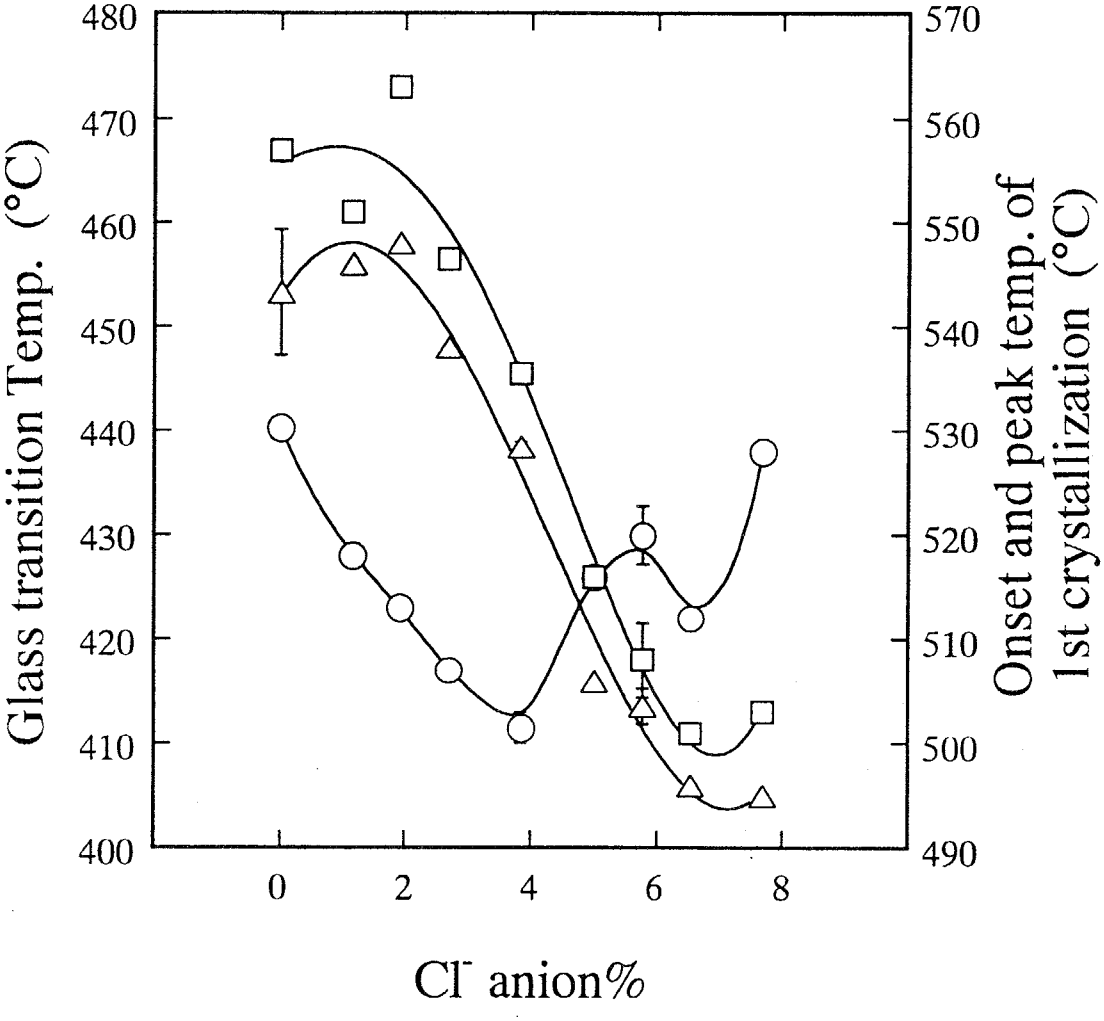

Fig. 6-6 Plots of the characteristic temperature of Tg, Tx and Tp against the chlorine content. The curves were drawn with the eye.

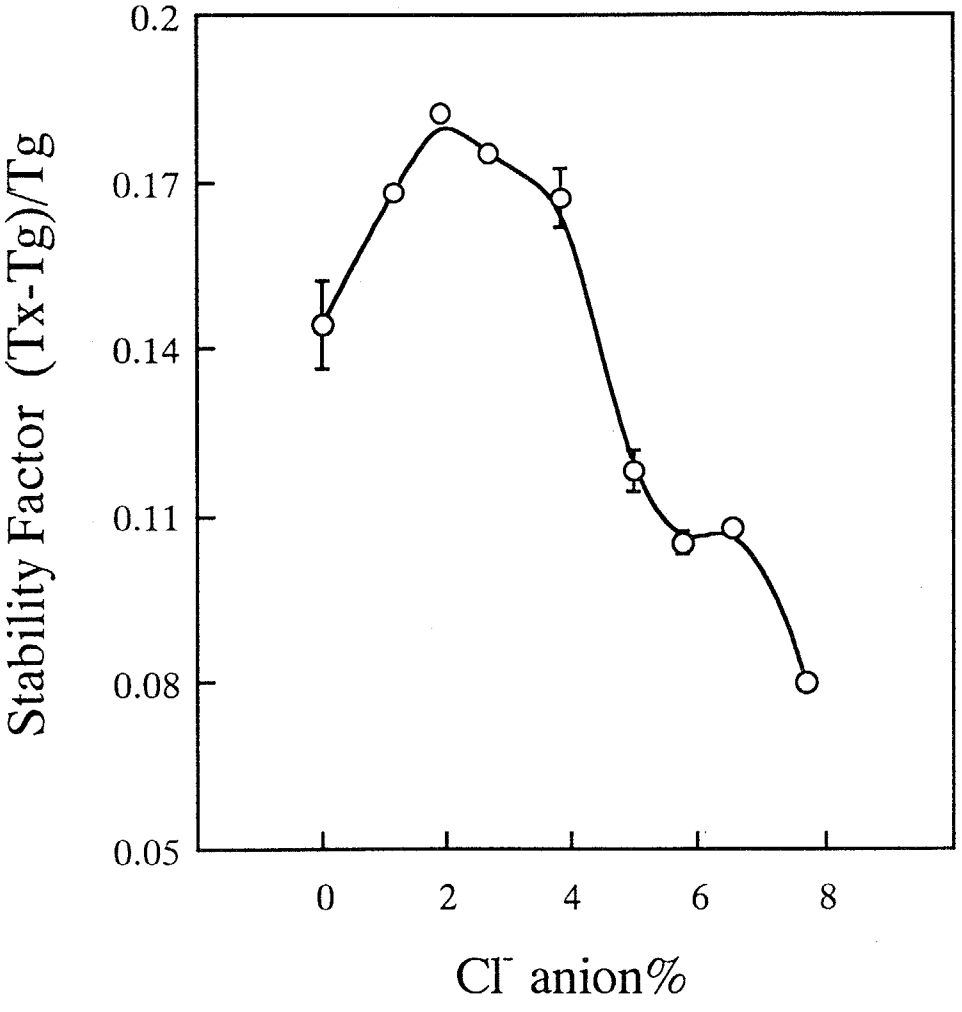

Fig. 6-7 Changes in stability factor (Tx-Tg)/Tg against chlorine content.

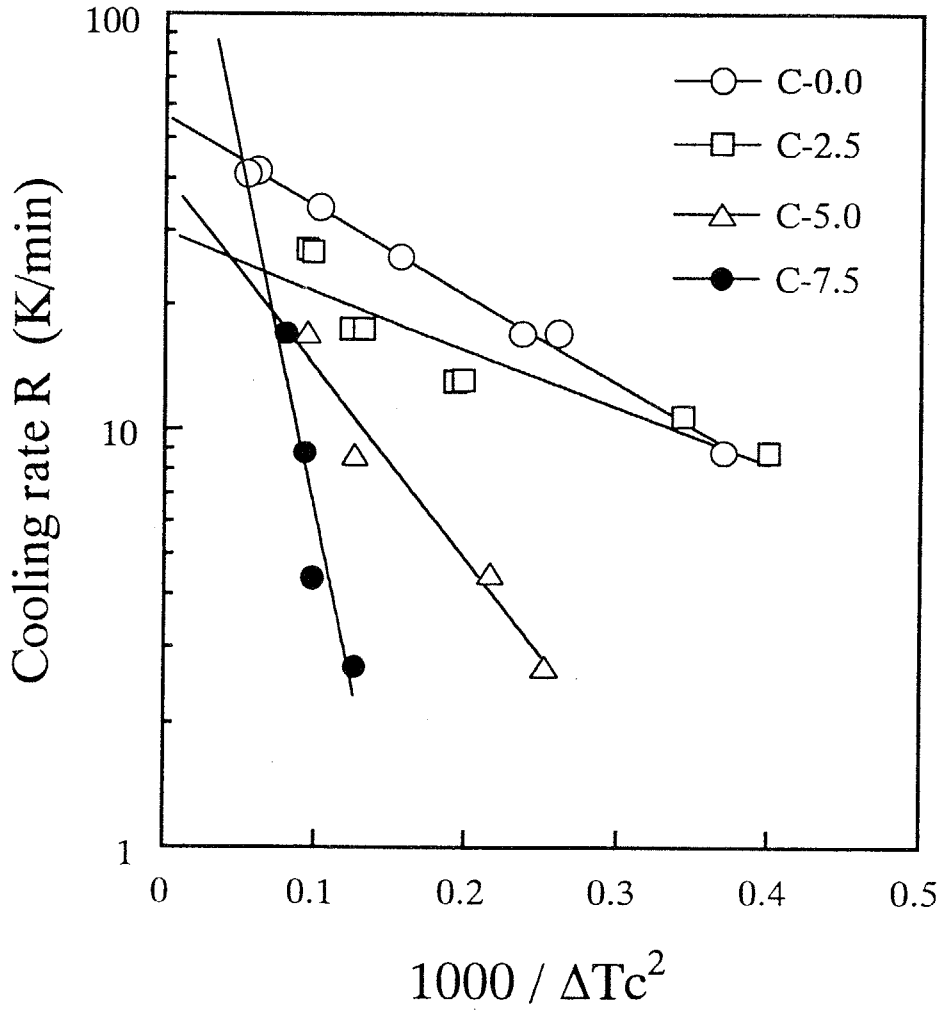

Fig. 6-8 The plots of the results of critical cooling rate measurements for the respective sample glasses.

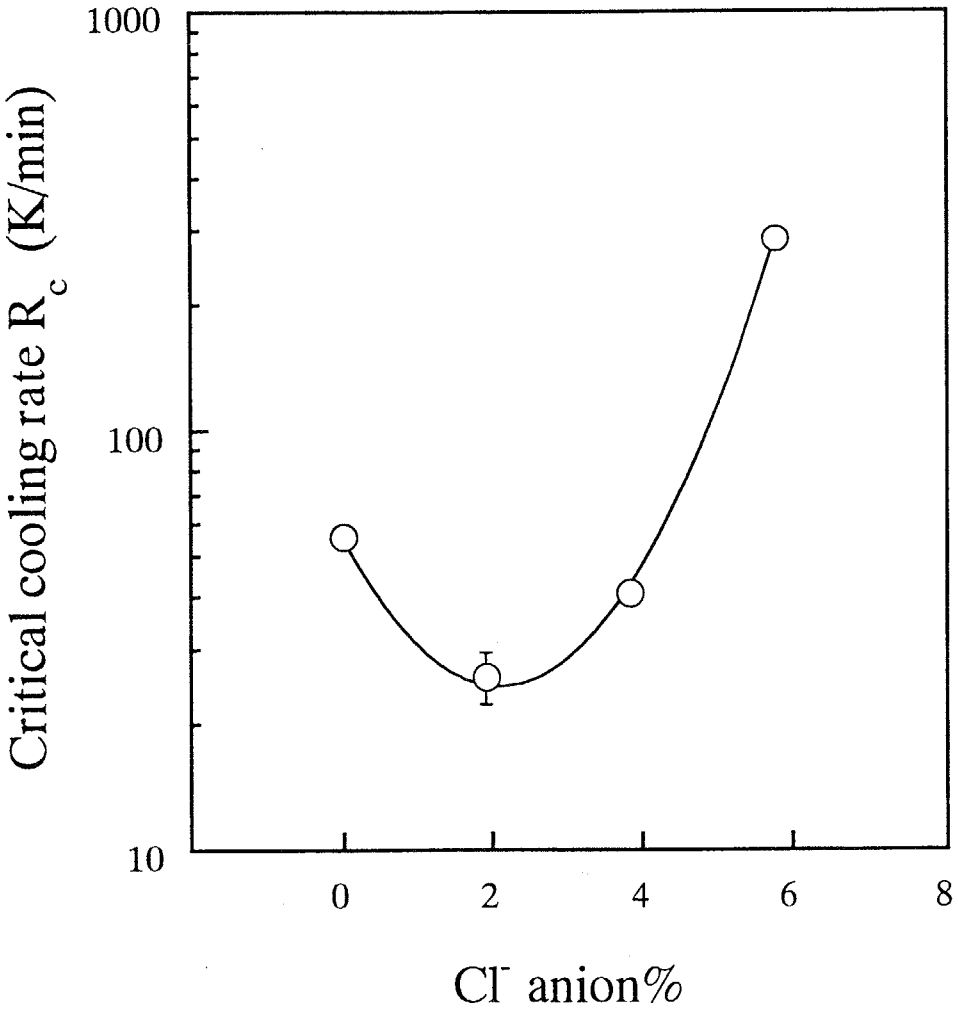

Fig. 6-9 The plot of the critical cooling rate R_c against chlorine content. Curve was drawn with the eyes.

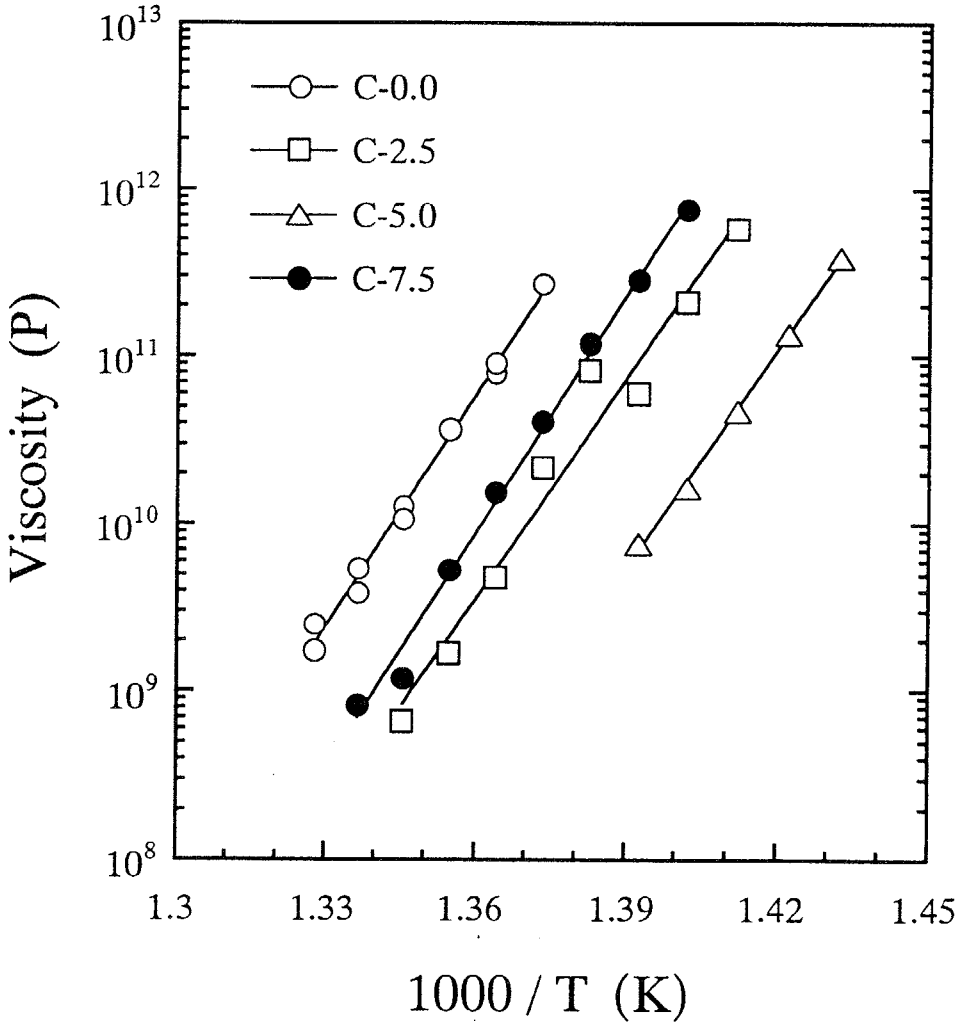

Fig. 6-10 Arrhenius plots of viscosity near glass transition temperature. The lines were obtained by the least square fitting to Arrhenius type equation.

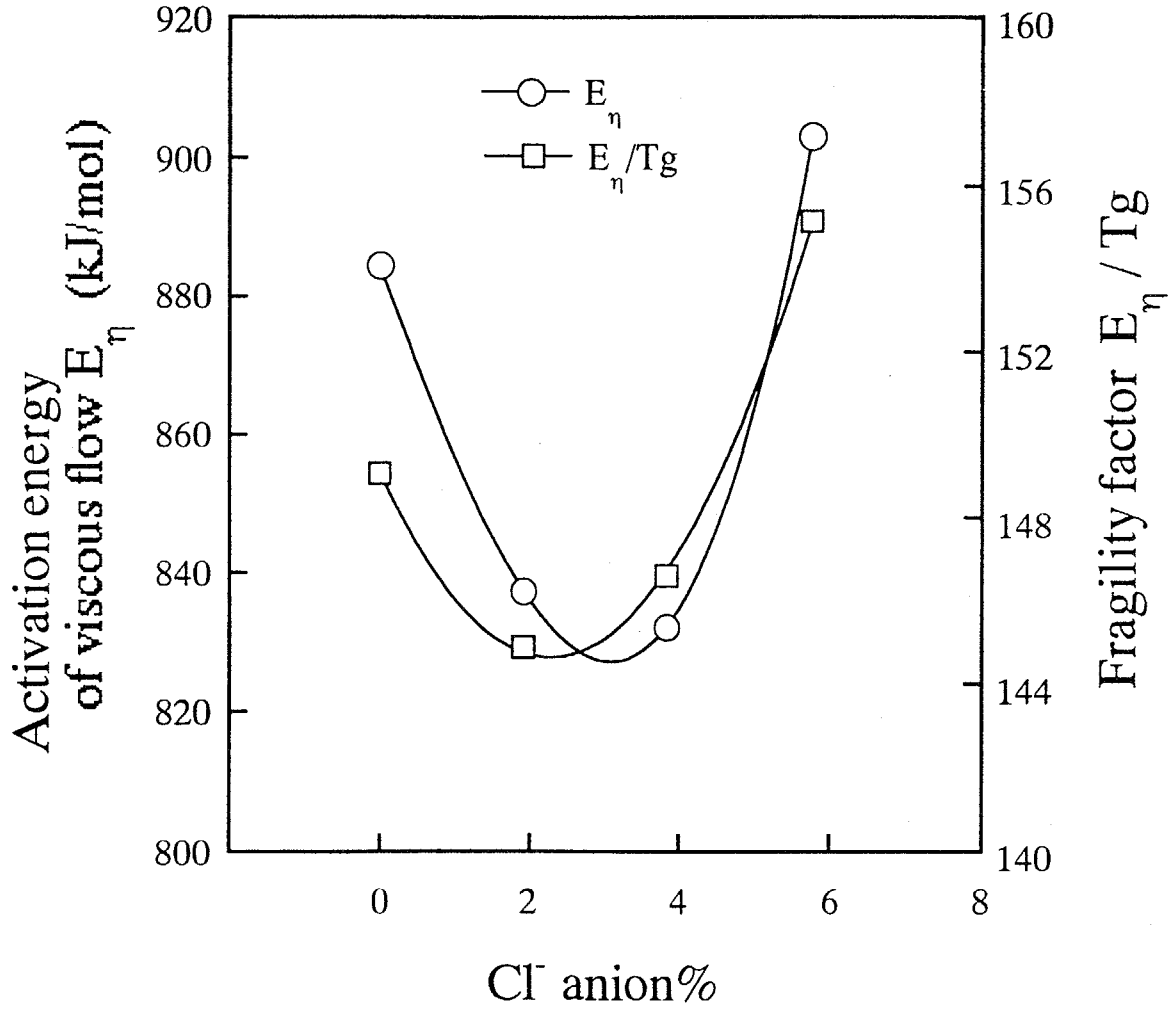

Fig. 6-11 Plots of activation energy of viscous flow near Tg and fragility factor against chlorine content.

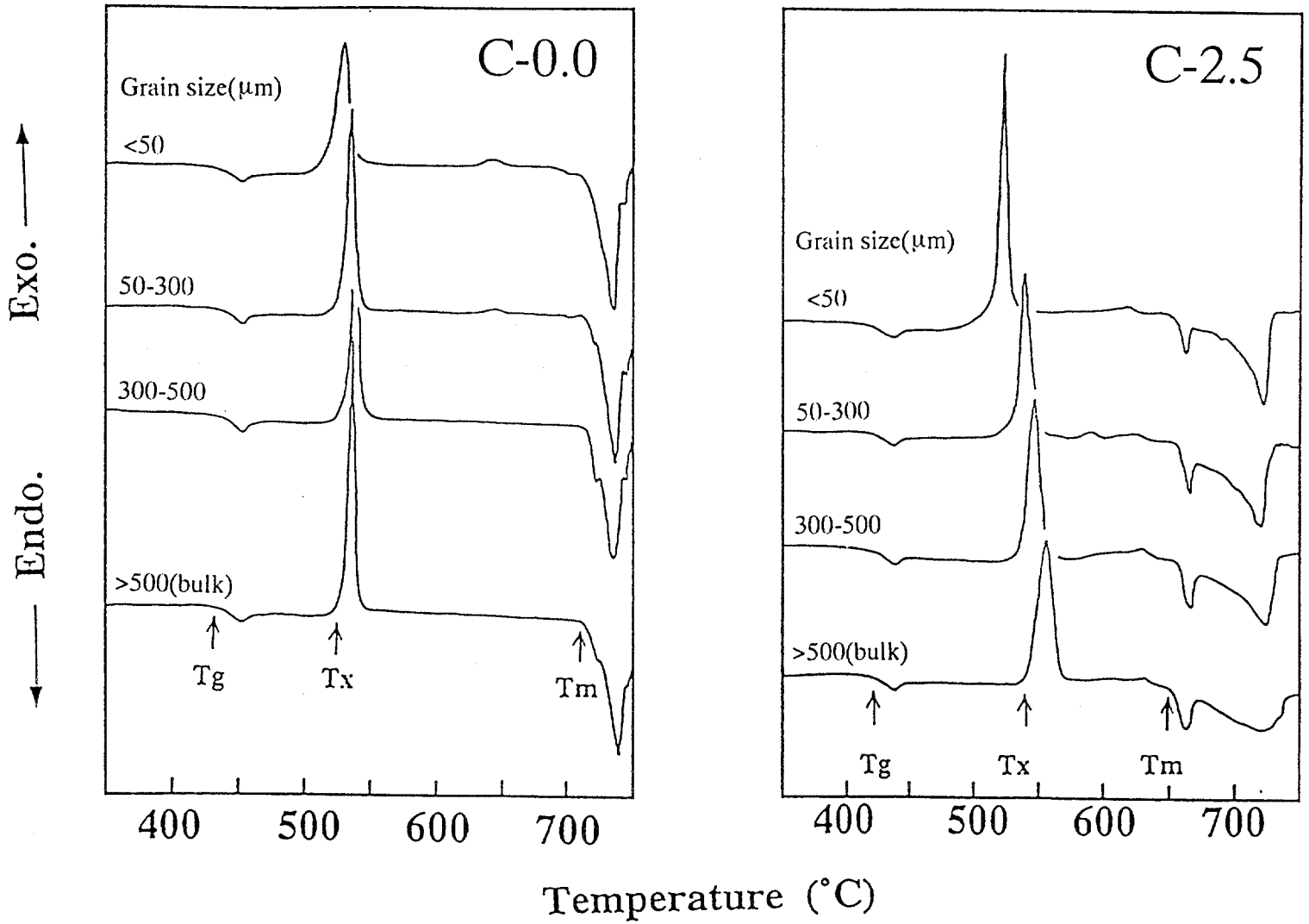

Fig. 6-12 DTA traces of the glass sample with different grain size. The heating rate was 10K/min and while measuring, dry N_2 gas was flowed.

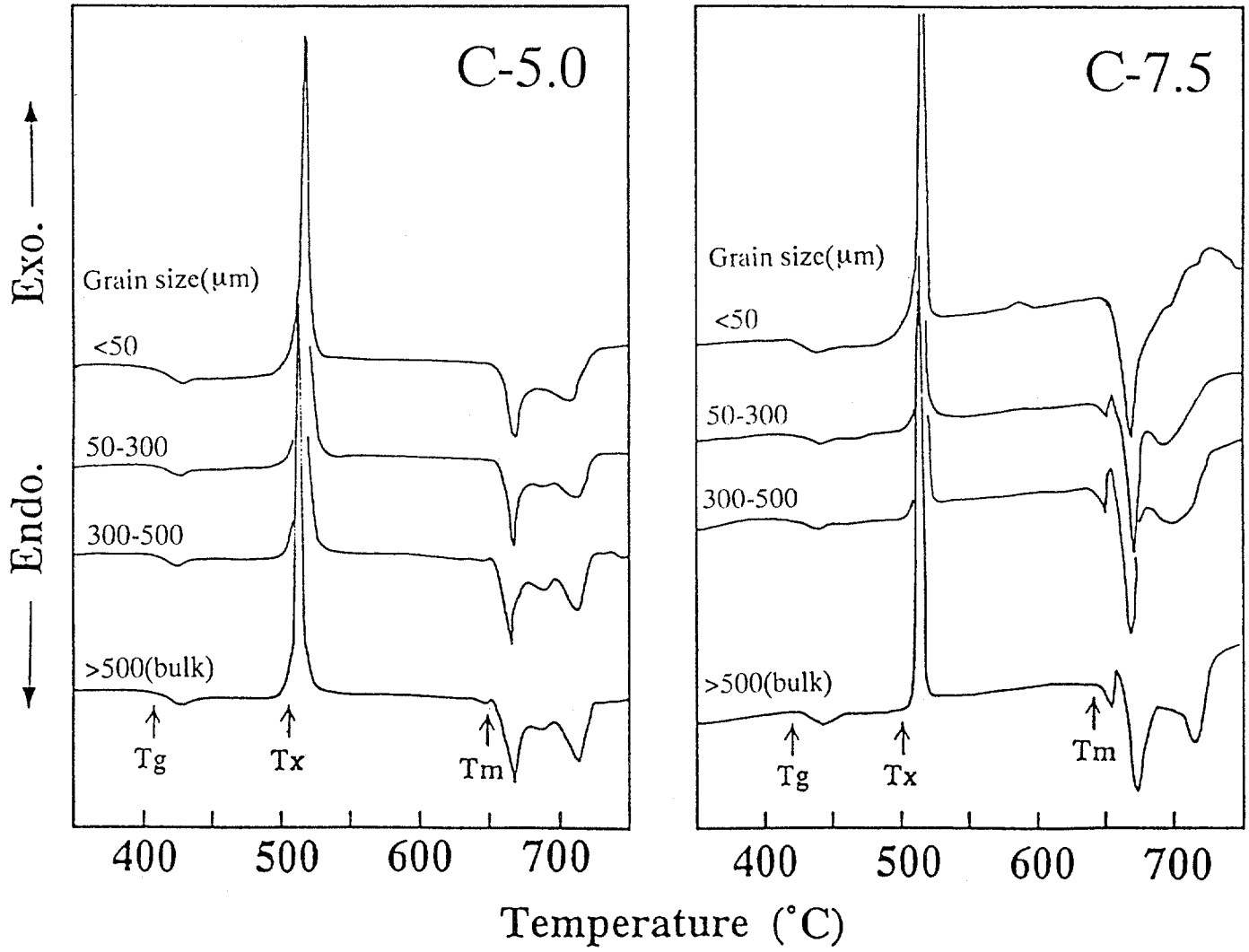
C-5.0
C-7.5
Exo.
Endo.
Grain size(μm)
<50
50-300
300-500
>500(bulk)
Tg
Tx
Tm
400
500
600
700
Temperature (°C)

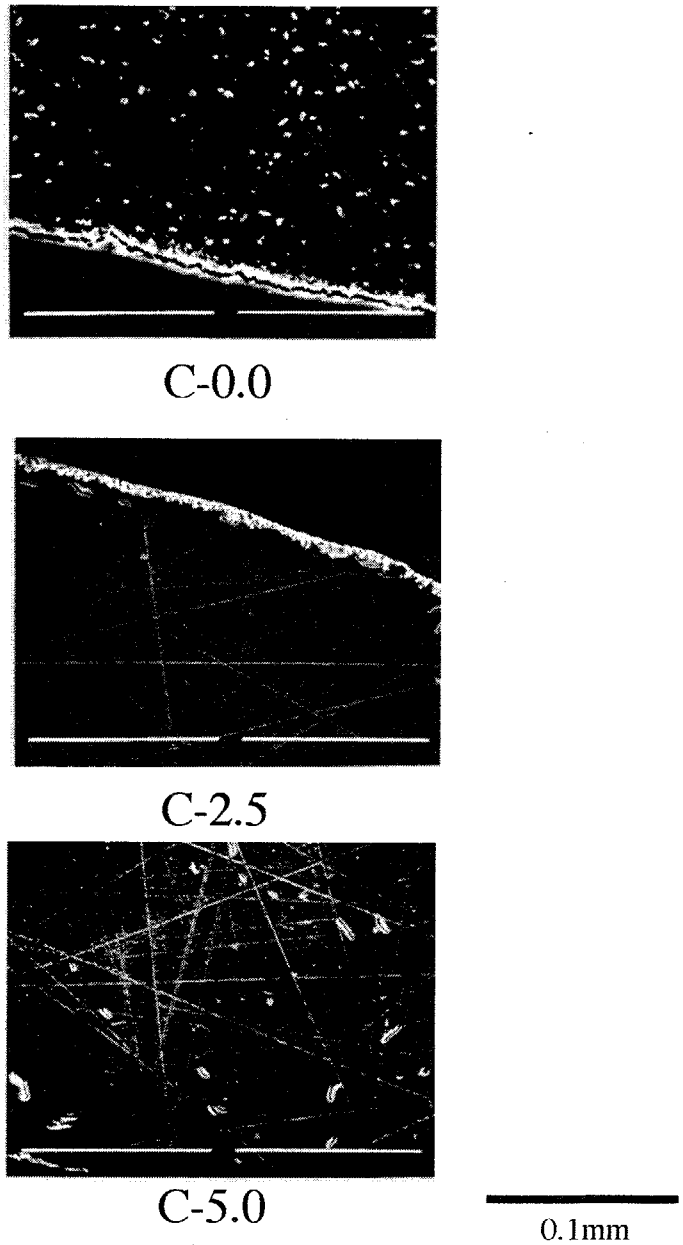

Fi. 6-13 SEM photographs of the heat-treated samples. The sample glasses were heat-treated isothermally at the peak temperature of DTA trace for 4 min, respectively. The fractured surface was polished foolowed by the chemical etching. The condition are dictribed in the text.

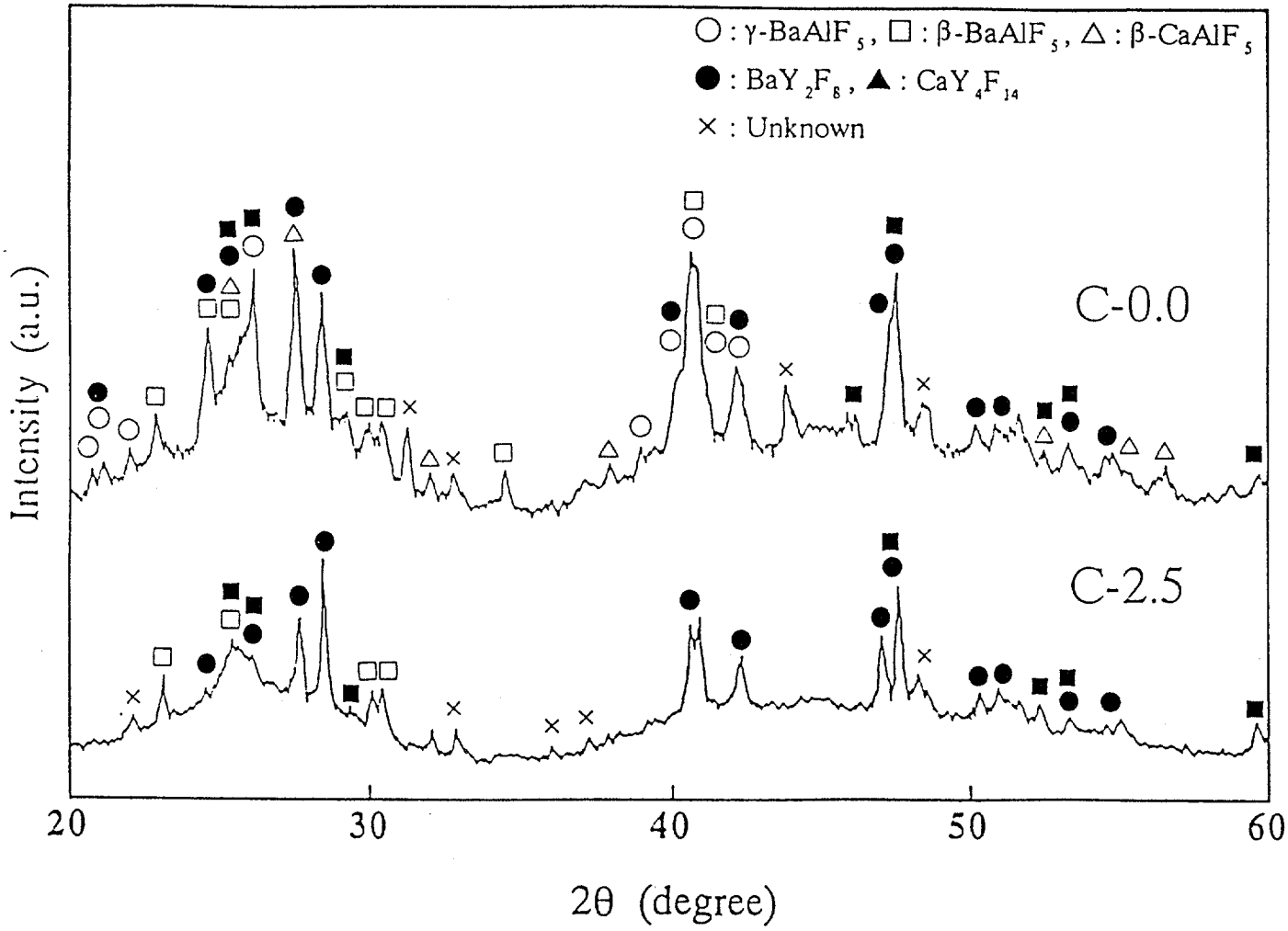

Fig. 6-14 XRD powder patterns for the heat-treated samples of C-0.0 and C-2.5, respectively. Before powdered, the surface crystallized parts were removed, in order to investigate the effect of bulk crystallizing phase.

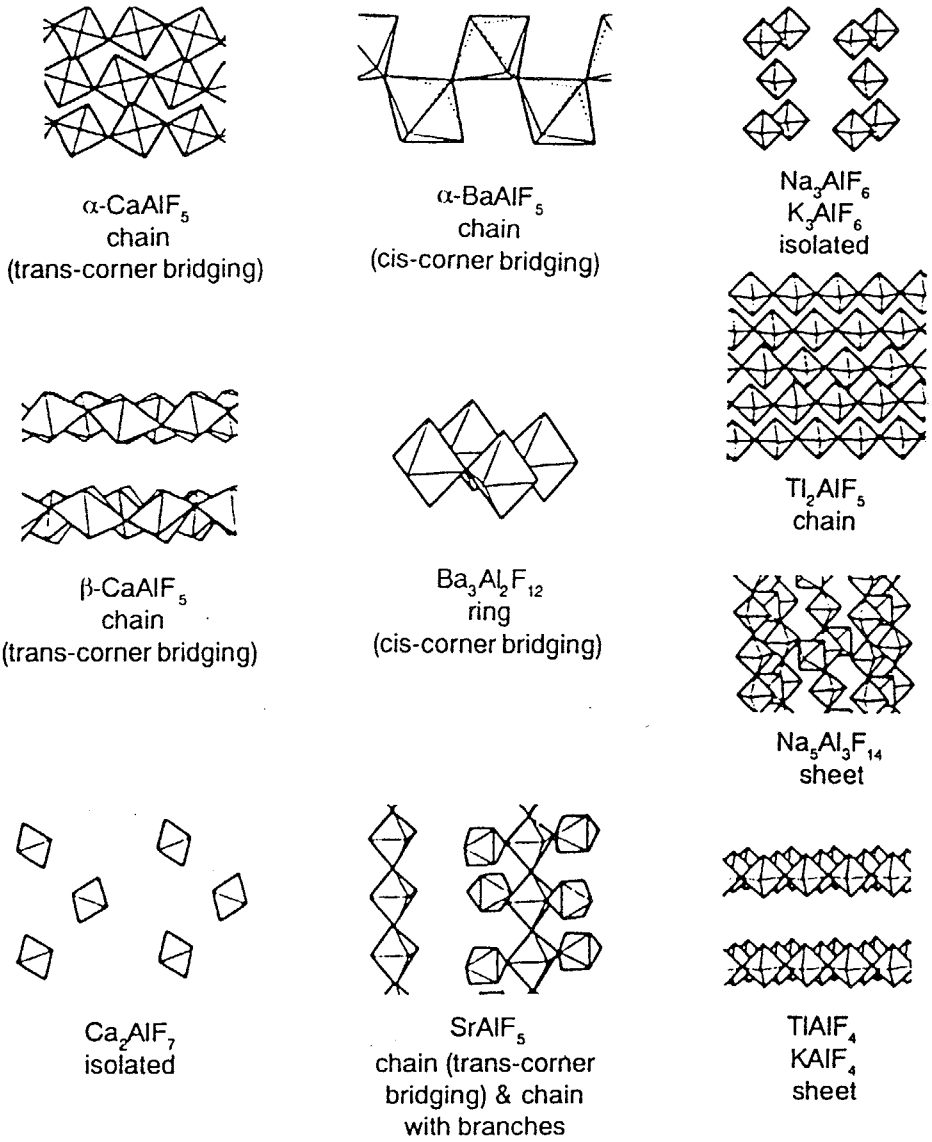

Fig. 6-15 the connection schemes found in metal-fluoroaluminate crystals. For clarity, only AlF_n polyhedra are represented.

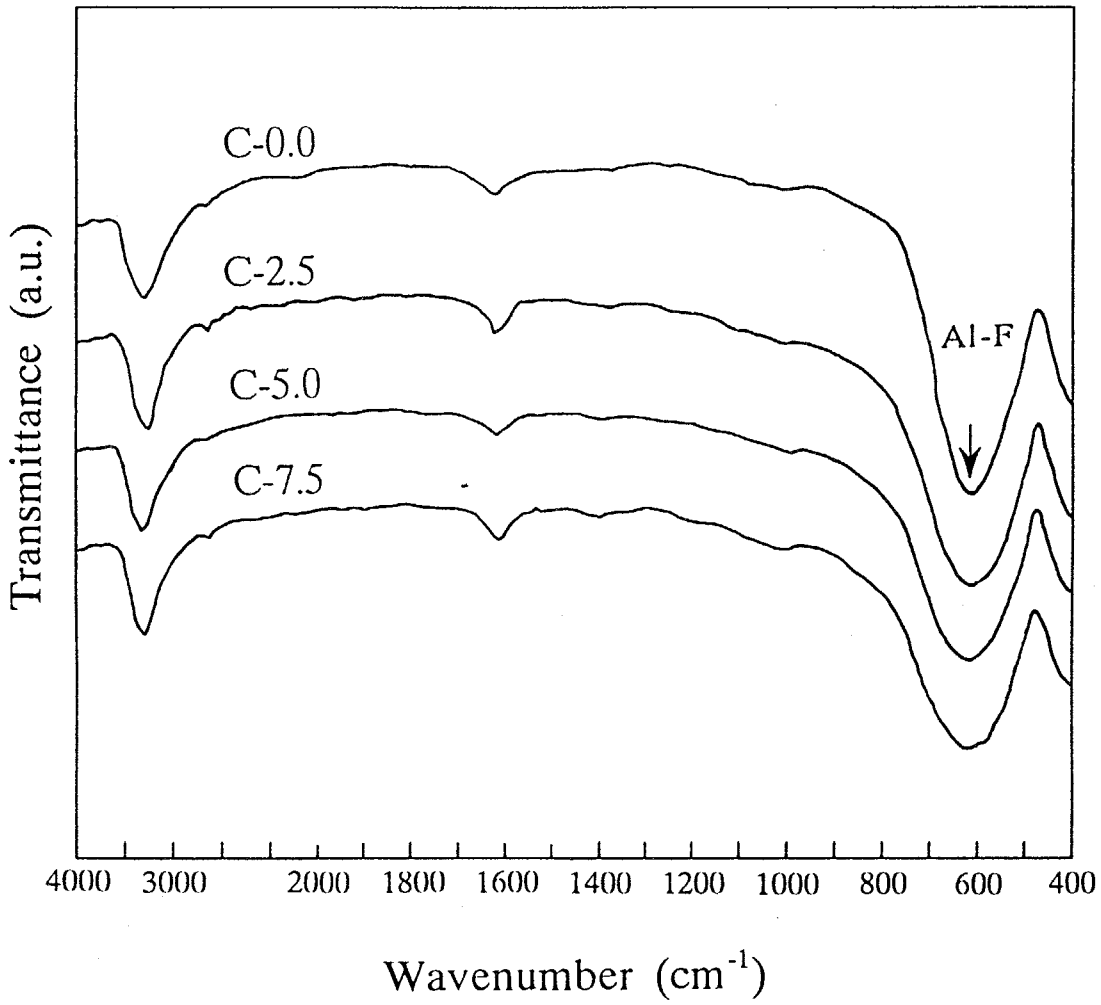

Fig. 6-16 IR spectra of the sample glasses by using KBr pellet method.

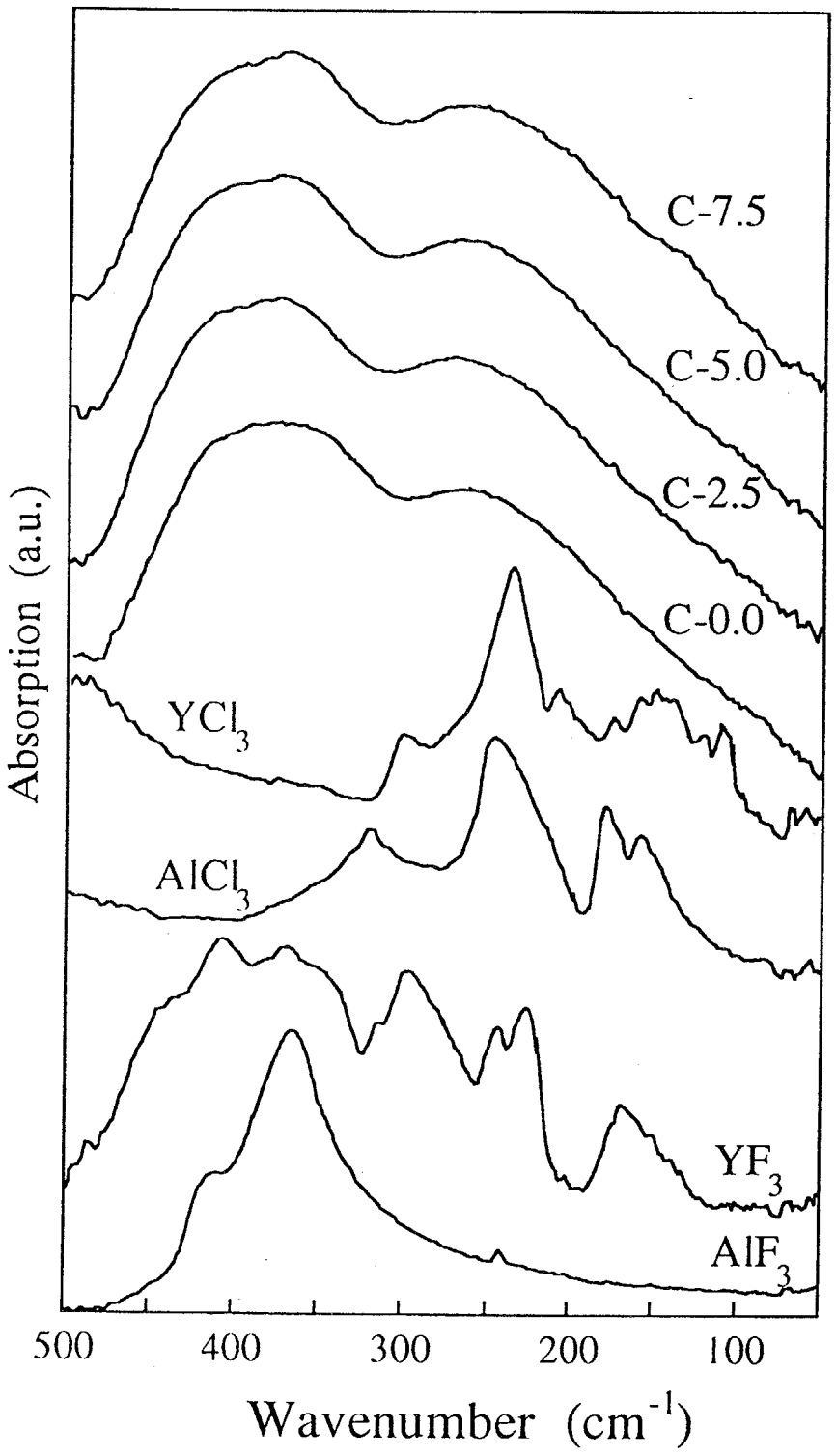

Fig. 6-17 FIR spectra of the sample glasses and the raw materials of aluminum and Yttrium halide compounds.

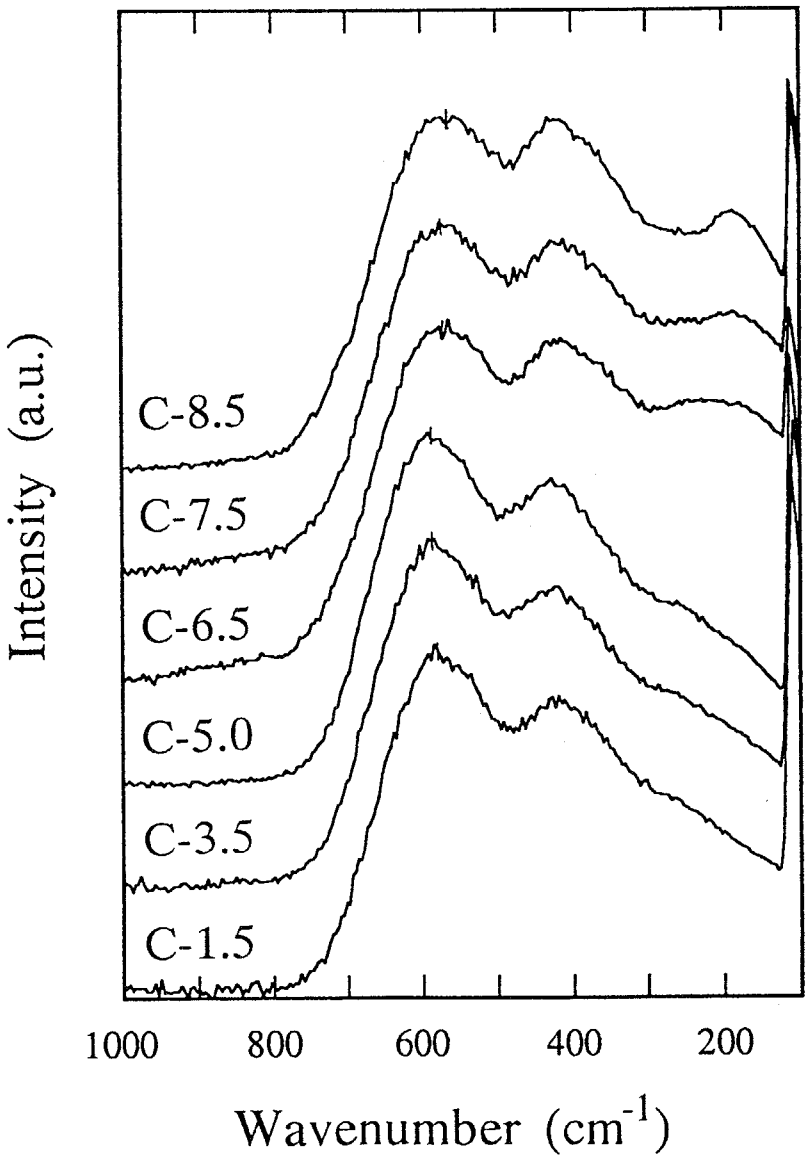

Fig. 6-18 Raman scattering spectra of the respective glass samples. The scattering intensity was corrected by Bose-Einstein factor.

CHAPTER 7

SUMMARY AND CONCLUDING REMARKS

7-1 SUMMARY

In this thesis, nature of the glass formation of fluoride glasses of ZrF_4- and AlF_3-based systems has been investigated through the viscosity and the crystallization behaviors of the melt. A new calculation method of Non-equilibrium Molecular Dynamics simulation for viscosity of the inorganic ionic melts has been developed and applied to the fluoride glass melt of Zr-Ba-Na-F system intending the structural illustration of the melt, which provides the microscopic point of view to the structural relaxation of viscous flow. The crystallization studies of the metal fluoride compounds offer the guideline to understand the precipitation of the crystalline from the melt and the structural features bringing about high glass forming ability are depicted through the coordination chemistry. The effect of the chemical agent of non-fluorine anions are examined and its analogy is applied to AlF_3-based fluoride glass of YF_3-AlF_3-BaF_2-CaF_2 system.

CHAPTER 1: The historical background of the development of fluoride glasses represented by ZrF_4-BaF_2-based systems are described. The problems concerning the poor glass forming ability of the melt are mentioned along with the glass forming criteria proposed at the present. The importance of both the viscosity and the crystallization of the melt are pointed out in order to consider the glass forming ability of fluoride glass systems and the purposes in this

thesis are mentioned.

CHAPTER 2: A new calculation method of Non-equilibrium Molecular Dynamics for viscosity of inorganic ionic melt have been developed based on the idea by Lees and Edwards. The calculation are performed to the simple alkaline halide melt of NaCl and the accuracy and the analysis way are examined. So-called Non-Newtonian viscosity behavior is pointed out to be expressed well with the empirical equation rather than the ordinary used KYG equation. The potential and the applicability to the inorganic ionic melt have been proved with high accuracy by the comparison with the experimental value.

CHAPTER 3: The characteristic viscosity-temperature relation of ZrF_4-BaF_2-NaF system was investigated by using Equilibrium and Non-Equilibrium Molecular Dynamics simulation method developed in this thesis. The viscosity-temperature relation near liquidus temperature has been well simulated by employing the appropriate cell size and the availability of the calculation method to the glass forming liquid has been shown. The detailed structural changes have been investigated through the coordination number of ZrF_n polyhedra and the bridging formula between them. The formation of edge sharing among ZrF_n polyhedra has been found to be the key to increase the cooperativity of the flow units, the steep increase of viscosity under supercooling condition and the glass formation.

CHAPTER 4: The experimental measurements of viscosity of ZrF_4-BaF_2-LaF_3-AlF_3-NaF melts with the different composition have been performed. The difference in the glass forming

ability are investigated from the view point of liquidus viscosity and the steepness of the viscosity increase near liquidus temperature region. The general rules about liquidus viscosity in oxide glass systems are also applicable to fluoride glass melt and the fragility of the melt has been found to describe the glass forming ability, but the quite low viscosity in supercooling condition has suggested that other factors concerning the stability of the melt against the crystallization also has to be taken into account in addition to the viscosity factor.

CHAPTER 5: The non-fluorine anion effects on the crystallization behavior have been investigated for ZBLAN glass system through the growth rate of the precipitated crystallines. The time-temperature relations of the respective crystalline growth precipitated from the melt have been obtained by using X-ray diffraction analysis. OH^- ions act as the nucleation agent to enhance the surface crystallization of β-$BaZrF_6$ phase even when a small amount in the order of 10^2 ppm. Cl^- ions show the characteristic changes in the crystallization and the appropriate amount incorporation plays a role to suppress the crystallization of the major phase which determines the glass forming ability of this melt. The structural study about the precipitated crystallines reveals the chlorine effect on the stability of the coordinates of ZrF_n polyhedra and the variety of the 7- and 8-coordinates plays the important role to induce some potential barrier to the crystallization.

CHAPTER 6: The chlorine incorporation effects have been investigated in AlF_3-based glass of YF_3-AlF_3-BaF_2-CaF_2 system. The thermal properties, the viscosity, the crystallization behavior and the spectroscopic measurements have been carried out. The appropriate amount

of chlorine improves both of the glass forming ability (the critical cooling rate) and the thermal stability. Its value was found to be comparable or superior to ZBLA and ZBGA glasses, which are actually drawn into the fibre. Heavily suppressed the bulk crystallization phases including AlF_3 compound and showing the higher onset temperature of crystallization on heating. The vibrational spectra suggests that chlorine affects mainly Y^{3+} ion, which has the same electric structure and the high coordination number, and the linking of AlF6 polyhedra is influenced to suppress the crystallization.

7-2. CONCLUDING REMARKS

From CHAPTER 3 to 5, the glass forming process of ZrF_4-BaF_2-based melt and their origins of higher glass forming ability among various fluoride glass systems could be depicted. The main factors can be summarized as follows;

1) Zr^{4+} has higher single bond strength and higher field strength.

2) Zr^{4+} takes various coordination number from 6-8, which are actually observed in metal fluorozirconate crystals.

3) The edge sharing linkage form exists.

4) The higher coordinates like 7 and 8 have various stereochemistries and their stability are affected by the surrounding anions (ligand).

5) Lager size modifier of Ba^{2+} assists the formation of higher coordination number of ZrF_n polyhedra.

Among these factors, 1-4 have their origins in the characteristics of Zr^{4+} ion. The large ionic radii of Zr^{4+} ion permit to form higher coordination number and this is not only the case of

fluoride. In oxide, cubic ZrO_2 are consist of the 8-coordinates and monoclinic ZrO_2 includes 7-coordinates. From the consideration based on the coordination stereochemistry, these high coordination number (more than 6) need the utilization of the d-orbital to construct the hybridized orbitals. In case of Zr^{4+} ion, it includes the empty d-orbitals and they can be utilized freely to build up the polyhedra with high coordination number. The empty d-orbitals also require no stereo-chemical selectivity to the ligand ions. This means that the lower activation energy to change the coordination number if Zr^{4+} ion is isolated enough in the solution, and they will depend on the electric character of ligand ions. These features are common in Zr, Hf, Th, U, which belong to IVA group. These flexibility in the coordinates brings about, at least, 3 types of stereochemistry in both of 7-coordinates and 8-coordinates respectively. In addition, concerning the factor 3, the edge sharing will cause more wide variety of stereochemistry, if the edge sharing is regarded as ' **bidentate** '. Fig. 7-1 shows the examples of 7-coordinates stereochemistry, $[M(bidentate)(unidentate)_5]$, which are calculated by Valence Shell Electron Pair Repulsion theory [1]. When observed bond length data in barium fluorozirconate crystals are applied to this theory, the stereochemistry of A and B are predicted as the most probable coordinates, where the edge sharing F's are treated as one bidentate, and terminal and corner bridging F's are treated as unidentate. Stereochemistry A and B are actually observed in α-$BaZrF_6$ and β-$BaZr_2F_{10}$ crystals respectively. These consideration can be also applied to 8-coordinate with $[M(bidentate)_2(unidentate)_4]$ and predicts the dodecahedron with two bidentate in trans position, which is the same as one observed in β-$BaZrF_6$. As seen in the above considerations, the very wide variety in the coordinates and their connection is considered to be caused in the glass melt and act as the origins of the

stability of the melt against the crystallization.

If the above mentioned consideration were applied to AlF_3-based systems, we can imagine easily their low glass forming ability, in spite of high single bond strength and high field strength. Al^{3+} ion dose not have the empty d-orbitals and have to use the outer d-orbitals to form the hybridized orbitals for octahedral coordination. The small ionic radii prohibits to take the higher coordination number and can not obtain the variation of the coordinates other than octahedron and tetrahedron. However, as shown in 6-11, there are some variety in the linkage form among them and they are dependent on the character of modifier ions like alkaline earth ions. These varieties in the linkage manner, which are called as ' polymorph ' can induce some potential barriers in the glass melt against the crystallization. The introduction of ' intermediates ' like YF_3 compound will play some assistant role in it. YF_n polyhedra can form the edge sharing with AlF_6 octahedra and add more varieties in the AlF_6 polyhedra.

Ga^{3+} and In^{3+} also have potential to form the glass as well as Al^{3+} ion, because they belong to the same IIIB group and show the similar characteristics. Recently, InF_3-based fluoride glass systems have been payed much attention because InF_3 has some favorable characteristic properties for the optical application. Basically, In^{3+} ion acts as the same structural features, but because it is located at the lower site in the periodic table, some exceptional features appear. Fig. 7-2 shows the linkage structures found in alkaline fluoroindate crystals [2]. The important features to be payed attention are that there exist the 7-coordinate structure and the edge sharing linkage form in it. This will cause more varieties in both of the coordinates and their linkages and will show the higher glass forming ability than AlF_3-based glasses.

There have been proposed some glass forming criteria at the present, but as mentioned

in CHAPTER 1, they are not enough to explain the glass formation. The definite defect is considered to be attributed to the lack of the description about the freedom of the structure. Recently, Cooper [3] proposed the modified Zackariasen rules in the abstract, which are re-interpreted to extend the ordinary ones to the subjects with higher coordination number. The above consideration about the variety of the coordinates are considered to be one of the chemical concrete descriptions of them.

REFERENCES

[1] D. L. Kepert, '*Inorganic Stereochemistry*', Springer-Verlag, Berlin, 1982

[2] J.-C. Champarnaud-Mesjard, Rev. Chim. Min., t. 15 (1978) 328

[3] A. R. Cooper, Mat. Sci. Forum, **67&68** (1991) 385

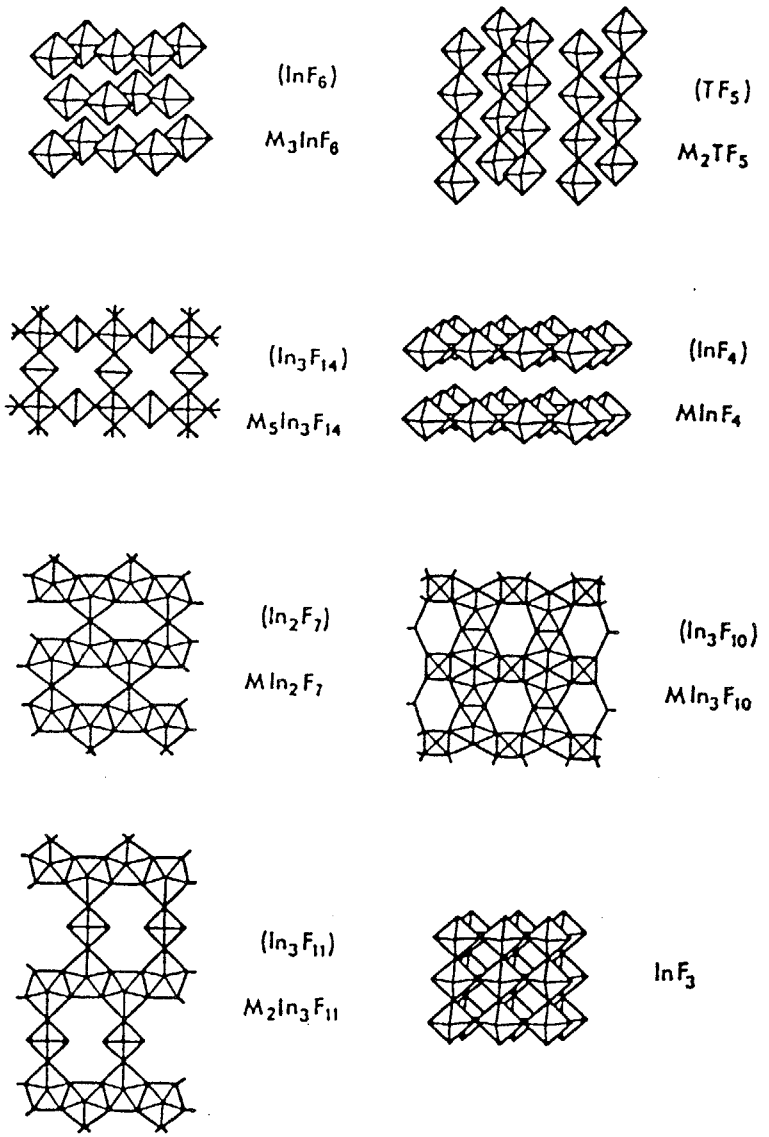

Fig. 7-2 The schematic illustration of M_xInF_y crystalline structures [2].

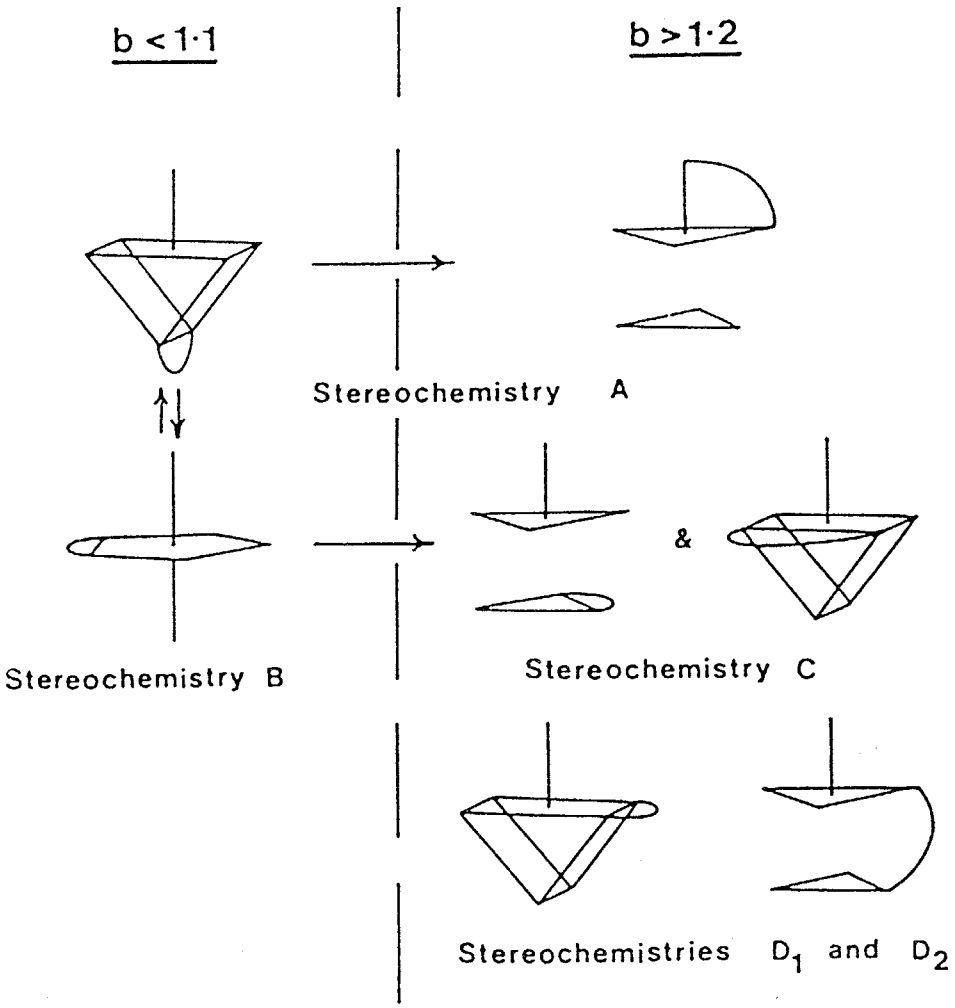

Fig. 7-1 Stereochemistries for [M(bidentate)(unidentate)$_5$] [1]

APPENDIX

PREPARATION PROCEDURES OF STANDARD CRYSTALS

In CHAPTER 5, in order to determine the crystallizing phase volume in the partially crystallized sample, internal standard method of powder X-ray diffraction method. In order to obtain the calibration draw lines, the standard single phase crystals were prepared. The procedures were as follows;

α-$BaZrF_6$

The 20g mixture with the same composition from ZrF_4 (99.999% purity, Rare Metallic Co.) and BaF_2 (99.999% purity, Rare Metallic Co.) was heated at 5°C/min and melted at 850°C for 30 min and then rate cooled down to the room temperature at 0.6°C/min.

β-$BaZrF_6$

The 20g mixture with the same composition from ZrF_4 (99.999% purity, Rare Metallic Co.) and BaF_2 (99.999% purity, Rare Metallic Co.) was heated at 5°C/min and melted at 850°C for 1 h. After cooled down to 730°C, the sample was held for 6 days, followed by the heating at 700°C for 5 days.

α-$BaZr_2F_{10}$

The 20g mixture with the same composition from ZrF_4 (99.999% purity, Rare Metallic Co.) and BaF_2 (99.999% purity, Rare Metallic Co.) was heated at 10°C/min and held at 700°C for 1 h. After cooled down to 610°C at 3°C/min and to 400°C at 2°C/h, it was kept at 400°C for 4 days.

β-$BaZr_2F_{10}$

The 50g mixture with the same composition from ZrF_4 (99.999% purity, Rare Metallic Co.) and BaF_2 (99.999% purity, Rare Metallic Co.) was heated at 5°C/min and melted at 850°C for 1 h. After stirred to improve homogeneity, the sample were kept at 560°C for 3 days and 525°C for 3 days.

$Na_7Zr_6F_{31}$

The 20g mixture with the same composition from ZrF_4 (99.999% purity, Rare Metallic Co.) and NaF (99.99% purity, Rare Metallic Co.) was heated at 5°C/min and melted at 850°C for 1 h. After stirred, the sample were rapidly cooled to 650°C and rate-cooled to the room temperature at 0.5°C/min.

Fig. A6-A10 show the powder X-ray diffraction patterns of the resulted samples. Although they were found to include some amount of undesired phases, the amount of them were considered to be small and the errors of the estimation of the crystalline volume would be small. The linearity of the calibration draw lines showed that the estimated volumes would include about ±10% in experimental error for measurement.

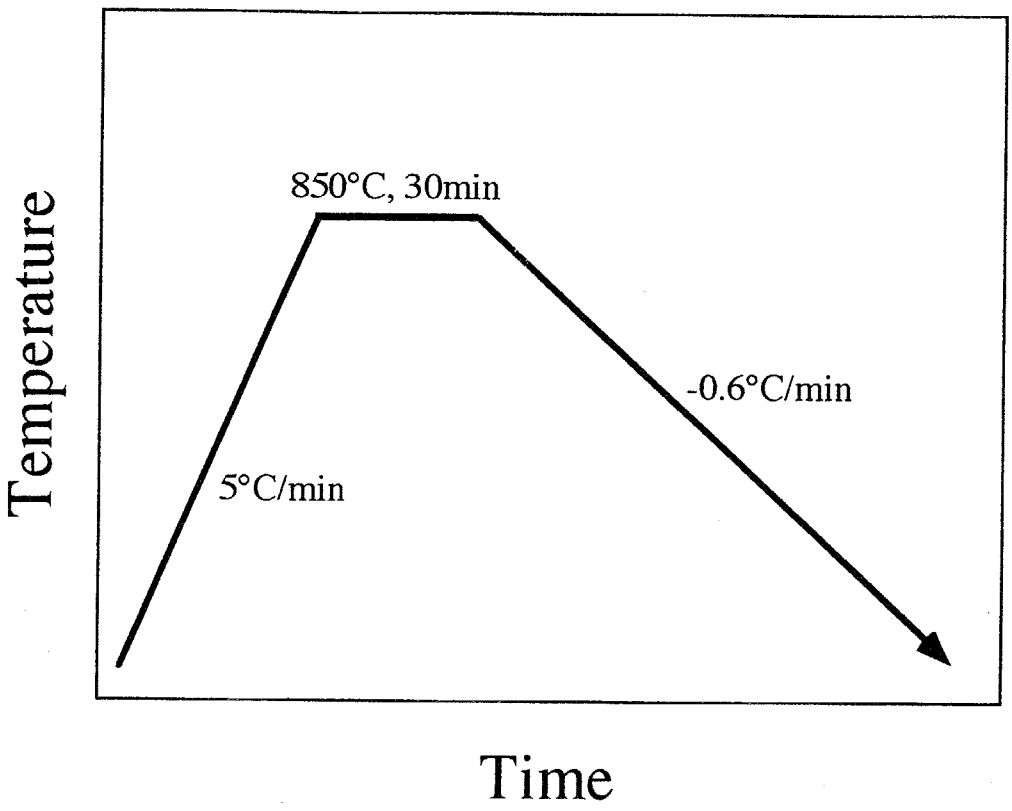

Fig. A-1 Preparation process of α-$BaZrF_6$ crystal.

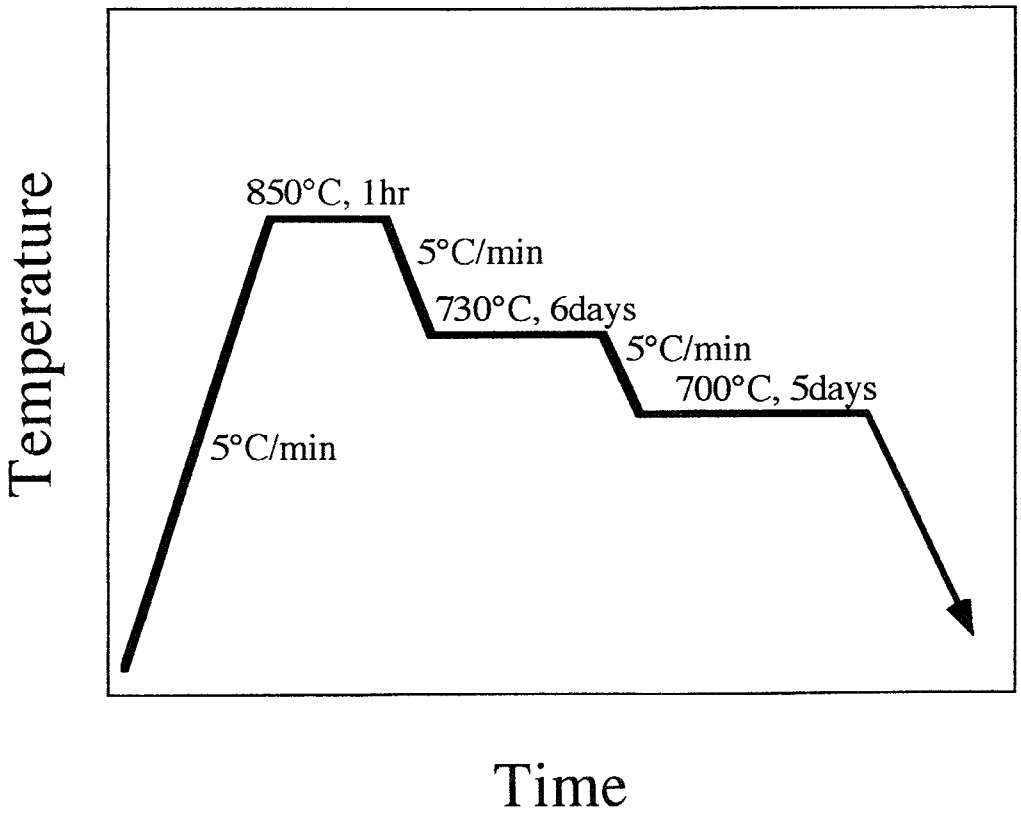

Fig. A-2 Preparation process of β-$BaZrF_6$ crystal.

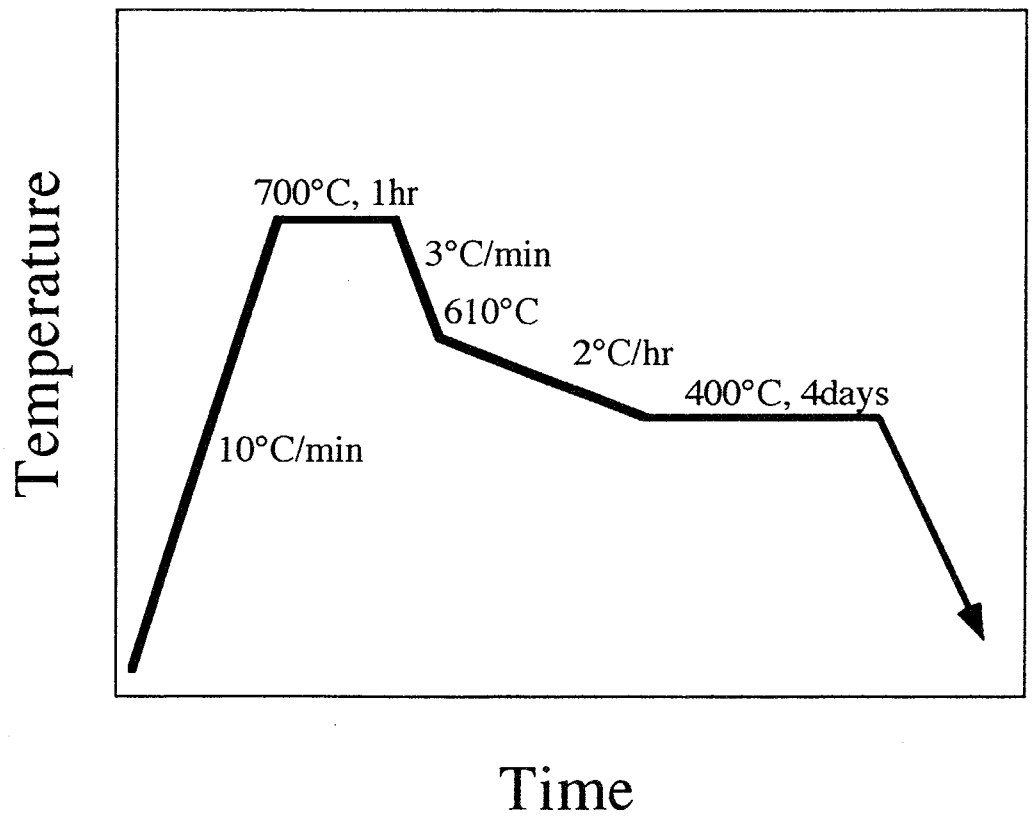

Fig. A-3 Preparation process of α-$BaZr_2F_{10}$ crystal.

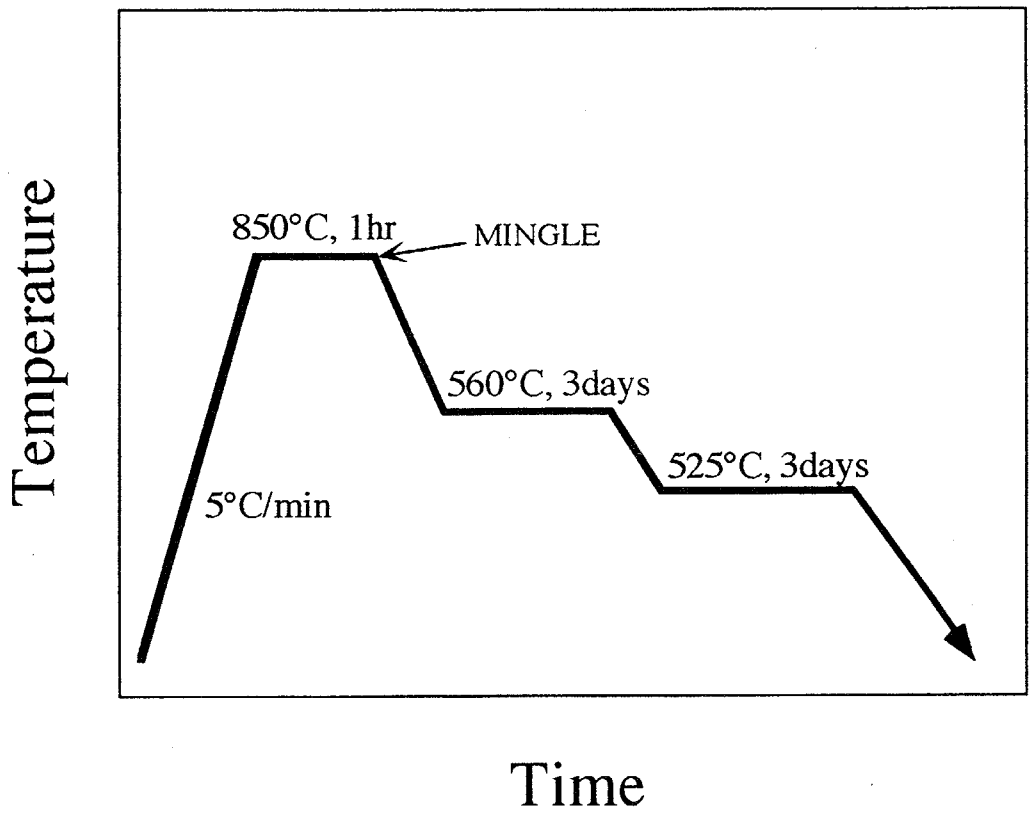

Fig. A-4 Preparation process of β-$BaZr_2F_{10}$ crystal.

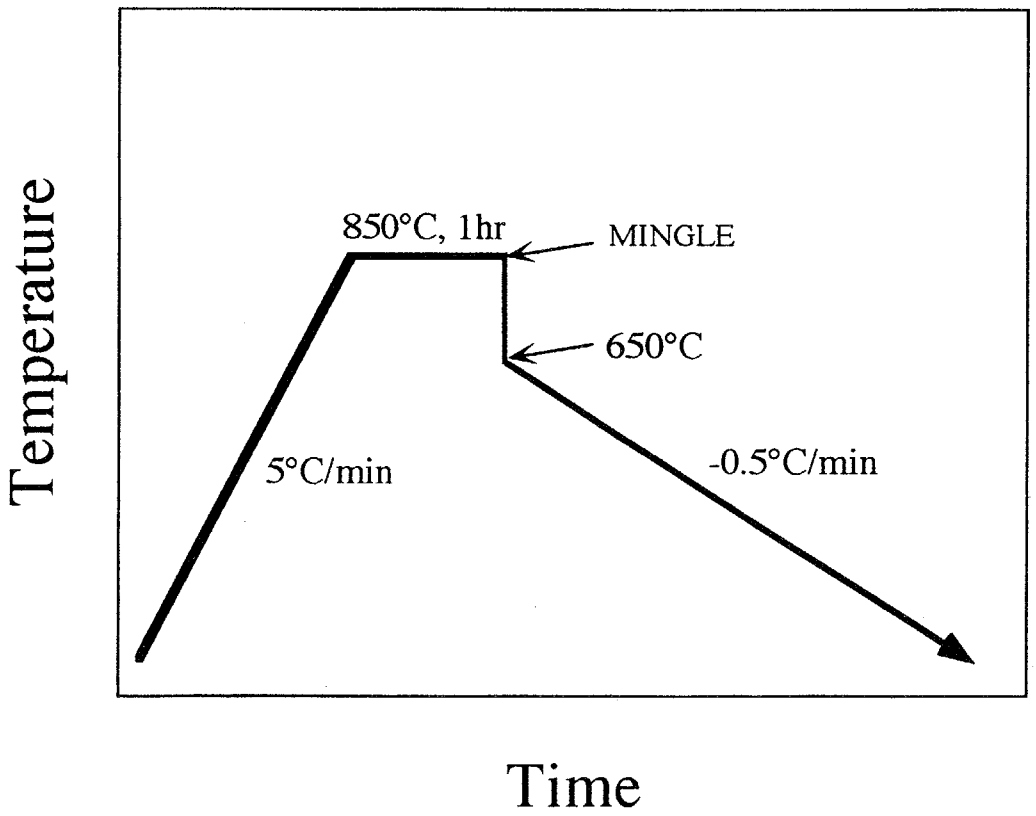

Fig. A-5 Preparation process of $Na_7Zr_6F_{31}$ crystal.

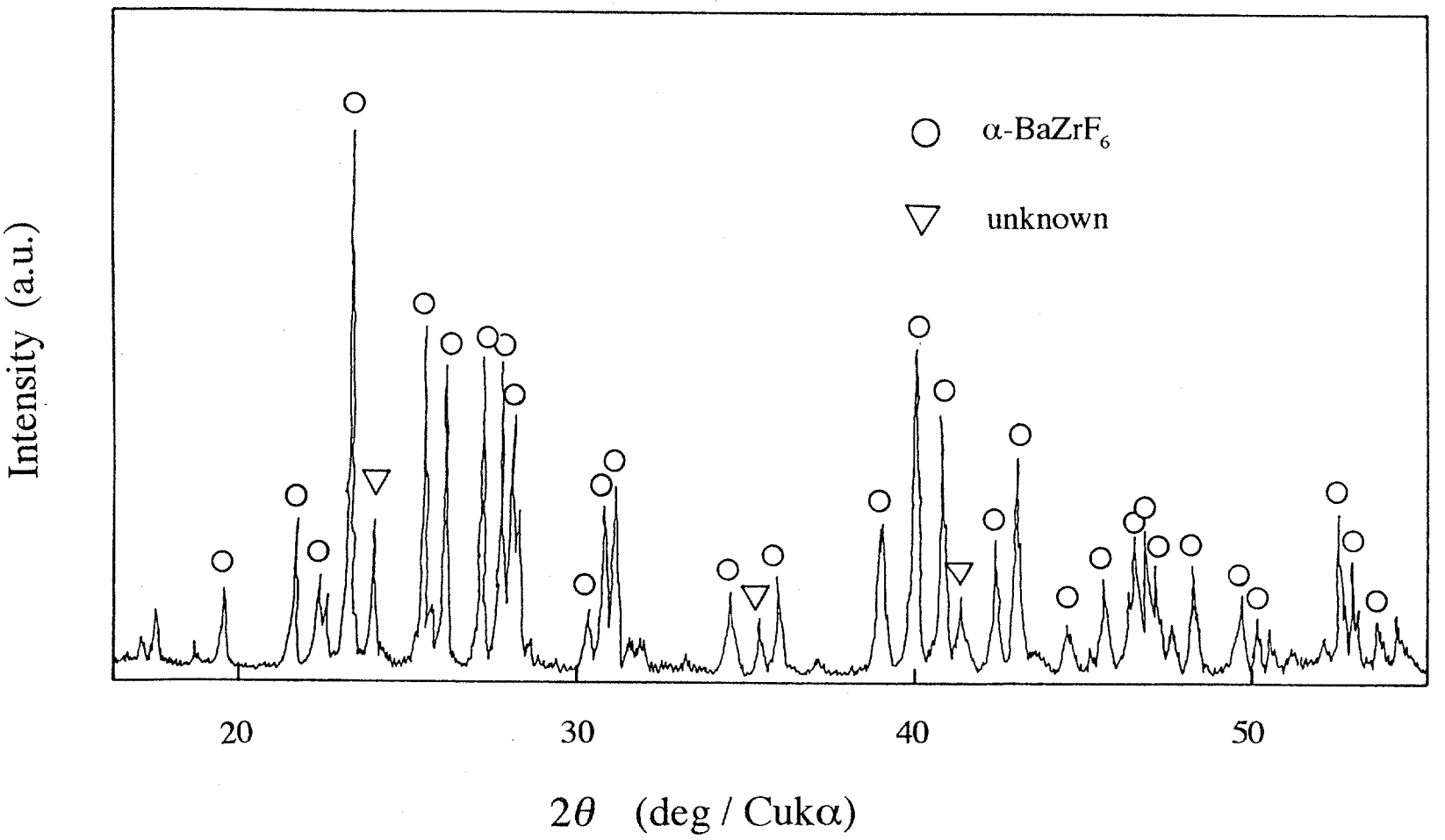

Fig. A-6 XRD powder pattern of the prepared α-$BaZrF_6$ crystal.

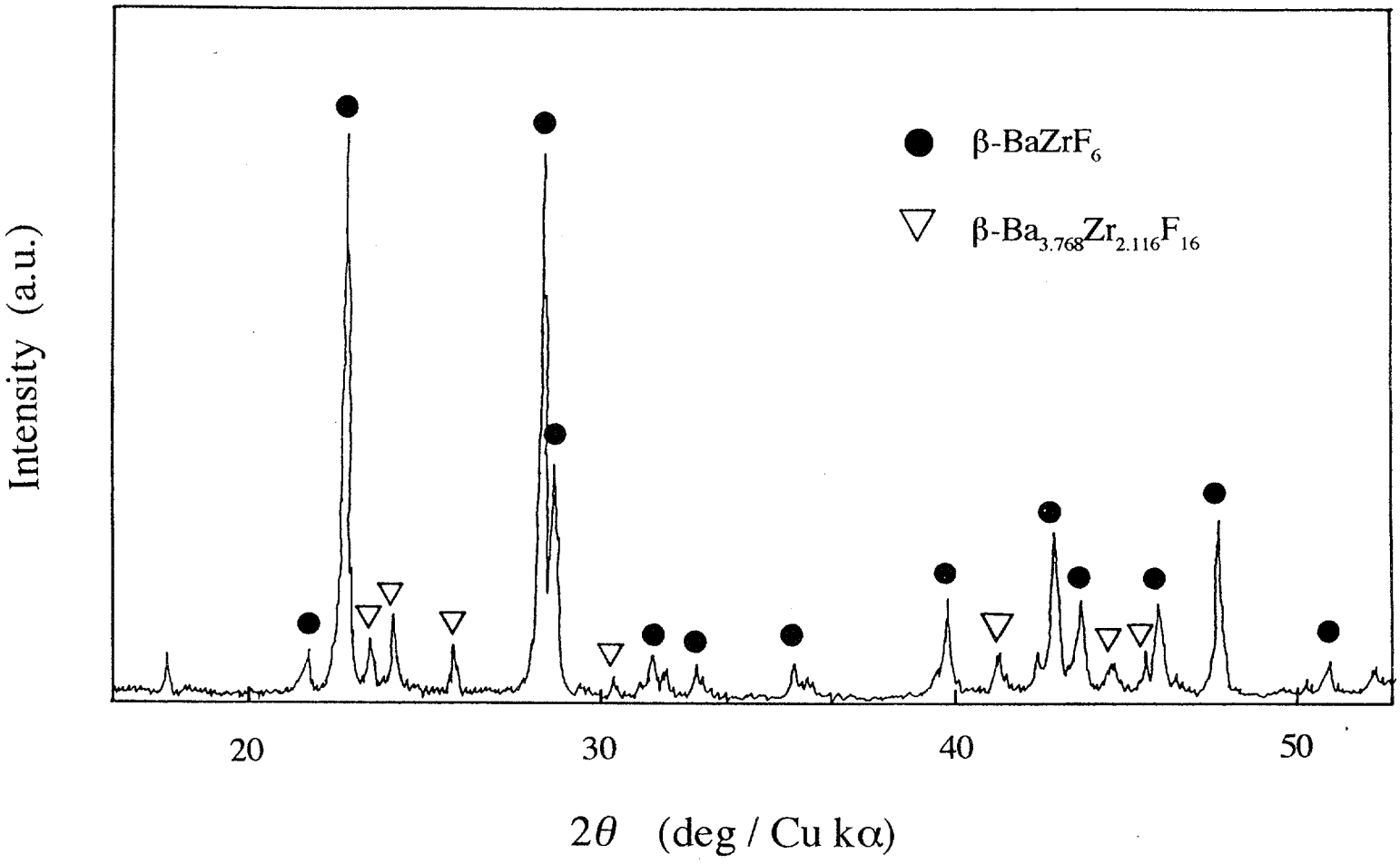

Fig. A-7 XRD powder pattern of the prepared β-$BaZrF_6$ crystal.

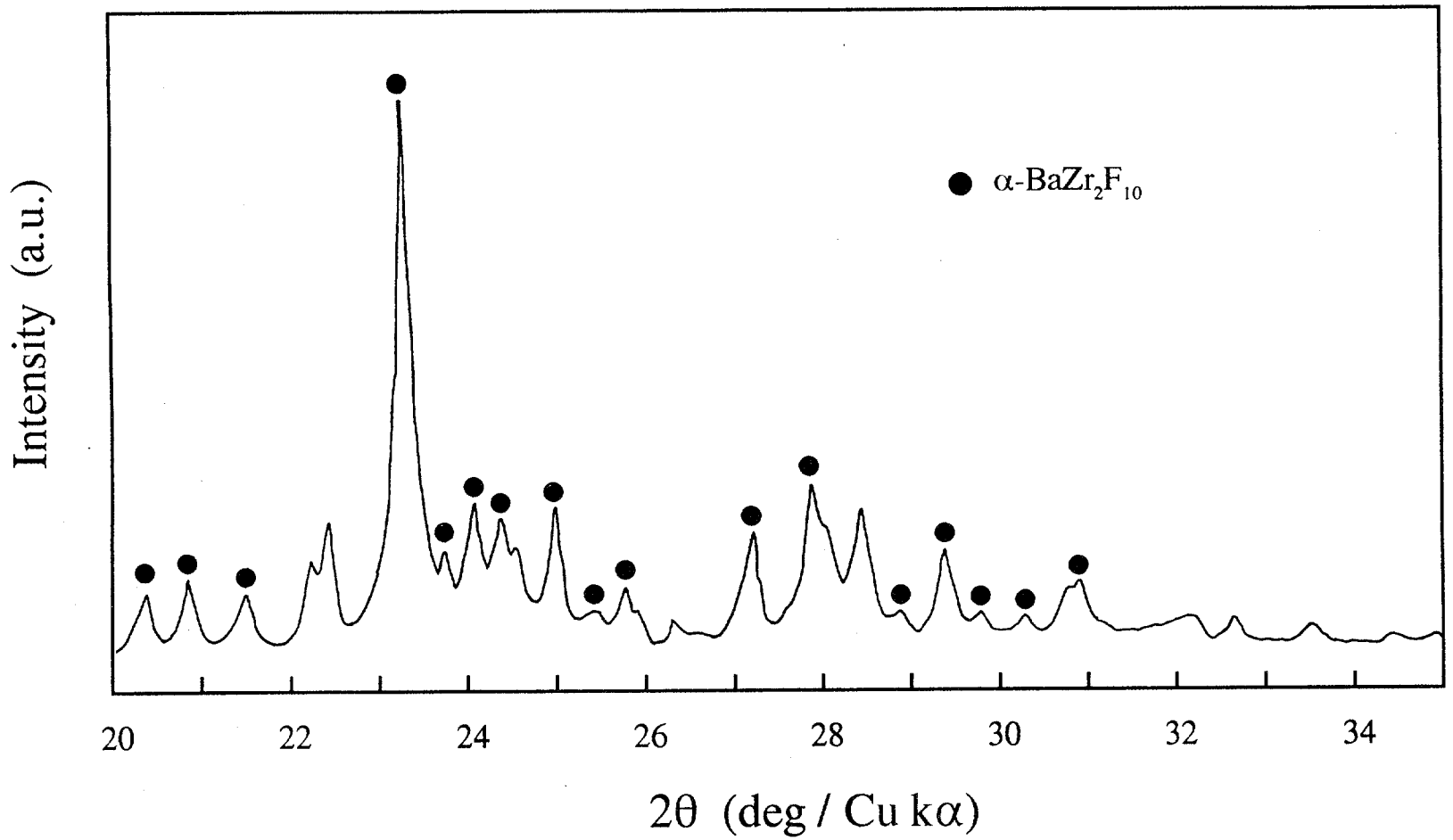

Fig. A-8 XRD powder pattern of the prepared α-$BaZr_2F_{10}$ crystal.

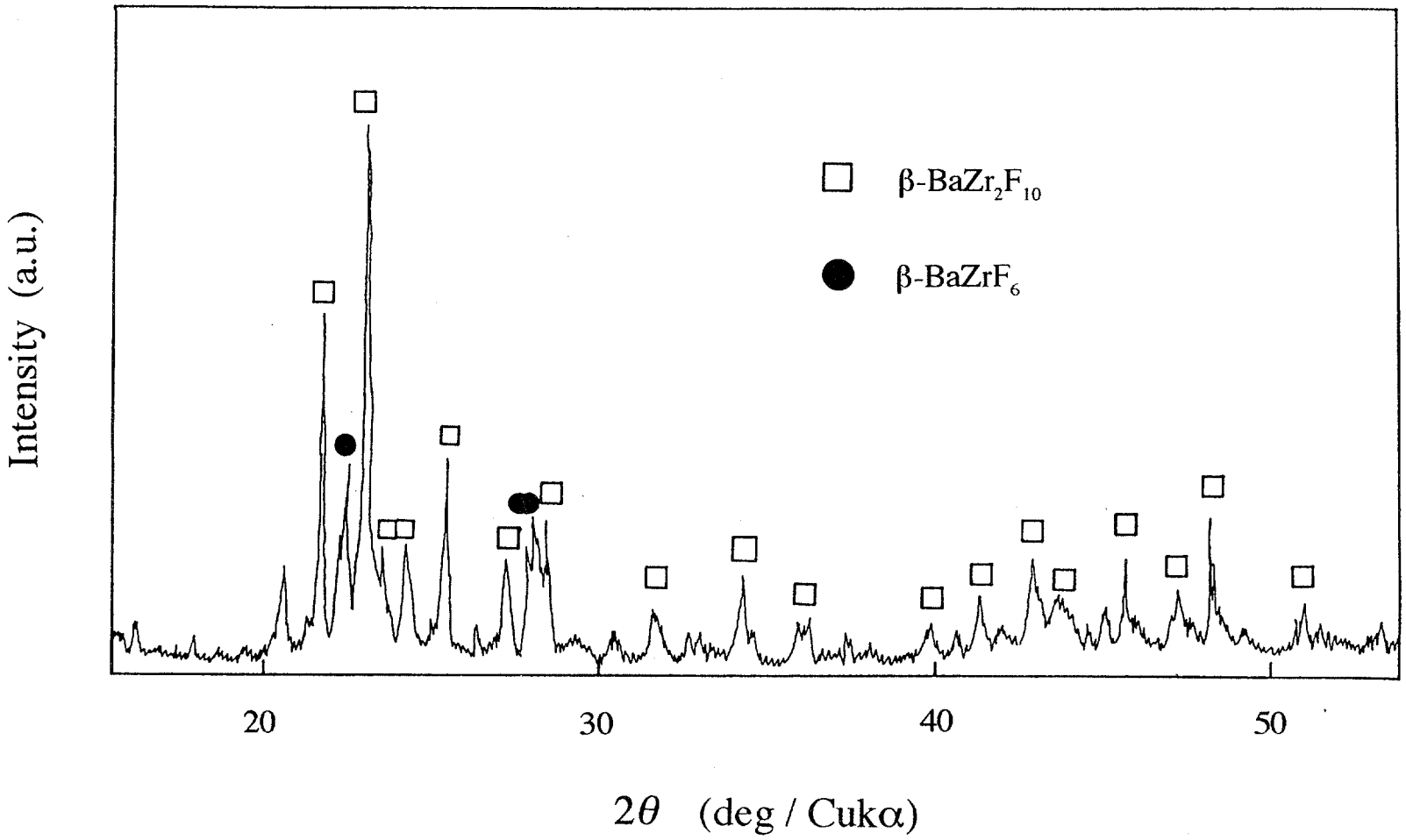

Fig. A-9 XRD powder pattern of the prepared β-$BaZr_2F_{10}$ crystal.

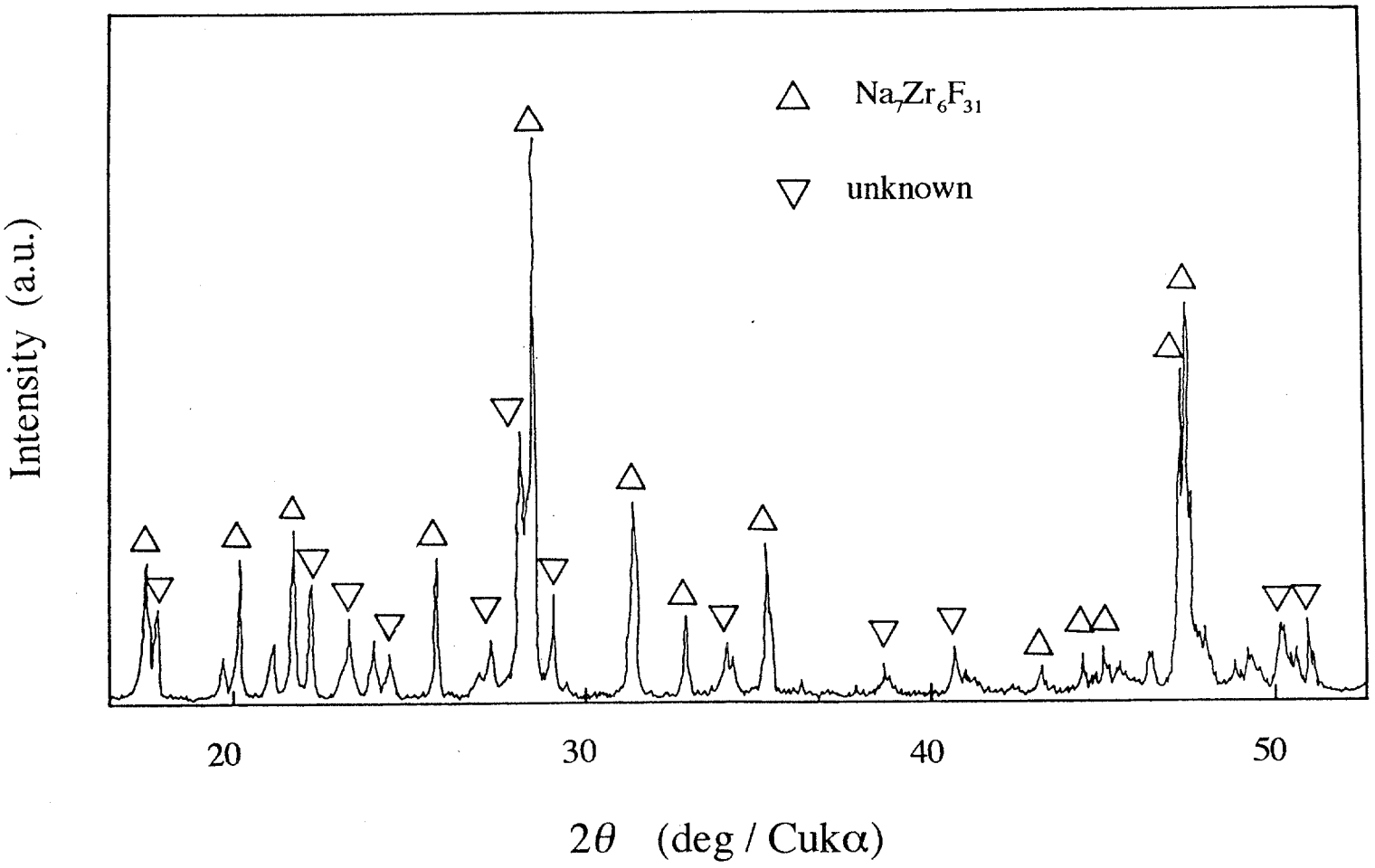

Fig. A-10 XRD powder pattern of the prepared $Na_7Zr_6F_{31}$ crystal.

Acknowledgment

I would like to give much gratitude to my wife and parents for their support and encouragement. The present study was carried out under the guideline of Prof. M. Yamane in Tokyo Institute of Technology. It gives me great pleasure to express my appreciation to Prof. M. Yamane for his precious guidance and advice in the field of the glass science and technology. I should like to acknowledge Assoc. Prof. S. Shibata for his kindly advice and support in the laboratory. I also wish to acknowledge Prof. H. Kawazoe of Tokyo Institute of Technology for giving me some scientific points of view in inorganic materials. I wish to express my special thanks to Dr. S. Inoue of National Institute of Research for Inorganic Materials, who proposed the exciting investigation field of the halide glasses and gave me the precious advises and encouragement. I would also like to give my thanks to all the colleagues in the laboratory, especially, to Mr. Y. Suzuki, Mr. T. Morohashi, Mr. M. Nakanishi, Mr. K. Yamazaki and Mr. J. Mizuno.

Finally, I am grateful to Prof. K. Okada, Prof. K. Kawamura, Assoc. Prof. S. Shibata, Assoc. Prof. T. Tsurumi and Assoc. Prof. A. Yasumori in Tokyo Institute of Technology for their careful reviewing of this thesis.

矢野哲司

Tetsuji Yano